Simultaneous Target and Multipath Positioning

by

Li Li

Department of Electrical and Computer Engineering
Duke University

Date:_____

Approved:

_____
Jeffrey L. Krolik, Supervisor

_____
Loren W. Nolte

_____
Lawrence Carin

_____
Ronald Parr

_____
Matthew S. Reynolds

Dissertation submitted in partial fulfillment of
the requirements for the degree of Doctor of Philosophy
in the Department of Electrical and Computer Engineering
in the Graduate School
of Duke University

2014

ABSTRACT

Simultaneous Target and Multipath Positioning

by

Li Li

Department of Electrical and Computer Engineering
Duke University

Date:_____

Approved:

_____
Jeffrey L. Krolik, Supervisor

_____
Loren W. Nolte

_____
Lawrence Carin

_____
Ronald Parr

_____
Matthew S. Reynolds

An abstract of a dissertation submitted in partial
fulfillment of the requirements for the degree
of Doctor of Philosophy in the Department of
Electrical and Computer Engineering in the Graduate School
of Duke University

2014

Abstract

In this work, we present the Simultaneous Target and Multipath Positioning (STAMP) technique to jointly estimate the unknown target position and uncertain multipath channel parameters. We illustrate the applications of STAMP for target tracking/geolocation problems using single-station hybrid TOA/AOA system, monostatic MIMO radar and multistatic range-based/AOA based localization systems. The STAMP algorithm is derived using a recursive Bayesian framework by including the target state and multipath channel parameters as a single random vector, and the unknown correspondence between observations and signal propagation channels is solved using the multi-scan multi-hypothesis data association. In the presence of the unknown time-varying number of multipath propagation modes, the STAMP algorithm is modified based on the single-cluster PHD filtering by modeling the multipath parameter state as a random finite set. In this case, the target state is defined as the parent process, which is updated by using a particle filter or multi-hypothesis Kalman filter. The multipath channel parameter is defined as the daughter process and updated based on an explicit Gaussian mixture PHD filter. Moreover, the idenfiability analysis of the joint estimation problem is provided in terms of Cramér–Rao lower bound (CRLB). The Fisher information contributed by each propagation mode is investigated, and the

effect of Fisher information loss caused by the measurement origin uncertainty is also studied. The proposed STAMP algorithms are evaluated based on a set of illustrative numeric simulations and real data experiments with an indoor multi-channel radar testbed. Substantial improvement in target localization accuracy is observed.

Contents

List of Figures

Acknowledgements

Throughout my five year graduate study at Duke University, I must give sincere thanks to the individuals who have provided me with encouragement, immense support and assistance. First and foremost, I would like to thank my dissertation advisor, Dr. Jeffrey Krolik for his guidance over the last five years. As a prominent mentor and scientist, Dr. Krolik provide me valuable insights into the world of signal process and the great opportunity to study such interesting and challenging research problems. I would also like to thank Dr. Loren Nolte, Dr. Matthew Reynolds, Dr. Ronald Parr and Dr. Lawrence Carin for serving on my committee of PhD defense, as well as all their kind comments and suggestions of my research projects.

I would like to thank Dr. Jeffrey Rogers, Dr. Ryan Goldhahn, Dr. William Lee, Dr. Jason Yu and Dr. Jonathan Odom for sharing their constructive insights in our discussions. I am also thankful all the support offered by my officemates, Itay Cnaan-on, Jonathan Soli, Juan Ramirez Jr., and Xu Chi, who have offered generous help and a collegial environment of my graduate work at Duke.

I would like to my parents, my families and and all my friends in both China and the States for their indispensable supports over the past few years. Finally, I would also like to thank the Office of Naval Research, for providing the funding for this research.

1
Overview

Remote sensing techniques have historically considered signals arriving via direct-path or line-of-sight (LOS) propagation. For localization purposes, target positions can be extracted from observations as Time of Arrival (TOA) [1], Time Difference of Arrival (TDOA) [2], Angle of Arrival (AOA) [3] or the Received Signal Strength (RSS) [4] based on various positioning systems, such as Radar [5], wireless LAN 802.1x infrastructures [6] or other distributed/collocated sensor platforms [7-10]. One of the biggest challenges faced by both non-cooperative and cooperative methods for RF geolocation of objects in complex terrain, such as indoor or urban environments, is the presence of multipath propagation. In such environments, reflections and scattering of RF energy from the target along different paths have largely precluded accurate geolocation without extensive training data (e.g. detailed environmental modeling) which is usually impractical to obtain. This work concerns the exploitation of multipath signals in uncertain multipath environments by considering how and when joint estimation of target location and channel parameters is possible. Previous work on the problem of non-cooperative target localization in multipath channels using varying amounts of a

priori channel modeling has addressed a variety of applications such urban GMTI radar [11], over-the-horizon radar (OTHR) [16], urban through-the-wall radar sensing [17] and underwater acoustic source localization [15]. For cooperative subjects, multipath has been exploited for navigation in GPS-denied indoor/urban environments [12-13] given accurate environmental modeling.

The type of multipath channel modeling varies significantly depending on the specific geolocation application [16-20]. For example, in Over-The-Horizon-Radar (OTHR) applications, the spatially-varying plasma frequency profile of ionosphere is measured using extensive ionospheric sounders; for indoor/urban radar synthetic aperture sensing, knowledge of the reflective geometry from building floor plans/local maps are used to obtain detailed physical models of multipath observations [17-20]. While in some situations, considerable environmental data is available, numerical multipath models are often both computationally intensive and sensitive to model mismatch. Alternatively, pattern classification-based approaches have been proposed based on matching received signals to templates obtained as a function of hypothesized source locations [21-22]. These methods, however, require extensive training data from measurements taken over a dense grid of possible source locations.

In more recent work, to avoid the need for high fidelity channel modeling, the dynamics of the target position have been included in the geolocation process to obtain estimates of both moving target positions and multipath parameters [24-26]. In [24], the

problem of indoor GPS using multiple, surrounding transmitters was treated by modeling only specular reflections from surfaces of uncertain position and using a probabilistic data association filter (PDAF) to link detected arrivals with multipath raymodes. In [25], a localization algorithm was developed to jointly estimate mobile transmitter positions and random scatter positions with angle-of-arrival (AOA), angle-of-departure (AOD), and time-of-arrival (TOA) measurements. Two serious issues, however, have limited the application of conventional tracking solutions to geolocation in complex environments for both non-cooperative (e.g. indoor radar) and cooperative (e.g. indoor GPS) applications. The first is the presence of false tracks due to multipath reflections from the same target which can be easily mistaken as multiple "ghost" targets. In particular, traditional single-scan data association approaches, such as the PDAF, are unable to associate multipath returns which can be widely separated in delay, Doppler, and/or angle. The second issue, more fundamental than the first, concerns the question of when there is sufficient information in the observed data to perform geolocation in presence of channel uncertainty.

In this paper, we derive a multi-scan geolocation method for both non-cooperative and cooperative target tracking in uncertain multipath environments, which we refer to as Simultaneous Target and Multipath Positioning (STAMP). STAMP is inspired by methods for Simultaneous Localization and Mapping (SLAM) used in robotics [17] where simultaneous navigation and mapping is performed. The general

framework for STAMP [16] uses a state vector which contains both the target position and multipath channel parameters. As in other recent approaches, STAMP requires: 1) a stochastic model for the dynamics of the targets and multipath channels parameters, and 2) a set of observations (e.g., TOA and AOA) which over time can be used to infer the underlying state sequence. STAMP, however, simultaneously tracks moving targets over an entire history of observation intervals which enables the algorithm to resolve ambiguities caused by "ghost" targets and learn the physical environmental parameters, e.g. wall locations, associated with each multipath, which are assumed to be stationary relative to the target dynamics. By using these environmental parameter estimates, STAMP can geo-locate targets even when they move into non-line-of-sight (NLOS) regions but have returns which reflect off the same multipath scattering centers.

The new approach for multi-dwell data association of multipath returns presented here is based on multi-hypothesis data association. In our previous related work [26], Viterbi Data Association (VDA) was proposed as a multi-scan method offering improved performance in clutter over the conventional single-dwell nearest neighbor (NN), joint probabilistic data association filter (JPDAF) [30, 40] and 2-D assignment methods [31-33], which was originally developed for tracking line-of-sight targets in high levels of backscatter clutter from the ground [28, 29]. This application of VDA can be interpreted as a dynamic programing approach to the multiple hypothesis tracking (MHT) problem with a specific "Viterbi Pruning scheme". Although dynamic

programming yields a suboptimal solution, the speed of VDA makes it computationally efficient [29]. In this paper, we present a VDA-liked multi-hypothesis data association method tailored to the STAMP problem using the framework given in [26, 34] to obtain a new pruning scheme derived as an H-best assignment. In addition, a multi-hypothesis extended Kalman Filter (EKF) based algorithm is proposed for STAMP. Finally, practical issues of track and multipath propagation ray mode initialization are also addressed to minimize the a priori information required.

In **Chapter 2** of this work, the multiple-hypothesis based STAMP technique is initially applied to a single station hybrid TOA/AOA RF source tracking problem. Firstly, the question of identifiability can be tractably explored by evaluating the Cramer-Rao Lower Bound (CRLB) for joint target and multipath parameter estimation with TOA/AOA observations. Although prior studies have addressed line-of-sight (LOS) and non-line-of-sight (NLOS) localization accuracies in terms of the mean-square-error based CRLB [38, 39] and a binary-error-metric based information theoretic bound [44], this work focuses on the question of how each propagation modes contributes to the Fisher information and when the target and multipath propagation parameters are identifiable as a function of available observations. Simulation and real data experimental results are presented using an S-band low-power bi-static radar testbed [36, 37] to track a mobile transmitter using the proposed multi-hypothesis STAMP algorithm. As an extension of the single station hybrid TOA/AOA problem, the STAMP

concept is also applied to a non-cooperative target tracking using a collocated two-way multi-input multi-output (MIMO) radar system in **Chapter 3**. The utilization of MIMO processing provides the extra degree of transmit diversity which permits angle of departure (AOD) measurements. This provides additional geometrical information that can be used to resolve the uncertain propagation model.

As applications of STAMP for one-way simplex RF source tracking and non-cooperative monostatic radar target tracking problem were studied, **Chapter 4** of this work also considers a multistatic range-based localization scenario: a Mobile Station (MS) is self-localizing using a Base Station (BS) network. Each node within the BS network shares the same system clock but is asynchronized with the MS, which makes the localization scenario equivalent to a Time-Difference-Of-Arrival (TDOA) problem. The multipath observations are modeled by single-bounce reflections from point-liked scatters within the area of interest, such as buildings, vehicles and other man-made structures. The scatters are assumed to be stationary, however, both the number of scatters and their associated ground positions are unknown. The previous multiple-hypothesis based STAMP implementation stacked the target position and multipath channel parameters as a single random vector. However, since the number of multipath modes (or the number of scatters in our case) is unknown and time-varying, mode validation steps must be performed over multiple successive dwells in order to obtain

an estimate of the number of modes, which results in fluctuating state dimensions of the STAMP state vector.

For this reason, we model states of all scatter positions by a random finite set [45], characterizing both the number of scatters and associated ground coordinates at a single time interval. Using range observations from each BS node, the multipath parameter state, conditioned on the MS position, is estimated using the first moment approximation of the Bayesian multi-target filter, known as the probability hypothesis density (PHD) filter [46]. The above formation yields the concept of single-cluster PHD filter, which has been applied to Simultaneous Localization and Mapping (SLAM) [48, 49], extend/group target tracking [50, 51] and sensor registration and calibration [47, 52]. The single-cluster PHD filter explores a hierarchical point process model. For the STAMP problem, we define the MS state the clock difference between the MS and the BS network as a parent process, whose probability distribution is approximated using a particle representation. Conditioning on each particle of the parent process, the random finite set of the scatter state is denoted as the daughter process, and its PHD intensity is represented using a Gaussian Mixture structure. Therefore, the distribution of parent process is updated using a particle filter; and for each particle, the associated PHD surface is updated via a multi-sensor iterated Gaussian Mixture PHD filter [47, 53]. The Single-Cluster PHD filter based STAMP algorithm is evaluated via a set of simulations and an illustrative real-data indoor RF source tracking experiment.

Similar to the multi-static range-based setup, **Chapter 5** explores the application of STAMP in a multi-static AOA-only target localization scenario. Using AOA observation from a single non-cooperative target collected by a distributed Uniform Linear Array (ULA) network, the multipath parameter state and the target state are jointly estimated using the Single-Cluster PHD filter concept. As an alternative of the previous particle filter based implementation, the target state (i.e., the parent process) is modeled as a single Gaussian distribution. We incorporate the multi-dwell multi-hypothesis data association in order to obtain a more accurate target position estimate. In this case, the multi-dwell multi-component likelihood is evaluated conditioned on a single association hypothesis between each observation and multipath channel, which can be evaluated recursively through time. Using previously estimated PHD of multipath channels, the Gaussian target state is then updated via conventional EKF. For the daughter process, the GM-PHD filtering of multipath parameters solely depends on the given estimate of target position, and avoids data association based on Finite Set Statistics (FISST). After obtaining a set of accurate estimate of target state based on various data association hypotheses, the PHD(s) of multipath parameters can be updated via GM-PHD filter framework.

As a summary, the organization of this thesis is as follows:

Chapter 2 formulates the STAMP recursive estimation problem for single station hybrid TOA/AOA target tracking. The multi-hypothesis data association algorithm is

derived and the CRLB analysis is provided. Demonstrations of practical implementations of the STAMP for indoor target tracking problem are also illustrated.

Chapter 3, the STAMP concept is extended to a mono-static Multiple-Input and Multiple-Output (MIMO) radar target tracking problem by using the multi-hypothesis based STAMP algorithm.

Chapter 4 extends the STAMP concept to a multi-static range-based geolocation problem. A Single-Cluster PHD filter framework is formulated and evaluated based on simulation and real data experiments. CRLB based identfifiability analysis is also provided.

Chapter 5 applies the STAMP technique to a multi-static AOA-only geolocation problem. The Single-Cluster PHD filter is modified by assuming that the target state follows a single Gaussian distribution. The proposed recursive Bayesian algorithm employs a multi-hypothesis tracker to obtain enhanced target state estimation.

Chapter 6 provides the conclusion and future work of the STAMP technique.

2

Single Station Hybrid TOA/AOA STAMP

In this chapter, we concentrate on applying the STAMP concept to a single station hybrid TOA/AOA geolocation problem. Fundamental analysis of the identifiability of unknown parameters is provided based on closed-from estimation-theoretic Cramer-Rao Lower Bound (CRLB). Although prior studies have addressed NLOS localization accuracy in terms of the CRLB, this work focuses on answering questions such as: how does each propagation mode contribute to the Fisher information and what is the identifiability of target and multipath channel as a function of the availability of LOS/multipath observations changes.

The framework of STAMP of dynamic target tracking is then formulated. We model the multipath measurements based on geometric optics in a 2D plane, where flat plane reflectors and point scatters are considered. The STAMP algorithm is derived based on the multi-dwell multi-hypothesis data association algorithm and the Extended

Kalman Filter, which is evaluated based on a set of simulation and real data experiments.

2.1 Identifiability of Hybrid AOA/TOA STAMP

We consider a single base station (BS) case for tracking a moving source with time of arrival (TOA) and angle of arrival (AOA) observations by a uniform linear receiver array (ULA) located at *origin*. This section discusses identifiability by examining the boundedness of the Cramer-Rao Lower Bound (CRLB) on joint target and multipath estimation. Under the assumptions of perfect detections and data associations, $N+1$ observations are obtained at a single time instance, corresponding to one direct-path observation and N multipath observations from N different multipath propagation modes. Each propagation mode i is modeled with a $L \times 1$ parameter vector $\boldsymbol{\theta}_i$, $i = 1,2,\dots N$, and among these N modes. The observation set Z is then defined as

$$Z = \{\mathbf{z}_d, \mathbf{z}_1, \dots, \mathbf{z}_N\} \quad \text{with} \quad \mathbf{z}_i = [\rho_i, \zeta_i]^T \tag{2.1}$$

where 2×1 observation vector $\mathbf{z}_i$ contains both TOA observation ρ_i and sine AOA observation ζ_i. Denoting the target position vector as $\mathbf{p} = [x, y]^T$, TOA and AOA observations for LOS observation (i.e., $i = d$) are given by:

$$\mathbf{z}_d = \begin{bmatrix} \rho_d \\ \zeta_d \end{bmatrix} = \begin{bmatrix} \sqrt{x^2 + y^2} \\ x/\sqrt{x^2 + y^2} \end{bmatrix} + \boldsymbol{\epsilon}_d \tag{2.2}$$

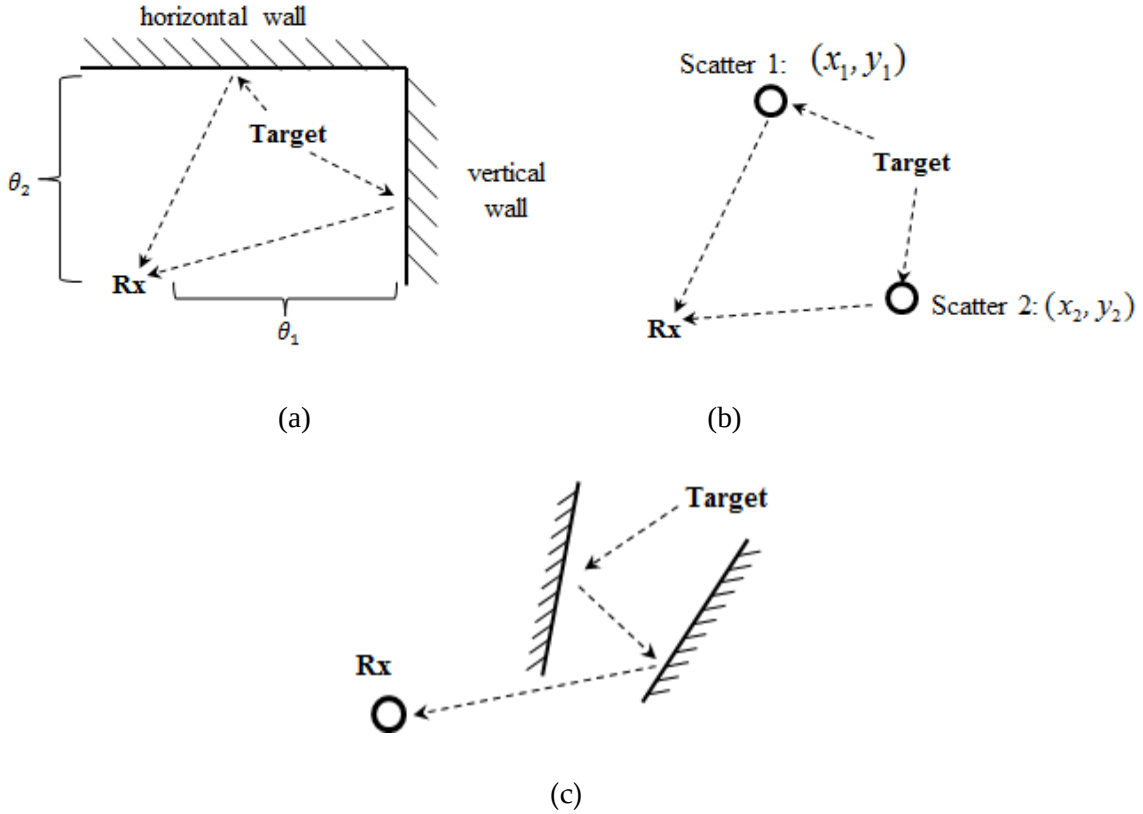

(a) (b)

(c)

Figure 2.1: **(a)** L **= 1: specular reflection produced by horizontal or vertical walls,** θ **represents the distances between walls and Rx; (b)** L **= 2: diffuse reflection by random scatters,** θ **represents the coordinates of the scatters; (c) L>2: multiple-bounce reflection, probably with both specular and diffuse reflections**

where $\boldsymbol{\epsilon}_d$ is zero-mean Gaussian observation noises with covariance matrix $\mathbf{R}_d$. For multipath observations (i.e., $i = 1, \ldots N$), $\mathbf{z}_i$ is given as:

$$\mathbf{z}_i = \begin{bmatrix} \rho_i \\ \zeta_i \end{bmatrix} = \mathbf{h}_i(\mathbf{p}, \boldsymbol{\theta}_i) + \boldsymbol{\epsilon}_i \tag{2.3}$$

where $\mathbf{h}_i(\mathbf{p}, \boldsymbol{\theta}_i)$ is the multipath observation function and similarly $\boldsymbol{\epsilon}_i$ is zero-mean Gaussian with covariance $\mathbf{R}_i$. The purpose of STAMP is to jointly estimate the target

position $\mathbf{p}$ and multipath parameters $\boldsymbol{\theta}_i, i = 1,..,N$, and the (2 + NL) × 1 STAMP state vector $\mathbf{x}$ is then defined by:

$$\mathbf{x} = [\mathbf{p}^T, \boldsymbol{\theta}_1^T, \ldots, \boldsymbol{\theta}_N^T]^T \tag{2.4}$$

Note that in addition to the observation set Z, supplementary observations of $\mathbf{x}$, denoted as $\tilde{\mathbf{x}}$, may also be available. For example, other sensing scheme may provide additional target position observations $\tilde{\mathbf{p}}$, and wireless channel probing may obtain the channel parameter observation $\tilde{\boldsymbol{\theta}}_i$ which could provide additional measurements on these parameters.

2.1.1 Derivation of Cramer-Rao Bound for STAMP

The CRLB provides lower limits for the variance (or covariance matrix) of unbiased estimation error of an unknown parameter vector $\mathbf{x}$. Denoting $\hat{\mathbf{x}}$ as an unbiased estimate of $\mathbf{x}$, the CRLB is provide the lower performance bound of $\hat{\mathbf{x}}$ as:

$$E_{\mathbf{x}}[(\hat{\mathbf{x}} - \mathbf{x})(\hat{\mathbf{x}} - \mathbf{x})^T] \geq \mathbf{J}(\mathbf{x})^{-1} \tag{2.5}$$

where $\mathbf{A} \geq \mathbf{B}$ denotes that matrix $\mathbf{A}$ - $\mathbf{B}$ is positive semidefinite, and $\mathbf{J}(\mathbf{x})$ is the nonsingular information matrix. In the STAMP case, $\mathbf{J}(\mathbf{x})$ consists two components:

$$\mathbf{J}(\mathbf{x}) = \mathbf{J}_l(\mathbf{x}) + \mathbf{J}_s(\mathbf{x}) \tag{2.6}$$

The first term $\mathbf{J}_l$ refers for the likelihood information as:

$$\mathbf{J}_l(\mathbf{x}) \triangleq E_Z[\nabla_{\mathbf{x}} \ln f(Z|\mathbf{x}) \, (\nabla_{\mathbf{x}} \ln f(Z|\mathbf{x}))^T] \tag{2.7}$$

where $f(Z|\mathbf{x})$ stands for the likelihood function of observation set Z. The second term $\mathbf{J}_s$ represents the supplementary observations on $\mathbf{x}$ given as:

$$\mathbf{J}_p(\mathbf{x}) \triangleq E_{\tilde{\mathbf{x}}}[\nabla_{\mathbf{x}} \ln f(\tilde{\mathbf{x}}|\mathbf{x}) \, (\nabla_{\mathbf{x}} \ln f(\tilde{\mathbf{x}}|\mathbf{x}))^T] \tag{2.8}$$

In the STAMP context, the log-likelihood is given as*:*

$$\ln f(Z|\mathbf{x}) \propto \begin{bmatrix} \sqrt{x^2+y^2} - \rho_d \\ x/\sqrt{x^2+y^2} - \zeta_d \end{bmatrix}^T \mathbf{R}_d^{-1} \begin{bmatrix} \sqrt{x^2+y^2} - \rho_d \\ x/\sqrt{x^2+y^2} - \zeta_d \end{bmatrix}$$

$$+ \sum_{i=1}^{N} \left(\mathbf{h}_i(\mathbf{p}, \boldsymbol{\theta}_i) - \begin{bmatrix} \rho_i \\ \zeta_i \end{bmatrix} \right)^T \mathbf{R}_i^{-1} \left(\mathbf{h}_i(\mathbf{p}, \boldsymbol{\theta}_i) - \begin{bmatrix} \rho_i \\ \zeta_i \end{bmatrix} \right) \tag{2.9}$$

In the case when direct-path is not present, $\mathbf{R}_d^{-1} \to 0$, and the first term in (2.9) is gone. We also assume Gaussian distributions of $\tilde{\mathbf{x}}$ as $\tilde{\mathbf{p}} \sim \mathcal{N}(\mathbf{p}, \boldsymbol{\Gamma}_{\mathbf{p}})$ and $\tilde{\boldsymbol{\theta}}_i \sim \mathcal{N}(\boldsymbol{\theta}_i, \boldsymbol{\Gamma}_i)$, given by*:*

$$\ln p(\tilde{\mathbf{x}}|\mathbf{x}) \propto (\mathbf{p} - \tilde{\mathbf{p}})^T \boldsymbol{\Gamma}_{\mathbf{p}}^{-1} (\mathbf{p} - \tilde{\mathbf{p}}) + \sum_{i=1}^{N} \left(\boldsymbol{\theta}_i - \tilde{\boldsymbol{\theta}}_i\right)^T \boldsymbol{\Gamma}_i^{-1} (\boldsymbol{\theta}_i - \tilde{\boldsymbol{\theta}}_i) \tag{2.10}$$

If no supplementary observations is available, $\boldsymbol{\Gamma}^{-1}$ becomes all zero matrix and has no contribution to $\mathbf{J}(\mathbf{x})$. The CRLB is asymptotically obtained by the maximum likelihood estimator defined as*:*

$$\hat{\mathbf{x}}_{MAP} = \underset{\mathbf{x}}{\operatorname{argmax}} \{\ln f(Z|\mathbf{x}) + \ln p(\tilde{\mathbf{x}}|\mathbf{x})\} \tag{2.11}$$

The asymptotic behavior is efficient when the signal-to-noise ratio is sufficiently large (i.e., observation noises are sufficiently small). With (2.5) to (2.11), the information matrix $\mathbf{J}(\mathbf{x})$ can be given in the form of

$$\mathbf{J}(\mathbf{x}) = \begin{bmatrix} \mathbf{L}_d + \sum_i \mathbf{L}_i + \boldsymbol{\Gamma}_{\mathbf{p}}^{-1} & \mathbf{C}_{1,\mathbf{p}} & \mathbf{C}_{2,\mathbf{p}} & \cdots & \mathbf{C}_{N,\mathbf{p}} \\ \mathbf{C}_{1,\mathbf{p}}^T & \boldsymbol{\Lambda}_1 + \boldsymbol{\Gamma}_1^{-1} & 0 & \cdots & 0 \\ \mathbf{C}_{2,\mathbf{p}}^T & 0 & \boldsymbol{\Lambda}_2 + \boldsymbol{\Gamma}_2^{-1} & & \vdots \\ \vdots & \vdots & & \ddots & 0 \\ \mathbf{C}_{N,\mathbf{p}}^T & 0 & \cdots & 0 & \boldsymbol{\Lambda}_N + \boldsymbol{\Gamma}_N^{-1} \end{bmatrix} \tag{2.12}$$

where

$$\mathbf{L}_i = \nabla_{\mathbf{p}} \mathbf{h}_i \big|_{(\mathbf{p},\boldsymbol{\theta}_i)}^T \mathbf{R}_i^{-1} \nabla_{\mathbf{p}} \mathbf{h}_i \big|_{(\mathbf{p},\boldsymbol{\theta}_i)} \tag{2.13}$$

$$\mathbf{C}_{i,\mathbf{p}} = \nabla_{\mathbf{p}} \mathbf{h}_i \big|_{(\mathbf{p},\boldsymbol{\theta}_i)}^T \mathbf{R}_i^{-1} \nabla_{\boldsymbol{\theta}_i} \mathbf{h}_i \big|_{(\mathbf{p},\boldsymbol{\theta}_i)} \tag{2.14}$$

$$\boldsymbol{\Lambda}_i = \nabla_{\boldsymbol{\theta}_i} \mathbf{h}_i \big|_{(\mathbf{p},\boldsymbol{\theta}_i)}^T \mathbf{R}_i^{-1} \nabla_{\boldsymbol{\theta}_i} \mathbf{h}_i \big|_{(\mathbf{p},\boldsymbol{\theta}_i)} \tag{2.15}$$

$$\mathbf{L}_d = \begin{bmatrix} \frac{x}{\sqrt{x^2+y^2}} & \frac{y^2}{(x^2+y^2)^{3/2}} \\ \frac{y}{\sqrt{x^2+y^2}} & \frac{-xy}{(x^2+y^2)^{3/2}} \end{bmatrix}^T \mathbf{R}_d^{-1} \begin{bmatrix} \frac{x}{\sqrt{x^2+y^2}} & \frac{y^2}{(x^2+y^2)^{3/2}} \\ \frac{y}{\sqrt{x^2+y^2}} & \frac{-xy}{(x^2+y^2)^{3/2}} \end{bmatrix} \tag{2.16}$$

where all elements in $\mathbf{J}(\mathbf{x})$ are evaluated at the true $\mathbf{x}$. Based on the special structure of $\mathbf{J}(\mathbf{x})$, the CRLB on target position estimates $\widehat{\mathbf{p}}$ yields the form of:

$$[\mathbf{J}(\mathbf{x})^{-1}]_{\mathbf{p}} = (\mathbf{L}_d + \boldsymbol{\Gamma}_{\mathbf{p}}^{-1} + \sum_i \underbrace{\mathbf{L}_i - \mathbf{C}_{i,\mathbf{p}} (\boldsymbol{\Lambda}_i + \boldsymbol{\Gamma}_i^{-1})^{-1} \mathbf{C}_{i,\mathbf{p}}^T}_{\triangleq \Delta \mathbf{L}_i})^{-1} \tag{2.17}$$

When neither direct path nor supplementary observation of target position is available, $\mathbf{L}_d + \boldsymbol{\Gamma}_{\mathbf{p}}^{-1} \to 0$, and the CRLB given in (2.17) only depends on multipath observations. Similarly, the CRLB on multipath parameter estimates $\widehat{\boldsymbol{\theta}}_k$ is given by:

$$[\mathbf{J}(\mathbf{x})^{-1}]_{\boldsymbol{\theta}_k} = (\boldsymbol{\Gamma}_k^{-1} + \boldsymbol{\Lambda}_k - \mathbf{C}_{1,\mathbf{p}}^T \mathbf{L}_k^{-1} \mathbf{C}_{1,\mathbf{p}} + \mathbf{C}_{k,\mathbf{p}}^T \mathbf{L}_k^{-1} (\mathbf{L}_k^{-1} + [\mathbf{J}(\mathbf{x})^{-1}]_{\mathbf{p}}^{(k)})^{-1} \mathbf{L}_k^{-1} \mathbf{C}_{k,\mathbf{p}})^{-1} \leq \boldsymbol{\Gamma}_k \tag{2.18}$$

where $[\mathbf{J}(\mathbf{x})^{-1}]_{\mathbf{p}}^{(k)}$ denotes the CRLB on $\hat{\mathbf{p}}$ excluded the contribution from mode k. The derivation of (2.17) and (2.18) will be given in Appendix A.

The 2 × 2 non-negative definite matrix $\Delta\mathbf{L}_i$ carries out the information obtained from propagation mode i, and as the number of modes N increase, the CRLB on $\hat{\mathbf{p}}$ decreases with the total information increasing. We can also derive the following bounds for $\Delta\mathbf{L}_i$:

$$\mathbf{L}_i - \mathbf{C}_{i,\mathbf{p}}\boldsymbol{\Lambda}_i^{-1}\mathbf{C}_{i,\mathbf{p}}^T \leq \Delta\mathbf{L}_i \leq \mathbf{L}_i \tag{2.19}$$

The upper bound of $\Delta\mathbf{L}_i$ is obtained when $\boldsymbol{\theta}_i$ is known exactly (i.e., $\boldsymbol{\Gamma}_i^{-1} \to \infty$), so that the uncertainty on $\boldsymbol{\theta}_i$ is eliminated and the CRLB on target position decreases. The lower bound is attained when no supplementary observation on $\boldsymbol{\theta}_i$ is available (i.e., $\boldsymbol{\Gamma}_i^{-1} \to 0$), resulting in Fisher information reductions and increases of the CRLB on target position. Therefore, the more accurate $\widetilde{\boldsymbol{\theta}}_i$ is (i.e., increase in $\boldsymbol{\Lambda}_i^{-1}$), the more Fisher information $\Delta\mathbf{L}_i$ can contribute, and lower the CRLB on $\hat{\mathbf{p}}$ can be achieved. Note that, for $L = 2$, $\mathbf{L}_i$ can be expanded as

$$\mathbf{L}_i = \mathbf{C}_{i,\mathbf{p}}\boldsymbol{\Lambda}_i^{-1}\mathbf{C}_{i,\mathbf{p}}^T \tag{2.20}$$

providing that the upper bound of $\Delta\mathbf{L}_i$ is $\mathbf{0}$; while for $L > 2$, the $L \times L$ matrix $\boldsymbol{\Lambda}_i$ is not invertible, so that $\Delta\mathbf{L}_i$ does not exist in this case. Therefore, non-zero Fisher information could be extracted only if $\widetilde{\boldsymbol{\theta}}_i$ is available for $L \geq 2$.

2.1.2 Blind NLOS Initiation

We are interesting in the case when the neither direct-path observation nor the supplementary observation is available, referring as blind NLOS initiation (BNI). The analysis of this problem depends on the property of $\Delta\mathbf{L}_i$ and the dimension of $\boldsymbol{\theta}_k$, L, the following part will explore the CRLB on different value of L.For $L = 1$, we have $\boldsymbol{\theta}_i = \theta_i$ and $\boldsymbol{\Gamma}_i = \eta_{\theta_i}^2$, In the case $\mathbf{L}_d + \boldsymbol{\Gamma}_{\mathbf{p}}^{-1} \to 0$, the singularity of information matrix $\mathbf{J}(\mathbf{x})$ is determined by $\Delta\mathbf{L}_i$, with the determinant given by:

$$\det(\Delta\mathbf{L}_i) = \det(\mathbf{L}_i)/\left(\eta_{\theta_i}^2\boldsymbol{\Lambda}_i + 1\right) \tag{2.21}$$

It suggests that as $\eta_{\theta_i} \to \infty$ (i.e., supplementary observation on θ_i is unavailable), $\det(\Delta\mathbf{L}_i) \to 0$ and therefore:

$$rank(\Delta\mathbf{L}_i) \to 1 \ \ as \ \ \eta_{\theta_i} \to \infty$$

resulting in singular $\mathbf{J}(\mathbf{x})$ and CRLB trends to infinity. In order to guarantee that $\mathbf{J}(\mathbf{x})$ is invertible and the solvability of BNI problem, observations from two or more multipath modes must be obtained, i.e., $N \geq 2$. (This intuitively makes sense, since solving $2 + N$ unknowns with $2N$ equations must satisfy $2N \geq 2 + N$ or $N \geq 2$.)

In the case of $L = 2$, utilizing the matrix inversion lemma:

$$(\boldsymbol{\Lambda}_i + \boldsymbol{\Gamma}_i^{-1})^{-1} = \boldsymbol{\Lambda}_i^{-1} - (\mathbf{I}_2 + \boldsymbol{\Lambda}_i^{-1}\boldsymbol{\Gamma}_i^{-1})^{-1}\boldsymbol{\Lambda}_i^{-1}\boldsymbol{\Gamma}_i^{-1}\boldsymbol{\Lambda}_i^{-1} \tag{2.22}$$

where $\mathbf{I}_2$ is a 2 × 2 identity matrix, $\Delta\mathbf{L}_i$ is rewritten as

$$\Delta\mathbf{L}_i = \mathbf{C}_{i,\mathbf{p}}(\mathbf{I}_2 + \boldsymbol{\Lambda}_i^{-1}\boldsymbol{\Gamma}_i^{-1})^{-1}\boldsymbol{\Lambda}_i^{-1}\boldsymbol{\Gamma}_i^{-1}\boldsymbol{\Lambda}_i^{-1}\mathbf{C}_{i,\mathbf{p}}^T \tag{2.23}$$

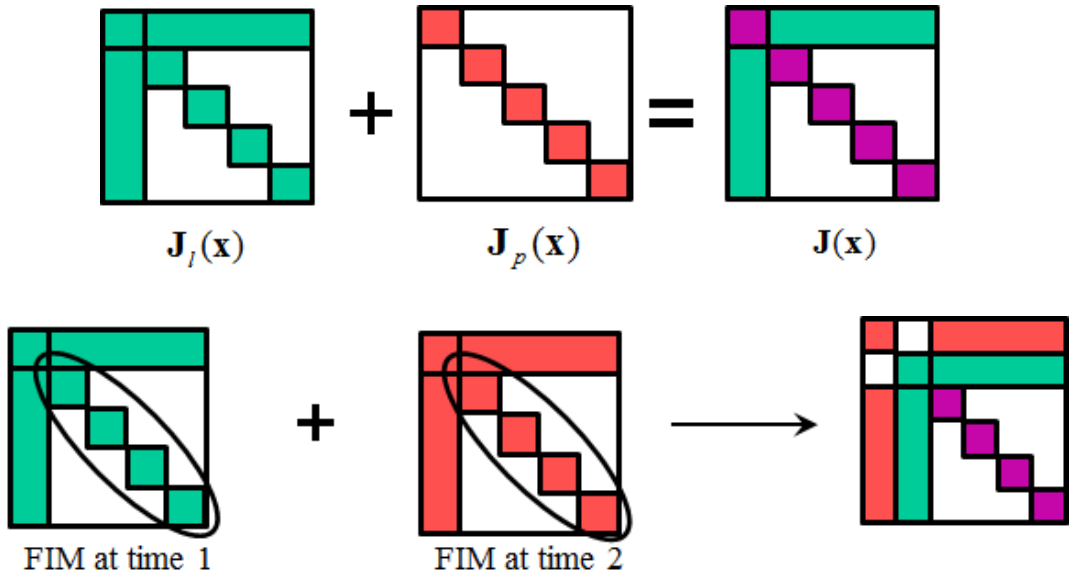

Figure 2.2: Essentially, the direct-path and complementary observations are regards as "diagonal loading" matrix term, which makes J(x) invertible; similarly, if the channels are time-invariant, we can use the Fisher information in time 2 to diagonal loading time 1, so that the J(x) is non-singular.

When supplementary observation on $\tilde{\mathbf{x}}$ is unavailable, $\mathbf{\Gamma}_i^{-1} \to 0$ and consequently $\Delta\mathbf{L}_i \to 0$. Therefore, CRLB on target position estimate only depends on and observations from direct-path, while observation from first-time observed multipath modes are all rejected, which yields the same intuition as discussed in [25].

$$[\mathbf{J}_l(\mathbf{p}_{1:2}, \boldsymbol{\theta}_{1:N})^{-1}]_{\mathbf{p}_{1:2}} = (\sum_i \underbrace{\begin{bmatrix} \mathbf{L}_{i,\mathbf{p}_1} & 0 \\ 0 & \mathbf{L}_{i,\mathbf{p}_2} \end{bmatrix} - \begin{bmatrix} \mathbf{C}_{i,\mathbf{p}_1} \\ \mathbf{C}_{i,\mathbf{p}_2} \end{bmatrix} (\mathbf{\Lambda}_{i,\mathbf{p}_1} + \mathbf{\Lambda}_{i,\mathbf{p}_2})^{-1} [\mathbf{C}_{i,\mathbf{p}_1}^T \; \mathbf{C}_{i,\mathbf{p}_2}^T]}_{\triangleq \Delta\mathbf{L}_{i,\mathbf{p}_{1:2}}})^{-1} \quad (2.24)$$

Given the relationship in (2.21), it can be shown that the 4 by 4 positive-semidefinite matrix $\Delta\mathbf{L}_{i,\mathbf{p}_{1,2}}$ satisfies:

$$rank(\Delta\mathbf{L}_{i,\mathbf{p}_{1:2}}) \leq 2 \quad (2.25)$$

which implies a minimal *two* to *four* first-observed multipath modes are required to obtain a finite CRLB in order to solve the BNI problem, depending on the specific multipath observation function $\mathbf{h}_i(\mathbf{p}, \boldsymbol{\theta}_i)$. For example, linear propagation models can be viewed as benchmark cases, which require only two modes. As for the nonlinear $\mathbf{h}_i(\mathbf{p}, \boldsymbol{\theta}_i)$, more than two modes need to be presented simultaneously to solve the problem.

In more complicated cases where $L > 2$, $\boldsymbol{\Lambda}_i$ is singular according to (2.15), suggesting that only the modes with complementary observation have contributions to the target position estimate. Consequently, it may be inferred that the BNI is doable if and only if $2T > L$ where T is the number of dwells observed, and the factor 2 refers to the number of degrees of freedom of observations (i.e., AOA and TOA).

Note that although regularized by complementary observation, the above analysis essentially describes an identifiability analysis driven by of the singularity of FIM. Although "global" Bayesian bounds could be computed, they involve computing the expected FIM $\mathbf{J}(\mathbf{x})$ with respect to the prior distribution of the STAMP state vector $\mathbf{x}$. This averaging often "regularizes" the FIM such that an average of singular matrices becomes non-singular. This limits the use of Bayesian bounds for studying identifiability of the joint estimation problem.

2.1.3 Multipath Propagations Modeling

Two types of stationary geometric features are considered: flat plane and point scatters as shown in Fig 5, each of which is represented by the parameter vector $\boldsymbol{\theta}$.

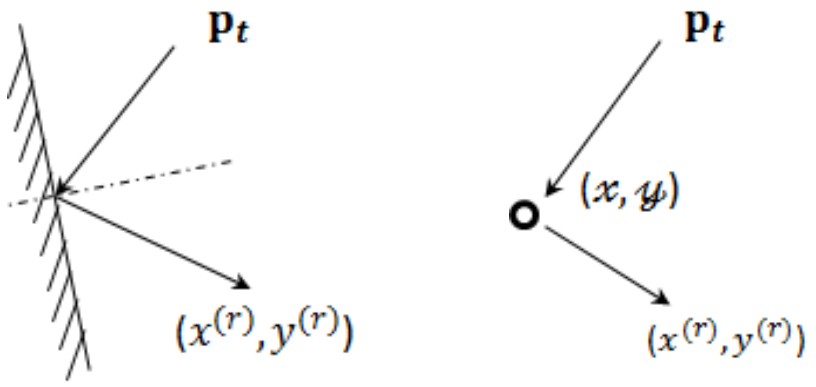

(a) (b)

Figure 2.3: Example of geometric multipath features as (a) flat planes and (b) point scatters

In this work, we consider physical optics based multipath propagating models including both specular reflections and point-scattering centers. In the case of $\boldsymbol{\theta} \in \mathbb{R}^2$, two types of reflectors are considered to produce multipath observations: flat planes and point scatters, shown in Figure 2.3. Flat planes reflectors are defined as straight lines based on Hessian normal form: $x\cos\psi + y\sin\psi + \rho = 0$, with parameter vector $\boldsymbol{\theta} = [\psi, \rho]^T$. The planes are assumed to be specular reflectors and are able to produce images source with a delay (aka "slant" range) and bearing depending on the position of the incident source as shown in Figure 2.3 (a). Point scatters are modeled as discrete points in a 2-D map defined by their location parameter vector $\boldsymbol{\theta} = [x, y]^T$, where x and y are (x, y) coordinates of the scattering point. The point scatters can be convex/concave edges

or irregular shaped objects, which produce diffusive reflections. Since angle-of-arrival (AOA) observations are constant for the point scatters, the multipath returns from point scatters provides only range information of target as illustrated in Figure 2.3 (b).

Denoting the number of reflector as N_t , the total number of possible propagation modes received by the ULA is then $1 + \mathrm{N_t}$ including the direct path. The Gaussian TOA and sine AOA observation noise introduced in Section II is modeled based on the CRLB model with covariance matrix

$$\mathbf{R} = SNR^{-1}\begin{bmatrix} c^2 BW^{-2} & 0 \\ 0 & 4N_a^{-2} \end{bmatrix} \tag{2.28}$$

where c and BW denote speed of light and signal bandwidth respectively, and N_a represents the number of array elements.

$$\mathbf{h}_i(\mathbf{p}(\mathrm{t}), \boldsymbol{\theta}_i) = \begin{bmatrix} \sqrt{x_i'(t)^2 + y_i'(t)^2} \\ x_i'(t)/\sqrt{x_i'(t)^2 + y_i'(t)^2} \end{bmatrix} \tag{2.29}$$

Collaborating with (2.3), the nonlinear multipath observation equation is given by

For flat plane reflectors, we have

$$x'(t) = -x(t)\cos 2\psi - y(t)\sin 2\psi - 2\rho\cos\psi \tag{2.30}$$

$$y'(t) = -x(t)\sin 2\psi + y(t)\cos 2\psi - 2\rho\sin\psi \tag{2.31}$$

while for point scatters:

$$x'(t) = x + x\sqrt{(x - x(t))^2 + (y - y(t))^2}/\sqrt{x^2 + y^2} \tag{2.32}$$

$$y'(t) = y + y\sqrt{(x - x(t))^2 + (y - y(t))^2}/\sqrt{x^2 + y^2} \tag{2.33}$$

In order to numerically evaluate the BNI result given in Proposition 2 for the model of flat reflectors and point scatters, consider the case that target locations at time dwell 1 and 2 are $\mathbf{p}(1) = [0,10]^T$ and $\mathbf{p}(2) = [2,13]^T$ respectively. Five plane reflectors are defined with parameters $[0,20]^T$, $[\pi/4,20]^T$, $[\pi/2,20]^T$, $[3\pi/4,20]^T$ and $[\pi, 20]^T$; while five points scatters are defined at $[3,15]^T$, $[-3,15]^T$, $[2,5]^T$, $[-2,5]^T$ and $[0,20]^T$. Since we assume the LOS path is always absent, to guarantee an invertible FIM, we assume Gaussian supplementary observations of targets at two time instances as $\tilde{\mathbf{p}}(t) \sim N(\mathbf{p}(t), 100^2\mathbf{I}_2)$, for $t = 1, 2$. The root-mean-square error (RMSE) predicted by the CRLBs for the position estimates $\hat{\mathbf{p}}(1)$ and $\hat{\mathbf{p}}(2)$ are shown in Figure 2.4 as function of SNR and the number of reflectors *N*. When BNI is not solvable, the resulting CRLB on $\mathbf{p}$ is determined by the supplementary observation which is constant independent of SNR. Figure 2.4 (a) illustrates the characteristics of flat plane reflectors and indicates that a minimum of three reflectors are required for the CRLB to decrease with SNR. Similarly, Figure 2.4 (b) illustrates the characteristics of scatter-induced multipath and suggests that a minimum of four point scatters are required to obtain a CRLB which improves with SNR. From this analysis we can infer that the BNI problem can be solved for both multipath scenarios in this example.

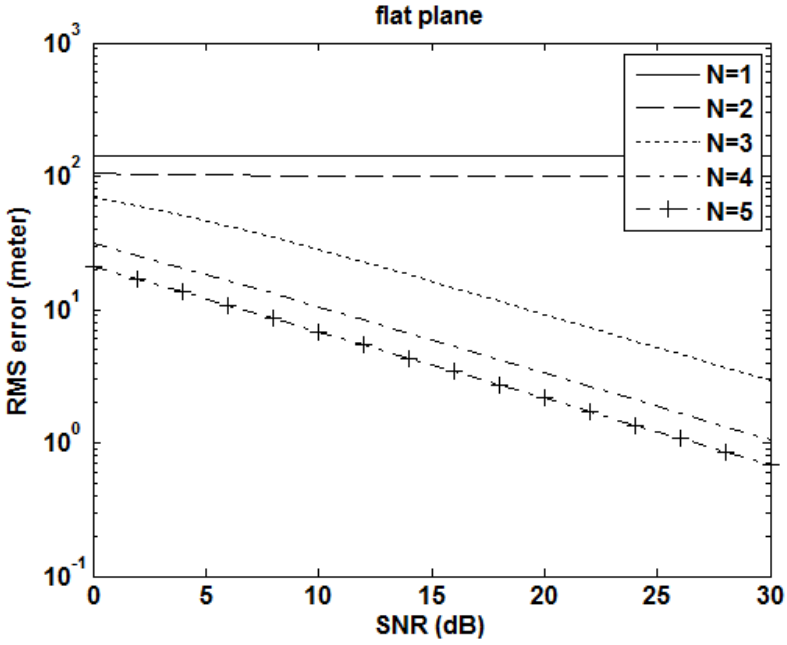

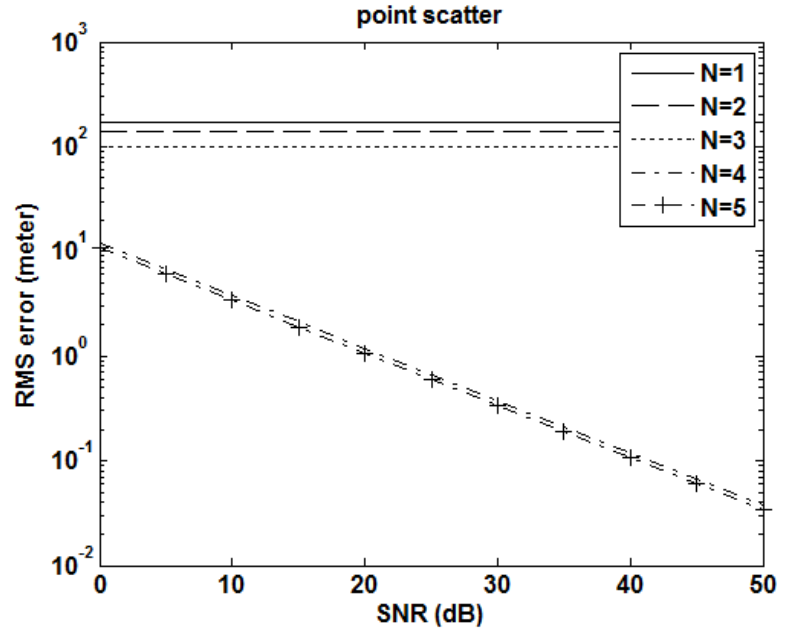

(b)

Figure 2.4: CRLB of target positions estimate for $\mathbf{p}(1)$ and $\mathbf{p}(2)$ for varying number of propagating modes *N*, a) flat plane reflectors and b) point scatters.

2.2 Hybrid TOA/AOA STAP Formulation

Denoting $\boldsymbol{p}(t) = [x(t), y(t)]^T$ as the target x-y ground coordinates $\boldsymbol{v}(t) = [\dot{x}(t), \dot{y}(t)]^T$ as the x-y vector velocity at scan t, the non-manoeuvring dynamics of the target is modeled as a simple linear discrete-time difference equation as:

$$\begin{bmatrix}\mathbf{p}(\mathrm{t}+1)\\ \mathbf{v}(\mathrm{t}+1)\end{bmatrix} = \mathbf{F}\cdot\begin{bmatrix}\mathbf{p}(\mathrm{t})\\ \mathbf{v}(\mathrm{t})\end{bmatrix} + \mathbf{G}\cdot\boldsymbol{\omega}(\mathrm{t}) \tag{2.34}$$

with

$$\mathbf{F} = \begin{bmatrix}\mathbf{I}_2 & \Delta\mathrm{t}\cdot\mathbf{I}_2\\ \mathbf{0} & \mathbf{I}_2\end{bmatrix},\ \mathbf{G} = \begin{bmatrix}\Delta\mathrm{t}^2/2\cdot\mathbf{I}_2\\ \Delta\mathrm{t}\cdot\mathbf{I}_2\end{bmatrix} \tag{2.35}$$

where $\boldsymbol{\omega}(\mathrm{t})$ is zero-mean Gaussian process noise representing the random acceleration of target movement, and $\Delta\mathrm{t}$ is the sampling interval between adjacent time instances.

We utilize the multipath modeling introduced in 2.1.3: flat planar reflector and point-like scatter. Under the assumption that all reflectors are invariant during the tracking period, we have

$$\boldsymbol{\theta}(\mathrm{t}+1) = \mathbf{I}_2\cdot\boldsymbol{\theta}(\mathrm{t}) = \boldsymbol{\theta} \tag{2.36}$$

Denoting the number of reflectors at t as N_t, the complete system state transition model of STAMP, analogous to the SLAM problem, is now given by

$$\begin{bmatrix}\mathbf{p}(\mathrm{t}+1)\\ \mathbf{v}(\mathrm{t}+1)\\ \boldsymbol{\theta}_1\\ \vdots\\ \boldsymbol{\theta}_{N_t}\end{bmatrix} = \begin{bmatrix}\mathbf{F} & 0 & \dots & 0\\ 0 & \mathbf{I}_2 & & \vdots\\ \vdots & & \ddots & 0\\ 0 & \dots & 0 & \mathbf{I}_2\end{bmatrix}\begin{bmatrix}\mathbf{p}(\mathrm{t})\\ \mathbf{v}(\mathrm{t})\\ \boldsymbol{\theta}_1\\ \vdots\\ \boldsymbol{\theta}_{N_t}\end{bmatrix} + \begin{bmatrix}\mathbf{G}\cdot\boldsymbol{\omega}(\mathrm{t})\\ \mathbf{0}\\ \vdots\\ \mathbf{0}\end{bmatrix} \tag{2.37}$$

The system error covariance matrix is given by

$$\mathbf{P}(t) = \begin{bmatrix} \boldsymbol{\Sigma}_t(t) & \boldsymbol{C}_{t1}(t) & \dots & \boldsymbol{C}_{tN_t}(t) \\ \boldsymbol{C}_{t1}^T(t) & \boldsymbol{\Gamma}_1(t) & \dots & \boldsymbol{C}_{1N_t}(t) \\ \vdots & \vdots & \ddots & \vdots \\ \boldsymbol{C}_{tN_t}^T(t) & \boldsymbol{C}_{1N_t}^T(t) & \dots & \boldsymbol{\Gamma}_{N_t}(t) \end{bmatrix} \tag{2.38}$$

The structure of STAMP system has some similarity to the SLAM set-up [23], where Dissanayake *et al.* provided convergence properties of SLAM for linear Gaussian system, so that the uncertainty of the time invariant multipath parameter **θ** estimate decreases monotonically as successive observations are obtained. In our problem, however, the challenge is to handle multipath propagation paths, which are not considered in modeling for SLAM.

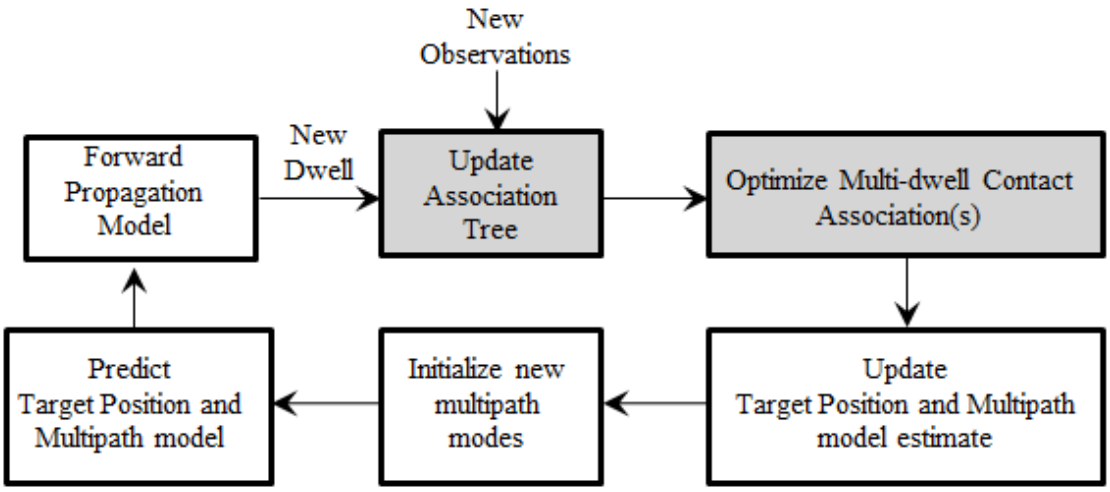

Figure 2.5: Block Diagram for STAMP Concept

2.3 The Simultaneous Target and Multipath Positioning (STAMP) Algorithm

The STAMP algorithm combines target tracking, data association, and multipath modeling within a recursive Bayesian estimation framework. An overview block diagram of STAMP is shown in Figure 2.5. Defining $Z_{1:t} = \{Z_1, \dots, Z_t\}$ and $X_{1:t} =$

$\{\mathbf{x}(1), \ldots, \mathbf{x}(t)\}$ as the set of measurements (e.g. scans or dwells) and STAMP states up to dwell t, and $H_{1:t}$ as a data association sequence for the total of t dwells, the STAMP algorithm maximizes the posterior probability $p(X_{1:t}, H_{1:t}|Z_{1:t})$ with respect to the state vectors and data associations, given the set of observations up to time t. In order to obtain computational tractable maximum a posteriori (MAP) estimates, STAMP decomposes the problem into two components: 1) data association to solve the unknown observation-to-mode correspondence, shown as gray blocks in Figure 2.5, and 2) a tracker to update the target position and multipath parameter estimates, shown as the white blocks in Figure 2.5. As new observations Z_t are obtained, a tree of hypothesized data associations $H_{1:t}$ is updated based on previous associations. The multi-dwell data association updates the cumulative joint-likelihood and finds the best association(s). Updating and prediction of target track and channel parameters $X_{1:t}$ are achieved by the extended Kalman filter (EKF), although alternative recursive Bayesian methods such as particle filters could be employed. In the following subsections, details of each STAMP component are presented.

2.3.1 Multi-Hypothesis Data Association

We utilize a multi-hypothesis algorithm where a sequence of detected observations is linked across multiple dwells in the presence of false alarms and the birth/death of multipath propagation modes. The multi-hypothesis algorithm is

essentially a multi-dwell batch algorithm employing a sequence of observations in contrast to conventional single-dwell methods (e.g., nearest neighbor association or probabilistic data association methods). Suppose at time *t*, the number of two-way propagation modes is $(N_t + 1)^2$, and define the observation set as $Z_t = \{\mathbf{z}_i(t)\}_{i=1}^{M_t}$ where M_t is the number of observations obtained. Let h_t represent the temporal data association hypothesis at time *t*, which can be interpreted as the association between the $(N_t + 1)^2$ modes and the M_t observations, e.g., *i*th observation originates from *j*th propagation mode. Let $H_{1:t}$: $\{h_1, h_2, \ldots h_t\}$ define a data association hypotheses sequence up to *t*. A hypothesis tree could then be constructed whose width (i.e. number of branches) expands exponentially with depth (i.e., time step *t*). Multi-hypothesis data association seeks to find the optimal hypothesis sequence by minimizing the negative logarithm joint likelihood function of the cumulative observation set $Z_{1:t}$ given cumulative target state $X_{1:t}$ as

$$\mathcal{H}_{1:t}^{*} = \underset{\mathcal{H}_{1:t}}{\operatorname{argmin}} - \ln \mathrm{p}(Z_{1:t}|H_{1:t}, X_{1:t}) \tag{2.39}$$

where $H_{1:t}^{*}$ is the most likely association hypothesis sequence. Since, in general, the computational complexity grows exponentially with the number of dwells, (2.39) is simplified by assuming:

$$\ln \mathrm{p}(Z_{1:t}|H_{1:t}, X_{1:t}) \cong \sum_{u=0}^{t} \ln \mathrm{p}(Z_u|\hat{\mathbf{x}}(u), H_{1:u}) \tag{2.40}$$

where $\mathrm{p}(Z_t|\hat{\mathbf{x}}(t), H_{1:t})$ is denoted as the transition likelihood at time *t*. The decomposition in (2.40) would be exact if the state sequence, $X_{1:t}$, were known exactly. The

approximation arises from the fact that a state sequence estimate, $\hat{\mathbf{x}}(t)$, is used which violates the strictly Markov model but facilitates computationally efficient optimization of (2.39) to be performed recursively at each time step.

The computation of transition likelihood $\mathrm{p}(Z_u|\hat{\mathbf{x}}(u), \mathcal{H}_{1:u})$ is solved as a 0-1 integer programming problem [43]. We assume that each measurement $\mathbf{z}_i(t), i = 1, \dots, M_t$, from Z_t can be 1) originated from one of the $(N_t + 1)^2$ existing propagation modes, 2) from a new propagation mode or 3) be a false alarm. In addition, some of the previously estimated propagation modes may not be detected or presented at the current dwell t. Therefore, we can define a binary assignment variable,$c_{i,j}(t) = \{0,1\}, i = 0,1, \dots, M_t, j = 0,1, \dots, (N_t + 1)^2$, based on a given association hypothesis h_t such that $c_{i,j}(t) = 1$ represents that ith observation corresponding to jth propagation mode, and $c_{i,j}(t) = 0$ otherwise. In particular, for $j > 0$, $c_{0,j} = 1$ implies that the jth propagation mode is not observed at time t, while for $i > 0$, $c_{i,0}(t)$ denotes ith observation originates from a false-alarm or a new propagation raymode. Under the assumption of the one-to-one correspondence between propagation modes and observations, each propagation mode can produce at most one observation and vice versa. Therefore, the following constraints can be derived for the binary assignment variable:

$$\sum_{i=0}^{M_t} c_{i,j}(t) = 1, \qquad j = 1,2 \dots, (N_t + 1)^2 \tag{2.41}$$

$$\sum_{j=0}^{N_t+1} c_{i,j}(t) = 1, \qquad i = 1,2, \dots, M_t \tag{2.42}$$

Assuming the unassociated measurements are uniformly distributed in a total

surveillance area V, the log transition likelihood, $\ln \mathrm{p}(Z_t, h_t|\hat{\mathbf{x}}(t), H_{1:t-1})$, can be then formulated as a two-dimensional assignment problem [31] as,

$$\ln \mathrm{p}(Z_t|\hat{\mathbf{x}}(t), H_{1:t}) = \sum_{i=0}^{M_t} \sum_{j=0}^{(N_t+1)^2} c_{i,j}(t) L_{i,j}(t) \tag{2.43}$$

with

$$L_{ij}(t) = \begin{cases} \ln\left(P_j(t) N\left(\mathbf{z}_i(t); \hat{\mathbf{z}}_j(t|t-1), \mathbf{S}_j(t|t-1)\right)\right), i,j > 0 \\ \ln\left(1 - P_j(t)\right), \quad i = 0 \\ -\ln V, \quad j = 0 \end{cases} \tag{2.44}$$

where $L_{ij}(t)$ is negative logarithm likelihood probability measuring the probabilistic correspondence between ith observation and jth mode, where $\hat{\mathbf{z}}_j(t|t-1)$ and $\mathbf{S}_j(t|t-1)$ denote the predicted measurement and innovation matrix. $L_{0j}(t)$ and $L_{i0}(t)$ represent the probabilities that raymode j is not presented at time t and observation i has no existing propagation mode to associate with respectively. Probability $P_j(t)$ denotes the probability that mode j can be observed at t.

The gating process described in [29] is utilized to reduce the increasing computational cost due to large M_t and N_t. At time t, observation $\boldsymbol{z}_i(t)$ is defined as a valid measurement for jth mode given hypothesis parent $H_{1:t-1}$, if it falls in the three dimensional validation region as,

$$\left[\boldsymbol{z}_i(t) - \hat{\boldsymbol{z}}_j(t|t-1)\right]^T \times \boldsymbol{S}_j(t|t-1)^{-1}\left[\boldsymbol{z}_i(t) - \hat{\boldsymbol{z}}_j(t|t-1)\right] \leq \gamma \tag{2.45}$$

where γ is Chi-squared distributed associated with the gate probability P_G, i.e., the probability that the validation region contains the true measurement. If an observation

falls outside the validation region, the log likelihood $L_{ij}(t)$ is assigned as $-\infty$, and all temporal hypotheses h_t with $c_{ij} = 1$ will be eliminated. Furthermore, we can also utilize physical constraints of the propagation model to eliminate impossible associations. For example, the TOA of the direct path must be shorter than any of the multipath TOAs, and the receiver and target must be on the same side of the planar reflectors.

Gating and mode validation can significantly reduce the number of child hypotheses h_t from each parent $H_{1:t-1}$. However, the total number of $H_{1:t}$ still grows exponentially as the hypothesis tree expands with depth. Further pruning in breath is thus required to facilitate real time processing in the presence of longer observation sequences. In this work, instead of brute-force computation of all hypothesis sequences, $H_{1:t}$, only the H-best hypothesis sequences are kept at each time t while others are pruned. This is performed by, 1) computing the H-best temporal hypothesis h_t from each hypothesis parent $H_{1:t-1}$, corresponding to the H largest values in (2.44) using dynamic programing or Murty's ranking algorithm [31, 35], and 2) selecting the H best $H_{1:t}$ sequences from the total H^2 candidates and prune the rest $H(H-1)$. This procedure ensures the number of hypothesis sequences remaining at each time step is made constant at each time which ensures the computational feasibility of this method.

2.3.2 Recursive Bayesian Estimation

Geolocation estimates may be obtained using the H-best raymode-to-data associations by employing a recursive Bayesian tracker to update the target position and

channel parameter estimates for all the H associations. In this work, for the sake of its computational efficiency, the EKF [40] is selected to deal with the nonlinear observation equations. A brief description of the tracking component of STAMP is given below

State Prediction: Let $\mathbf{P}(a|b) = E_{\mathbf{x}}[\big(\hat{\mathbf{x}}(a|b) - \mathbf{x}(a)\big) \times (\hat{\mathbf{x}}(a|b) - \mathbf{x}(a))^T]$ represent the error covariance matrix of the state estimate $\hat{\mathbf{x}}(a|b)$ for $a \geq b$. Given $\hat{\mathbf{x}}(t-1|t-1)$ and $\mathbf{P}(t-1|t-1)$, the state prediction step computes the means and covariance matrix of the Gaussian prior distribution of $\mathbf{x}(t)$ as

$$\hat{\mathbf{x}}(t|t-1) = \mathbf{F}\hat{\mathbf{x}}(t-1|t-1) \tag{2.46}$$

$$\mathbf{P}(t|t-1) = \mathbf{F}\mathbf{P}(t-1|t-1)\mathbf{F}^T + \mathbf{Q}(t) \tag{2.47}$$

Observation Prediction: Following state prediction, the observation from jth mode can be is predicted as:

$$\hat{\mathbf{z}}_j(t|t-1) = \mathbf{h}_j(\hat{\mathbf{x}}(t|t-1)) \tag{2.48}$$

The system innovation and its covariance matrix of a specific association h_t are then given by:

$$\mathbf{y}(t) = \bigoplus_{c_{i,j}(t)=1} \Big(\mathbf{z}_i(t) - \hat{\mathbf{z}}_j(t|t-1)\Big) \tag{2.49}$$

$$\mathbf{S}(t) = \mathbf{H}(t)\mathbf{P}(t|t-1)\mathbf{H}(t)^T + \mathbf{R}(t) \tag{2.50}$$

$$\mathbf{H}(t) = \bigoplus_{c_{i,j}(t)=1} \mathbf{H}_j(t), \ \mathbf{R}(t) = \underset{c_{i,j}(t)=1}{\text{DIAG}} \mathbf{R}_i(t) \tag{2.51}$$

where $\oplus$ and DIAG denote vertical and diagonal concatenation operations respectively when $c_{i,j}(t) = 1$, and $\mathbf{H}_j(t)$ is the linearized observation matrix for jth mode.

State Update: Given the prior and likelihood distribution of $\mathbf{x}(t)$ above, the posterior mean can be computed in terms of the state estimate and corresponding error covariance matrix as:

$$\hat{\mathbf{x}}(t|t) = \hat{\mathbf{x}}(t|t-1) + \mathbf{K}(t)\mathbf{y}(t) \tag{2.52}$$

$$\mathbf{P}(t|t) = \mathbf{P}(t|t-1) - \mathbf{K}(t)\mathbf{H}(t)\mathbf{P}(t|t-1) \tag{2.53}$$

where the Kalman gain matrix $\mathbf{K}(t)$ is given by

$$\mathbf{K}(t) = \mathbf{P}(t|t-1)\mathbf{H}(t)^T\mathbf{S}(t)^T \tag{2.54}$$

The above recursion estimation algorithm requires initialization of the multipath parameters and target position, which must be addressed in practice. For multipath channels in particular, the total number of ray modes is often unknown. This necessitates an approach for new reflector or scatterer initiation and validation. Furthermore, the track initialization of target position is also a well-known challenge due to the uncertainty and difficulty of LOS ray mode identification. If the LOS path observation is present, the target position can be directly initialized from the LOS observation. If the LOS path is absent, however, the target position and multipath parameters are jointly initialized until STAMP identifiability requirements (as discussed in the sequel) are achieved, or until the first LOS observation appears. Typically it is not known a priori whether the LOS path is present, nor which observation corresponds to the LOS path. To address this issue, multiple hypotheses of the initial target position are utilized at the first dwell $t = 1$. As successive measurements are obtained, incorrect

initial hypotheses are eliminated using the proposed multi-hypothesis data association. At time t, all unassociated observations are viewed as newly observed propagation ray modes. A validation process is performed in the next few time dwells, so that the newly initiated ray modes with low recurrence frequencies are also be eliminated. An visual example of the pruning scheme is described in Figure 2.6 for $H = 3$.

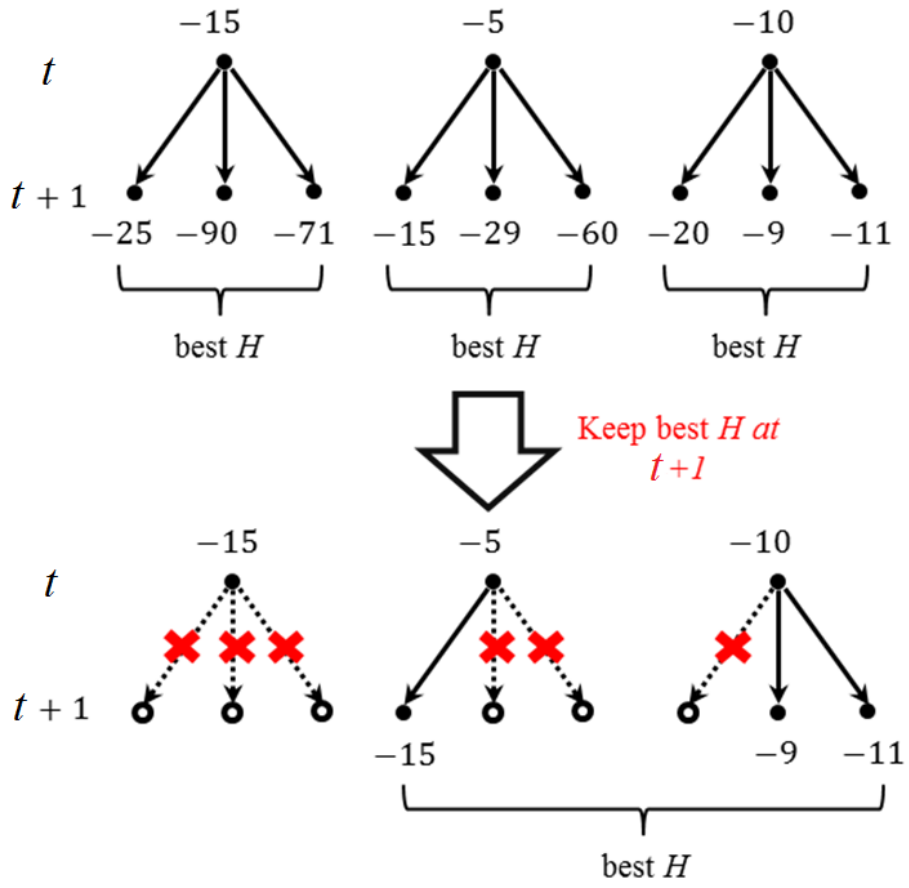

Figure 2.6. Example of the proposed pruning scheme for $H = 3$. Firstly project H-best hypothesis child h_t from parents, then keep the H best $\mathcal{H}^t$ sequence and prune the rest $H(H-1)$ sequences

2.3.3. Track and New Reflector Initiation

We consider a multi-hypothesis track initiation of STAMP with minimum track latency. Given an initial guess of the x-y coordinate for target position with large uncertainty, we uniformly select a number of initial guesses of the target location $\widehat{\mathbf{p}}(1)$ from the x-y space, and each location refers as an individual hypothesis h_1. It is also possible that the direct path observation is included in the first set of observations Z_1, hence, each of the observations $z_i(t)$ can be assumed as direct-path, so that $\widehat{\mathbf{p}}(1)$ and its error covariance matrix $\mathbf{P_p}(1)$ are given by

$$\widehat{\mathbf{p}}(1) = \begin{bmatrix} \rho_i(1) \cdot \zeta_i(1) \\ \rho_i(1) \cdot \sqrt{1 - \zeta_i^2(1)} \end{bmatrix} \tag{2.55}$$

$$\mathbf{P_p}(1) = \mathbf{G}_i(1)\mathbf{R}_i\mathbf{G}_i^T(1) \tag{2.56}$$

with

$$\mathbf{G}_i = \begin{bmatrix} \rho_i(1) & \zeta_i(1) \\ \left(1 - \zeta_i^2(1)\right)^{1/2} & -\rho_i(1)\zeta_i(1)\left(1 - \zeta_i^2(1)\right)^{-1/2} \end{bmatrix} \tag{2.57}$$

Based on each of the initial guess, reflectors also can be initiated from Z_1. Since the BNI guarantees unique solution of target position, as successive observations are obtained and processed, false initiation hypothesis will be eliminated.

Given a hypothesis sequence, all unassociated observations $\mathbf{z}_i(t)$ are considered as a new reflector as

$$\widehat{\boldsymbol{\theta}}_i(t) = \mathbf{h}_i^{-1}(\widehat{\mathbf{p}}(t), \mathbf{z}_i(t)) \tag{2.58}$$

$$\mathbf{P}_{\boldsymbol{\theta}_i}(t) = \begin{bmatrix} \nabla_{\mathbf{z}} \mathbf{h}_i^{-1} \big|^T_{(\hat{\mathbf{p}}(t), \mathbf{z}_i(t))} \\ \nabla_{\mathbf{p}} \mathbf{h}_i^{-1} \big|^T_{(\hat{\mathbf{p}}(t), \mathbf{z}_i(t))} \end{bmatrix}^T \begin{bmatrix} \mathbf{R}_i & 0 \\ 0 & \mathbf{P}_{\mathbf{p}}(t) \end{bmatrix} \begin{bmatrix} \nabla_{\mathbf{z}} \mathbf{h}_i^{-1} \big|^T_{(\hat{\mathbf{p}}(t), \mathbf{z}_i(t))} \\ \nabla_{\mathbf{p}} \mathbf{h}_i^{-1} \big|^T_{(\hat{\mathbf{p}}(t), \mathbf{z}_i(t))} \end{bmatrix} \tag{2.59}$$

where $\mathbf{h}_i^{-1}(\hat{\mathbf{p}}(t), \mathbf{z}_i(t))$ is the inverse observation function to initialize parameter vector $\boldsymbol{\theta}$ given target position estimate $\hat{\mathbf{p}}(t)$ and observation $\mathbf{z}_i(t)$. A newly initiated reflector will be denoted as a valid reflector if it appears T times in the next T+T' dwells, and otherwise deleted. In addition, since it is also difficult to distinguish the types of reflector for a single time dwell, we can then initialize all types of reflectors on a single hypothesis, and eliminate the false initiation guess during the validation step.

2.4. Experimental Evaluation

This section describes the results of applying STAMP to real data from an experiment conducted on the first floor atrium of an engineering building at Duke University. An indoor S-band radar testbed was used [41, 42] to track the bistatic transmitter with a linear frequency modulated waveform sweeping from 2.1 to 2.7 GHz shown in Figure 2.7 (a). The 600 MHz swept bandwidth of the system provides approximately 0.5 meter range resolution. The receiver array contains 16 array elements and both transmit and receive antennas were omnidirectional. Figure 2.7 (b) provides views of the experiment environment with red line as the measured trajectory of the transmitter that was used as the target in this experiment. No information about the building floor plan was used by the geolocation algorithm.

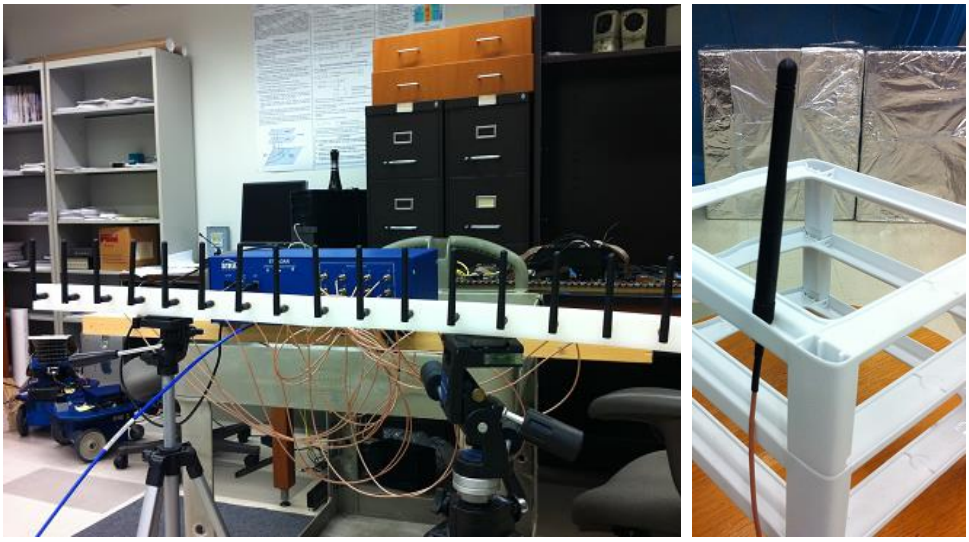

(a)

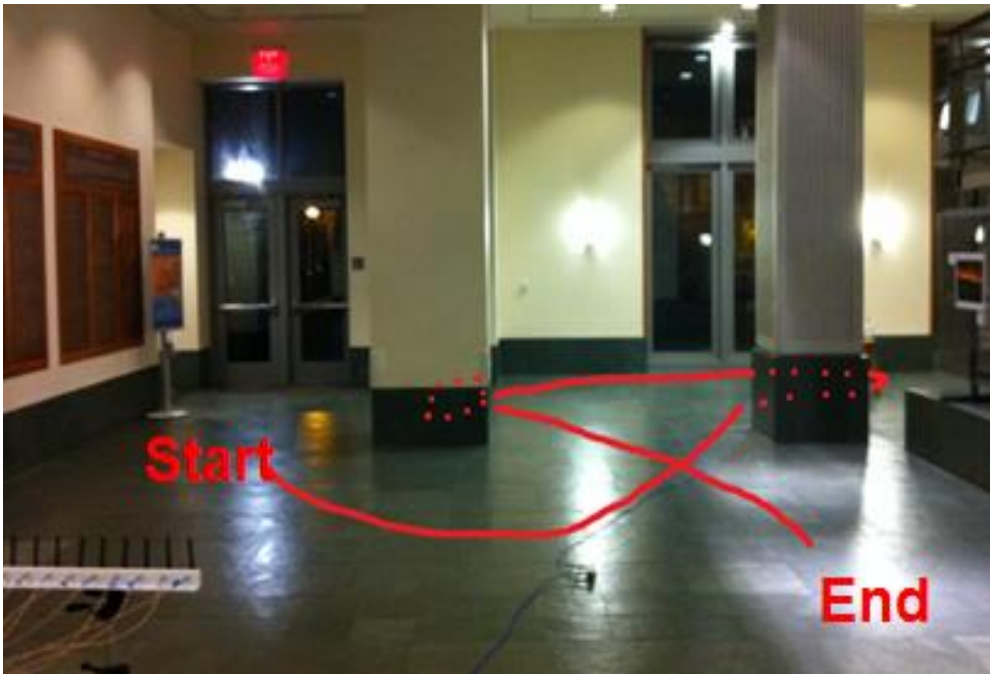

(b)

Figure 2.7: (a) The radar testbed utilized for the experiment: the receiver array and (b) Illustration of the experimental environment with red line as the target path

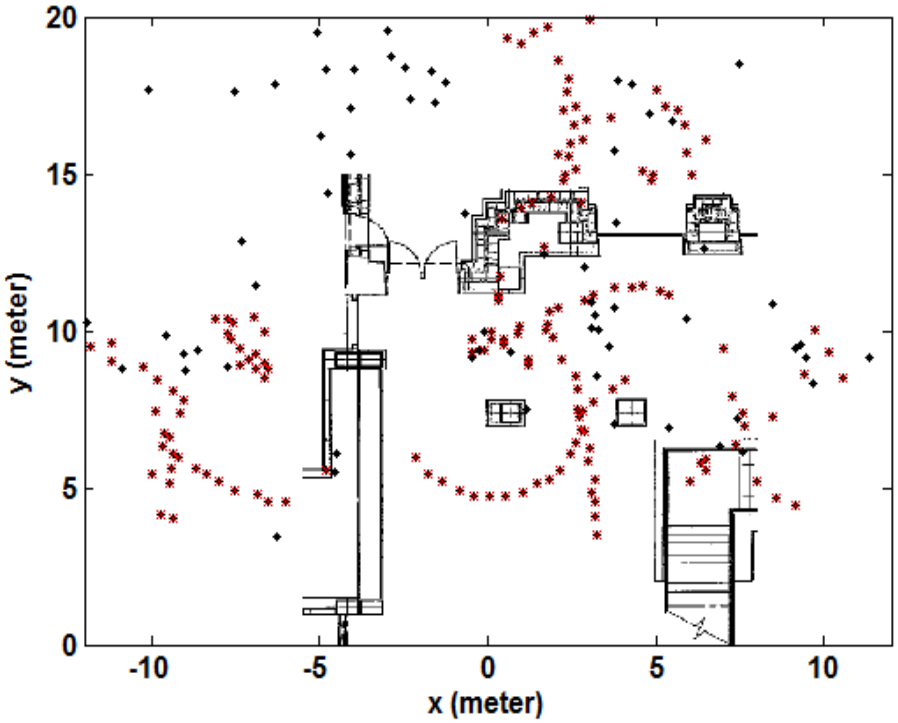

Figure 2.8: All observations in Cartesian coordinates. Red asterisks refer to the target oriented measurements

We implemented the multi-hypothesis tracking algorithm with the number of hypothesis per dwell as $H = 100$. All detected TOA/AOA observations, transformed into Cartesian coordinates as if they were LOS observations, are shown in Figure 2.8, where target-observations are marked as red dots as obtained by employing our multi-hypothesis data association algorithm. The estimated target path and reflector positions are shown in Figure 2.9, with the measured path ground truth (black solid line) and the actual floor plan. The NLOS areas are given in the gray regions due to the blockage of two large reinforced concrete pillars. Although both plane reflectors and point scatters are considered, the data association output suggests that mainly specular reflectors are

useful for geolocation in this environment. The red solid lines refer to the position of the five estimated plane reflectors as being numbered from 1 to 5, all of which correspond to real planar wall locations as indicated on the floor plan.

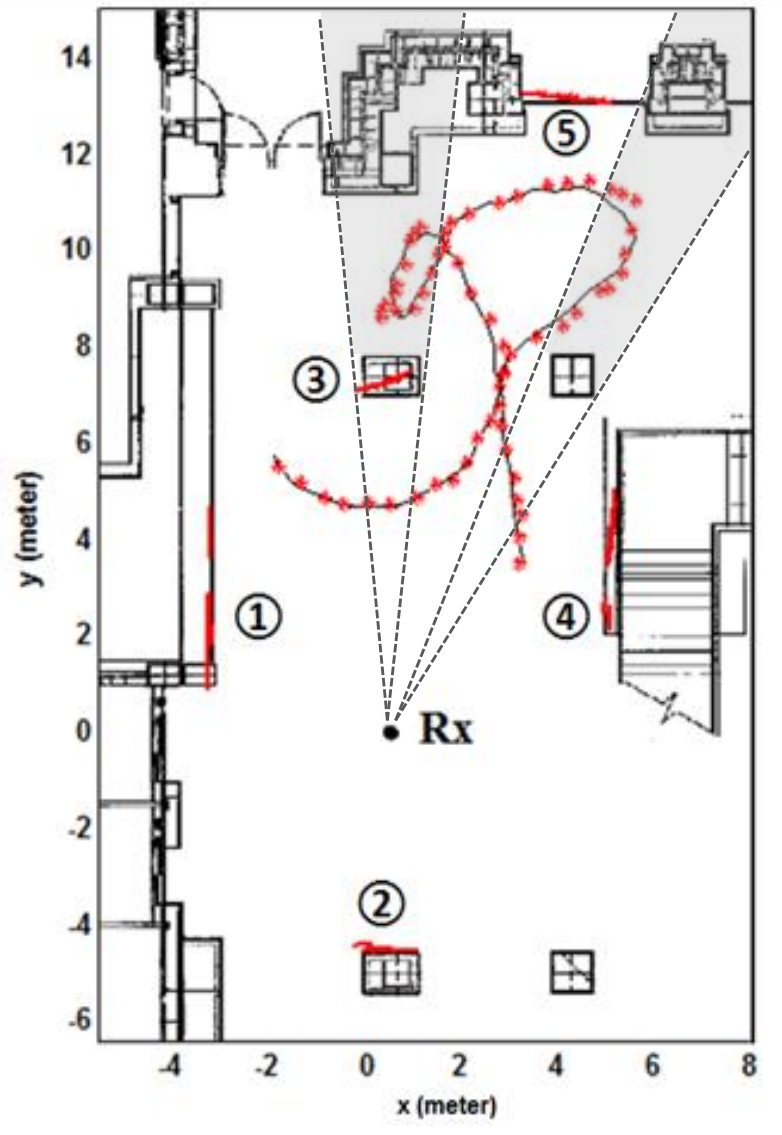

Figure 2.9: Estimation result for the proposed STAMP: red lines refer to estimated reflectors; the black solid line represents the path ground truth and red asterisks refer to target position estimates. The gray areas refer to the NLOS regions

The difference between the target position estimates and the ground truth versus time is plotted in Figure 2.10. Assuming the measured ground truth has RMS error of 0.1 m in both x and y directions, the 95% (2σ) confidence intervals of the estimate error (computed from the EKF posterior error covariance matrix), incorporating the ground truth uncertainties, are also illustrated in this figure as dashed lines. Note that when the target is in a NLOS region (i.e., time dwells 18-25 and 35-51 marked in gray), the positioning errors are larger compared to the LOS regions. However, using the multipath observations with estimated multipath parameters, STAMP is able to maintain the target localization errors to within ±1.5 m. For comparison, target localization errors using LOS observations only are shown in Figure 2.11 with 95% error bounds. The data association is solved using the same multi-hypothesis STAMP algorithm, but only LOS observations are utilized for localization. In this case, observe that the estimation error in the LOS region approximates that of STAMP. However, since no observation is present in the NLOS regions, the location error and bounds diverge rapidly with time compared the STAMP results in Fig. 11 (i.e., over ±5 m in both x and y directions). Overall, these results suggest that the STAMP algorithm is able to perform indoor geolocation in a real environment by exploiting both LOS and NLOS observations.

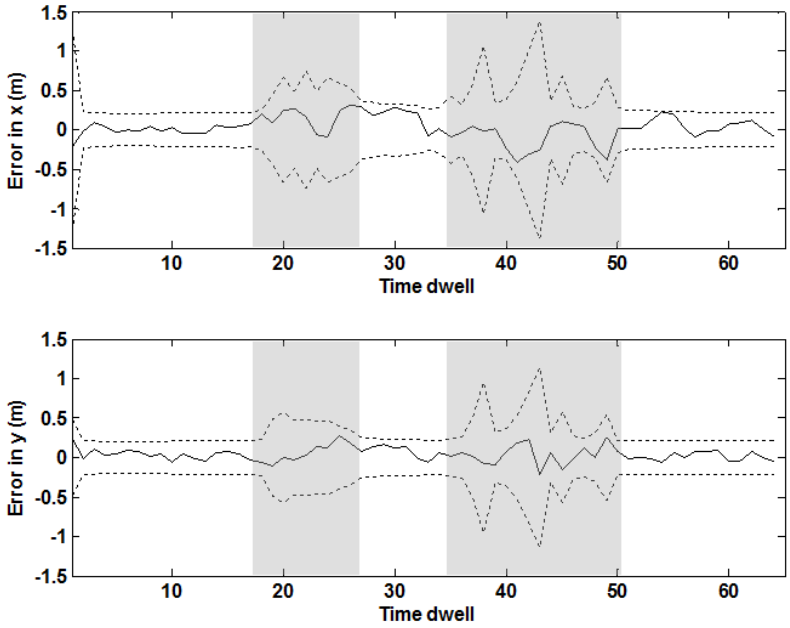

Figure 2.10: Target location estimate error via STAMP in x and y (solid line), with 95% confidence bounds (dotted lines). The reduction in the estimated location accuracy during the intervals 18 to 25 and 35 to 50 is due to NLOS propagation (gray area).

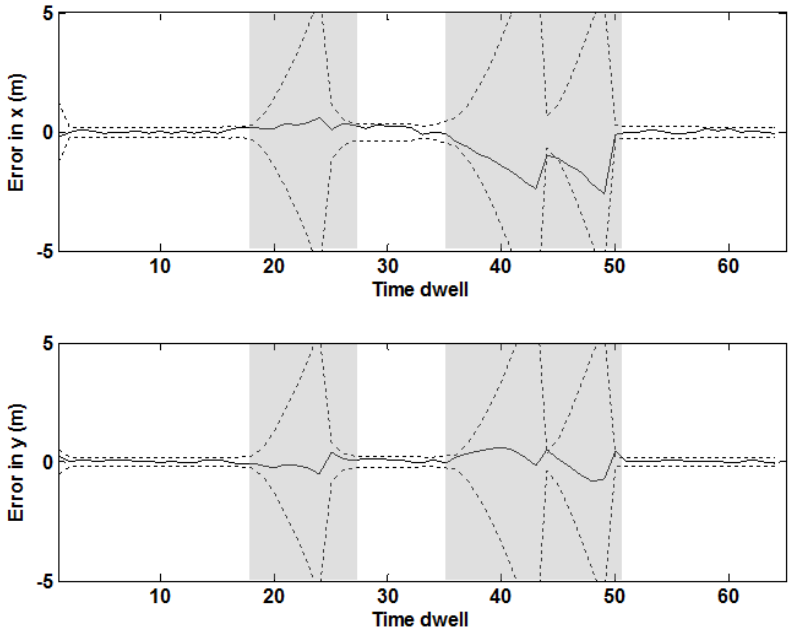

Figure 2.11: Target location estimate error based on direct path observations only in x and y (solid line), with 95% confidence bounds (dotted lines).

In addition to target geolocation, Figure 2.12 and 2.13 illustrate errors between the estimated multipath parameters for planar reflectors, ψ and ρ, and the measured ground truth for reflector 1 and 5 respectively. Reflector 1 appears at the first dwell and reflector 5 appears at dwell 20. The 95% confidence intervals of error bounds are also shown as dashed lines representing the uncertainty of the estimate error. Since the reflectors are assumed to be time-invariant, the error bounds decrease monotonically as successive observations obtained.

2.5. Summary

In this chapter, joint target and multipath position estimation has been presented for single-station hybrid TOA/AOA target tracking in complex terrain. A recursive Bayesian algorithm, including multi-scan multi-hypothesis data association, has been presented for estimating target position without detailed knowledge of multipath channel parameters. The approach has been evaluated via a real data experiment using an indoor S-band bi-static radar testbed. The experimental results demonstrate that accurate target localization is possible even when line-of-sight propagation is absent over a significant fraction of the observation interval. The identifiability of both target position and multipath parameters was analyzed by studying the singularity of the Fisher information matrix associated with source location and channel parameter estimates for the one-way cooperative source scenario.

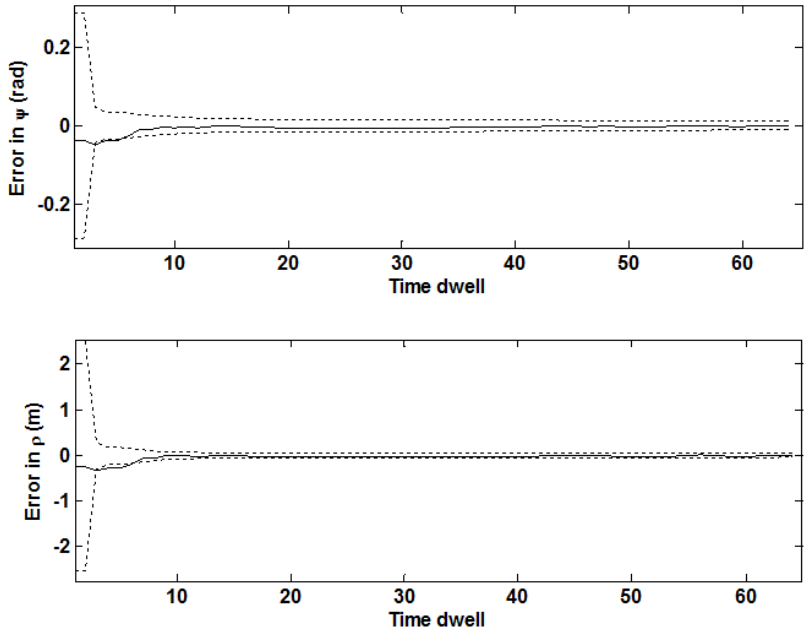

Fig. 2.12: Multipath parameters estimate error for reflector 1 with 95% confidence bounds (dotted lines).

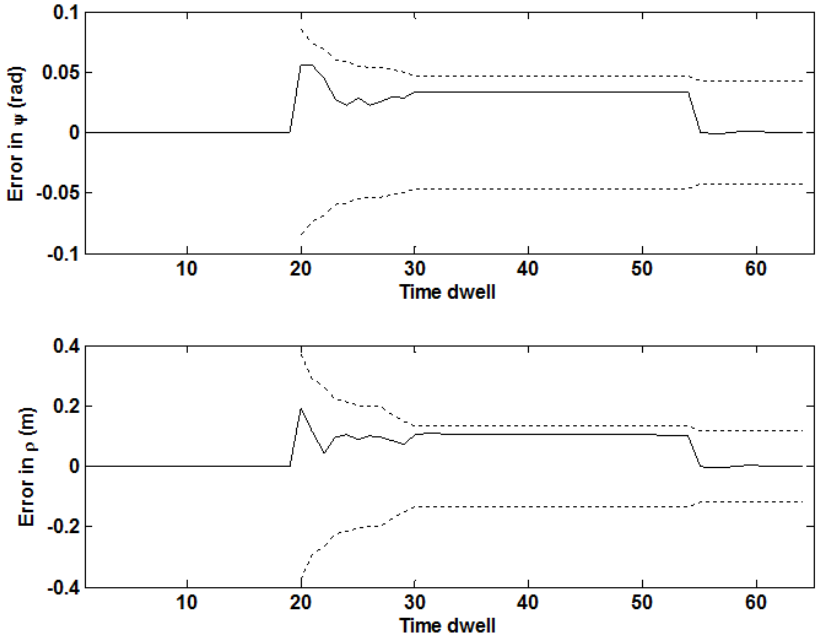

Figure 2.13: Multipath parameters estimate error for reflector 5 with 95% confidence bounds (dotted lines).

3

STAMP for Mono-static MIMO Radar

In this Chapter, STAMP is formulated for target tracking based on a collocated two-way MIMO radar system. According to Chapter 2, multipath propagation measurements are modeled based on specular reflections produced by flat plane reflectors and non-specular returns from point scatters. The utilization of MIMO processing provides the extra degree of transmit diversity which permits angle of departure (AOD) measurements. This provides additional geometrical information that can be used to resolve the uncertain propagation model. The multi-hypothesis data association can be directly applied to the new observation system and an illustrative simulation is presented in the later section.

3.1 Two-Way MIMO Radar Observation Model

Suppose a monostatic MIMO radar system, locating at known position $(x^{(r)}, y^{(r)})$, transmits and receives RF radar echoes with time of arrival (TOA), angle of arrival (AOA) and angle of departure (AOD) observations. The target is assumed to be

essentially non-manoeuvring and the multipath channels are modeled with stationary geometric features as flat plane reflectors and point scatters according to Chapter 2.

The MIMO radar is able to produce a 3 x 1 observation vector $\boldsymbol{z}_t$ with TOA, AOA and AOD measurements for a two-way radar echo consisting of different transmit and receive paths. Denoting the number of reflector as N_t, the total number of possible two-way propagation modes received by radar is $(1 + N_t)^2$ including the direct path. In the absolute NLOS situation (i.e., neither transmit nor receive path is direct path), an echo includes two one-way indirect paths from the same or two different reflectors as illustrated in Figure 3.1. The nonlinear observation function is then given by

$$\boldsymbol{h}(\mathbf{p}_t, \boldsymbol{\theta}_{tx}, \boldsymbol{\theta}_{rx}) = \begin{bmatrix} \sum_{i=tx,rx} \sqrt{x_i'(t)^2 + y_i'(t)^2} \\ x_{rx}'(t) / \sum_{i=tx,rx} \sqrt{x_i'(t)^2 + y_i'(t)^2} \\ x_{tx}'(t) / \sum_{i=tx,rx} \sqrt{x_i'(t)^2 + y_i'(t)^2} \end{bmatrix} \tag{3.1}$$

where $x_i'(t)$ and $y_i'(t)$ are referred (2.30) to (2.33). The observation noise term is modeled as zero-mean Gaussian based on the Cramer-Rao Lower Bound model with covariance matrix

$$\mathbf{R} = SNR^{-1} \begin{bmatrix} c^2 BW^{-2} & 0 & 0 \\ 0 & 4N_{rx}^{-2} & 0 \\ 0 & 0 & 4N_{tx}^{-2} \end{bmatrix} \tag{3.2}$$

where SNR refers to the signal to noise ratio at radar receiver, c and BW denote speed of light and signal bandwidth respectively and N_{tx}/ N_{rx} represent the numbers of Tx/Rx elements.

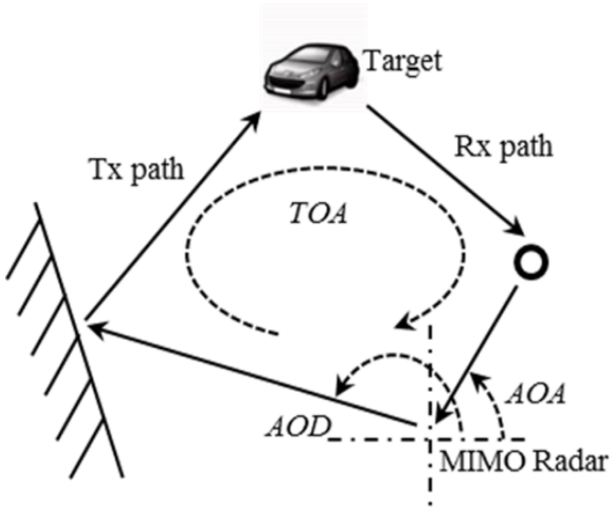

Figure 3.1: Illustration of the two way propagation Radar case.

3.2 Simulation Evaluation

Consider a target tracking problem in an uncertain urban environment shown in Figure 3.2. A MIMO radar is located at the origin with $N_t = N_r = 8$ and $BW = 600MHz$. The environment is constructed with 3 plane reflectors and 2 point reflectors. The point target starts from the LOS region in the upper- right corner of the figure, moves along the red trajectory to enter the NLOS area where the direct path is unobservable due to the obstructions (grey area in Figure 3.2), and eventually returns to LOS area. The total number of radar observation dwells is 120. Target detectability is considered as a realistic case that the probability of detection varies with positions. Assuming a Swerling 1 model [35] for the target SNR fluctuation, we have

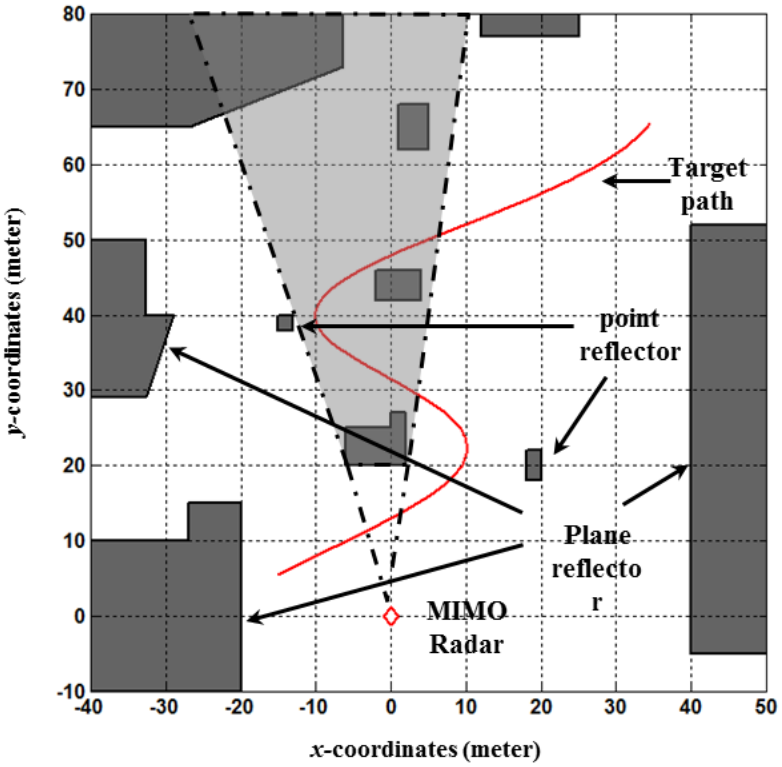

Figure 3.2: Illustration of the simulated scenario

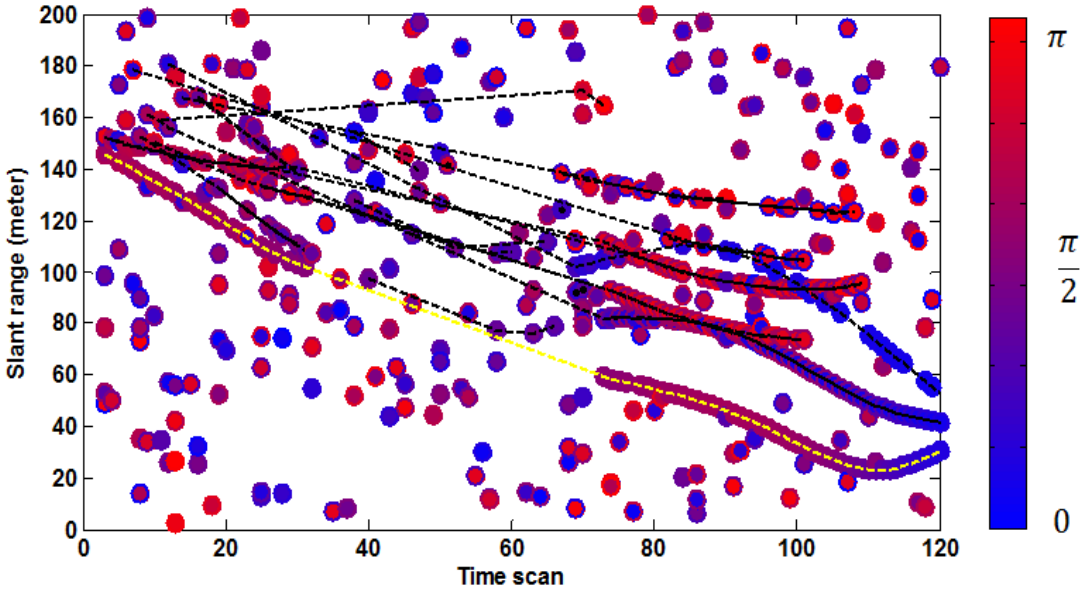

Figure 3.3: Observations bubble plots for $SNR_0 = 10\,dB$: the inner face color represents AOA, outer ring color as AOD; yellow line denotes the direct path and black lines as multipath observations

$$P_d = P_{fa}^{1/(1+SNR)} \tag{6.3}$$

where

$$SNR = (r_0/r)^4 SNR_0 \times RL \tag{6.4}$$

r denotes the two way propagating distance, and r_0 and SNR_0 refer to initial target slat range and SNR in LOS situation. RL represents SNR loss due to reflections; in particular, we assume specular reflections produce -4 dB loss per bounce and -8 dB for point reflectors. The total number of reflectors is assumed to be known a priori (i.e., $N_t \equiv 5$) and the multipath parameters are assumed to be initialized with large uncertainties. In the simulation SNR_0 is assumed to be known, however, the detection probability and measurement noise is estimated from state vectors while the true state noise covariance matrix $\mathbf{Q}$ of the target is known exactly. A constant false alarm rate detector is utilized with $P_{fa} = 0.001$.

To illustrate the concept of the STAMP algorithm, the data association is assumed be known exactly for the first few tests. Figure 3.3 illustrates all observations in the detection space for a single realization for $SNR_0 = 10\ dB$. Each bubble in the graph represents a single observation: the inner face color represents the AOA, the outer ring color denotes the AOD and the y coordinate as the slant range (TOA). The yellow line marks the direct path which is intermittent from $t = 33$ to $t = 71$. The black lines denote the multipath observations and the remaining bubbles are false alarms. One can observe

that when the target approaches to the radar, the detection performance is highly improved compared with the earlier stages. Since the certain multipath observations are still present inside the NLOS region, information of target positions can be extracted from multipath returns.

The convergence and consistence properties of STAMP estimates are shown in

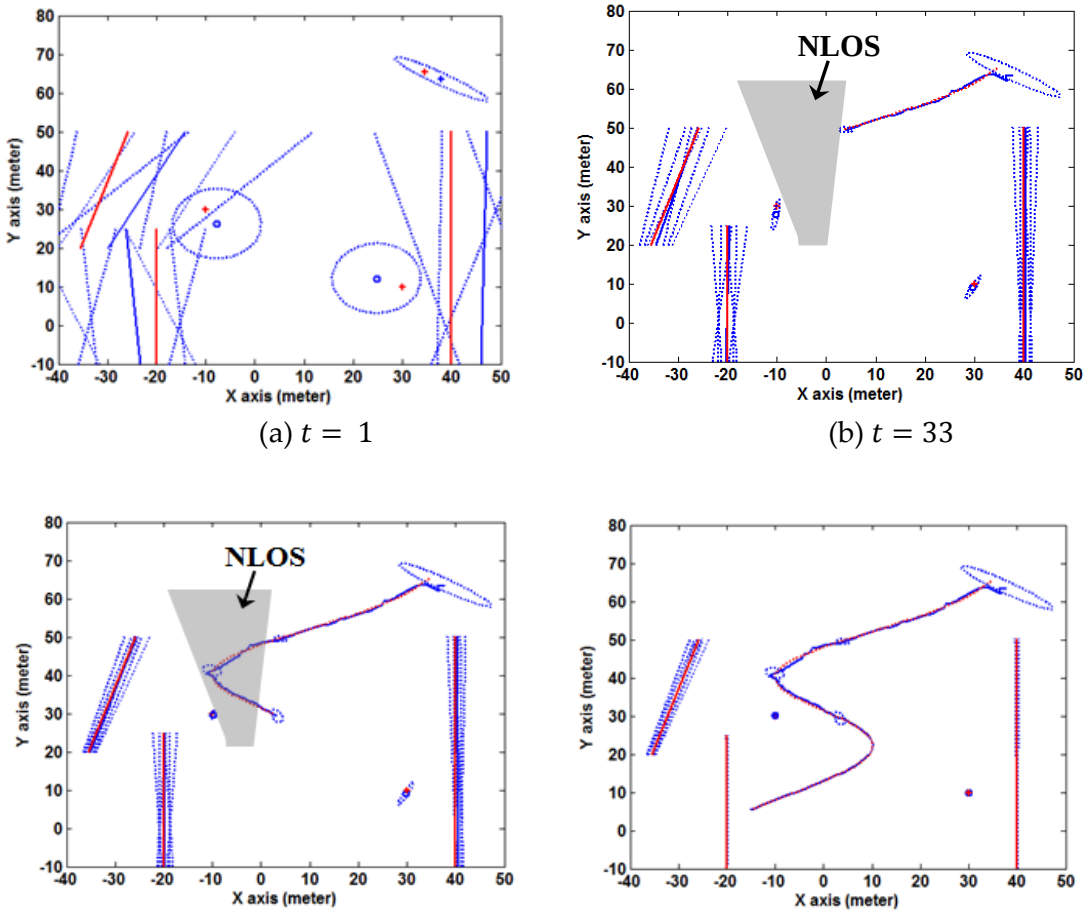

(a) $t = 1$ (b) $t = 33$

(c) $t = 71$ (d) $t = 120$

Figure 3.4: Convergence and Consistency properties for the STAMP algorithm at 4 time instance: (a) track is initialized; (b) target enters the NLOS region; (c) target reenters LOS region and (d) track is terminated

Figure 3.4 with four different time instances also for $SNR_0 = 10\,dB$. The red solid lines denote the ground truth of the target trajectory and the reflector positions. The blue solid lines are the estimates with the dashed lines as the 2σ confident boundaries (for plane reflector, the correlation between ψ and ρ are ignored for visible simplicity). Figure 3.4 (a) illustrates the initial condition for each estimate, exhibiting large biases and uncertainties. At $t = 33$, Figure 3.4 (b), the target enters the NLOS region, and at this moment, the target position and reflector estimates approach the ground truth and the error variance reduced dramatically. Figure 3.4 (c) shows the instance when the target return to the LOS region at $t = 71$. During the NLOS interval, the estimate error of target position increases with the error covariance ellipse increases compared with Figure 3.4 (b). The estimate error covariance matrices of the reflectors still decrease monotonically since they are stationary. For $t > 71$, when the direct path is observable again, the target position estimate error significantly reduces compared with the NLOS period visually, and all estimates converge to the ground truth when the track is terminated.

To evaluate the effectiveness of the data association algorithm, Monte Carlo simulations are utilized to compare it with the perfect data association case as the performance bound and some alternatives as local nearest neighbour (LNN) and joint nearest neighbour (JNN) data associations which are both single scan hard decision association schemes. LNN is the simplest association method which computes the

distance between each propagation mode and observation pair in the scene and associates the closest pairs independently. JNN is generally a modified version of LNN which estimates the most likely temporal association hypothesis at each time step. In other words, JNN is a special case for the proposed semi-batched algorithm with $H = 1$. The parameters assumed for the simulation are $P_G = 0.99$ with $\gamma = 11.3$ and the mode presence transition probability α and β are assumed to be both 0.9 for all modes. For the proposed method, The number of hypotheses kept for each time step H is selected to be 20. Figure 3.5 illustrates the off-track rate (i.e., percentage of the number of realizations whose instantaneous target position estimation error is greater 3 meter at any time instance) as a function of SNR_0 for 100 independent runs. At $SNR_0 = 10\ dB$, due to the low detectability even perfect data association produces a 40% off-track rate and no data association method provides satisfactory results. When SNR_0 increases to $15\ dB$, the proposed multi-hypothesis algorithm only produces a 10% off-track rate while the JNN and LNN are both greater than 50%. The proposed method approaches to 0% off-track rate at $SNR_0 = 20\ dB$ which is approximately 10 dB leading the other two.

The second metric utilized to quantify the data association accuracy, as in Figure 3.6, is the cumulative probability distribution function (CDF) of the cumulative joint negative log likelihood function which is minimized over the 100 runs. We assume SNR_0 as $15\ dB$, and the perfect data association is marked as the red curve as an upper bound of performance. Compared to the JNN method, the proposed multi-hypothesis

algorithm is much closer to the upper bound. The "step jump", which appears when CDF is greater than 0.8, is due to missing reflectors (i.e., one or more reflectors are missed associating during the whole tracking process, even though the target and other reflectors can be simultaneously estimated, the resulting likelihood is far off the upper bound).

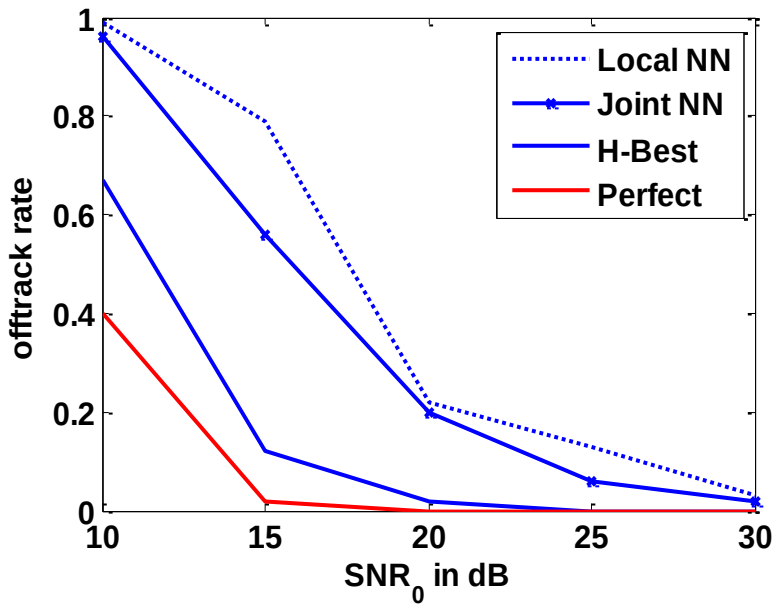

Figure 3.5*:* Data association off-track rate test as a function of SNR_0

3.3 Summary

This paper has presented the MIMO radar application of STAMP for the problem of jointly estimating target positions and geometric based multipath channels for flat planes reflectors and point-like scatters. The data association uncertainty in presence of imperfect detections was solved via a computational feasible multi-

hypothesis association algorithm. An illustrative simulation of a single target tracking problem in a dense multipath urban environment was presented which demonstrates that both multipath parameters and target positions can be jointly estimated even when the direct path propagation is not always present.

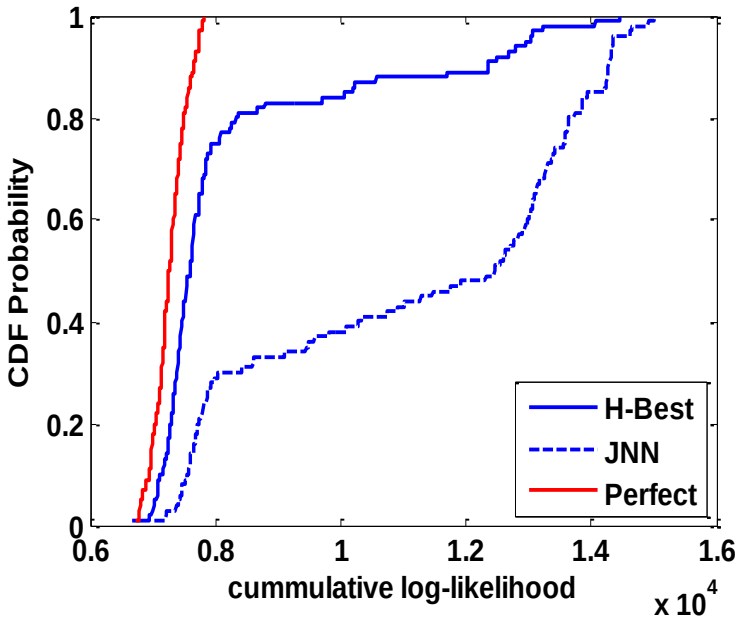

Figure 3.6*:* **CDF of cumulative negative log-likelihood for $SNR_0 = 15\ dB$**

4

Multi-static AOA STAMP

This chapter considers the problem of range-based self-localization of a mobile station (MS) using multi-static base station (BS) signal beacons in dense multipath environments with low Line-Of-Sight availability. The multipath propagation is modeled as single-bounce reflections from a set of unknown random scatters. STAMP problem is formulated by jointly estimating the MS state and the uncertain scatter multipath parameters. Since the number of multipath channels is unknown and time varying, a single cluster process is formulated using a recursive Bayesian estimation framework: the MS state and the MS-BS clock difference are together defined as a parent process and the scatter state is defined as the daughter process, which can be implemented based on particle/Gaussian mixture filtering. The Cramer-Rao Lower Bound (CRLB) is derived for the STAMP method and analyzed to establish the identifiability of this joint estimation problem. The CRLB is also extended to the case of

data association uncertainty in term of the Fisher Information Reduction Matrix, analogous to the problem of multi-sensor/multi-target tracking in clutter [62, 63]. Simulation and experimental results using real data for an indoor target positioning problem demonstrates substantial improvements in localization accuracy with the proposed method.

4.1 Problem Formulation

In this work, a mobile station (MS, aka, the target of interest) is considered in a two-dimensional space, and the target state vector is defined by $\mathbf{p}_k = [x_k, y_k, \dot{x}_k, \dot{y}_k]^T$ including the target *x*-*y* ground coordinates and vector velocities at discrete time k. Assuming a linear constant velocity target dynamics with white Gaussian process noise, the Markov probability density function of a state transition is given as

$$f(\mathbf{p}_{k+1}|\mathbf{p}_k) = \mathcal{N}(\mathbf{p}_{k+1}; \mathbf{F}\mathbf{p}_k, \mathbf{D}\mathbf{Q}_k\mathbf{D}^T) \tag{4.1}$$

where $\mathcal{N}(.; \mathbf{m}, \mathbf{P})$ denotes a Gaussian density function with mean vector $\mathbf{m}$ and covariance matrix $\mathbf{P}$. For a non-maneuvering target, the state transition function is defined:

$$\mathbf{F} = \begin{bmatrix} \mathbf{I}_2 & \Delta t \cdot \mathbf{I}_2 \\ \mathbf{0} & \mathbf{I}_2 \end{bmatrix}, \quad \mathbf{D} = \begin{bmatrix} {\Delta t^2}/{2} \cdot \mathbf{I}_2 \\ \Delta t \cdot \mathbf{I}_2 \end{bmatrix} \tag{4.2}$$

and $\mathbf{Q}_k$ is the 2 × 2 covariance matrix representing random target accelerations, $\mathbf{I}_N$ denotes a $N \times N$ identity matrix, and Δt is the temporal sampling interval.

The multi-static localization system is constituted with S base stations (BS), with

an overlapping coverage, whose x-y ground coordinates are defined by a 2×1 vector $\mathbf{r}_i$, $i = 1,\ldots,N$. Assuming the transmitting waveform is known exactly, all nodes are able to produce a set of range observations through the match filtering process. Additional to the LOS propagation, multipath propagations are also considered. In this work, we consider a number of random scatters located in the area of interest, and the scatter x-y coordinates are defined by a 2×1 vector $\mathbf{s}_j$, $j = 1,\ldots,S_k$, where S_k refers to the number of scatters at time k. Since all scatters are assumed to be static, $\mathbf{s}_j$ is time invariant and independent of the time index k. The geolocation scenario is illustrated in Figure 3.1.

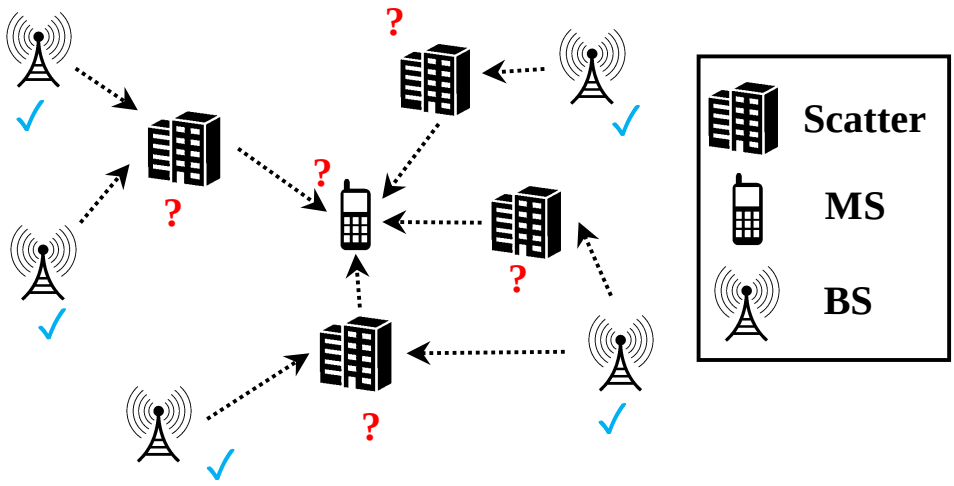

Figure 4.1: Illustration of the Mobile Station (MS) geolocation problem in a dense multipath environment, where MS locations and Scatter locations are both uncertain

We also assume that all BS's share the same oscillator clock time, however, the MS and the BS network are asynchronized. Let b_k refer to a time varying unknown range offset between the MS and BS network, and the MS localization formulation is

then equivalent to a TDOA case. In real world RF geolocation system, the bias b_k is time varying due to the effect of clock drifts. Therefore, we model the fluctuation of b_k as a random walk process, i.e.,

$$f(b_k|b_{k-1}) = \mathcal{N}(b_k; b_{k-1}, \sigma_b^2) \tag{4.3}$$

Since at each time *k*, only one MS or target is presented, we define the MS state and the range offset as a single system random vector:

$$\mathbf{x}_k = [\mathbf{p}_k^T, b_k]^T \in \mathbb{R}^5 \tag{4.4}$$

Based on the above assumptions, the LOS Gaussian observation noise model of *i*th BS at time *k* is given by:

$$\pi_i^0(z|\mathbf{x}_k) = \mathcal{N}(z; g_i^0(\mathbf{x}_k), \sigma_i^2) \tag{4.5}$$

with

$$g_i^0(\mathbf{x}_k) = \left\|\mathbf{p}_k - \mathbf{r}_j\right\| + b_k \tag{4.6}$$

While for multipath measurement, the observation noise model is given by

$$\pi_i(z|\mathbf{x}_k, \mathbf{s}) = \mathcal{N}(z; g_i(\mathbf{x}_k, \mathbf{s}), \sigma_i^2) \tag{4.7}$$

with

$$g_i(\mathbf{x}_k, \mathbf{s}) = \|\mathbf{p}_k - \mathbf{s}\| + \left\|\mathbf{s} - \mathbf{r}_j\right\| + b_k \tag{4.8}$$

where the model $g_i^0(\mathbf{x}_k)$ and $g_i(\mathbf{x}_k, \mathbf{s})$ denote nonlinear observation models for LOS path and multipath propagation respectively, and the operator $\|\mathbf{a}\|$ defines the euclidean norm of vector **a**.

For MS localization in an uncertain multipath environment, the number of scatters (i.e., number of multipath propagation modes) S_k is a time-varying random unknown variable. Therefore, the scatter, or multipath channel state can be modeled as a random finite set (RFS) on $\mathcal{S} \in \mathbb{R}^2$.

$$\mathbf{S}_k = \{\mathbf{s}_1, \dots, \mathbf{s}_{N_k}\} \in \mathcal{F}(\mathcal{S}) \tag{4.9}$$

where $\mathcal{F}(\mathcal{S})$ denotes collections of all finite subsets of $\mathcal{S}$ [45]. An RFS is a finite-set-valued random variable, whose cardinality is characterizes by a discrete probability distribution, and each element of a RFS is followed by a family of joint probability densities for a given cardinality. Similarly, in the presence of imperfect detection, the observation set at time *k* is also modeled as a RFS on space $\mathcal{Z} \in \mathbb{R}$

$$\mathbf{Z}_{i,k} = \left\{z_{i,k}^{(1)}, z_{i,k}^{(2)}, \dots, z_{i,k}^{(|\mathbf{Z}_{i,k}|)}\right\} = Z_{i,0}(\mathbf{x}_k) \cup Z_i(\mathbf{x}_k, \mathbf{S}_k) \cup C_{i,k} \in \mathcal{F}(\mathcal{Z}), i = 1, \dots, N \tag{4.10}$$

where $Z_0(\mathbf{x}_k)$ denotes the LOS path observation, $Z(\mathbf{x}_k, \mathbf{S}_k)$ represents the observation set of multipath from random scatters, and $C_{i,k}$ denotes the set of false alarms detected at time *k*. In order to estimate the joint STAMP state $\mathbb{X}_k = \{\mathbf{x}_{1:k}, \mathbf{S}_{1:k}\}$, a single-cluster point process is modeled, where the MS and range bias state $\mathbf{x}$ represents the parent state vector and the multipath mode parameter $\mathbf{S}$ represent its daughter process. Letting $\mathbf{Z}_k = \mathbf{Z}_{1,k} \cup \mathbf{Z}_{2,k} \dots \cup \mathbf{Z}_{S,k}$, the Bayesian recursion of the posterior density for $\mathbb{X}$ can be written as

$$p(\mathbb{X}_k|\mathbf{Z}_{1:k}) = \frac{f(\mathbf{Z}_k|\mathbb{X}_k)p(\mathbb{X}_k|\mathbf{Z}_{1:k-1})}{\int f(\mathbf{Z}_k|\mathbb{X}_k)p(\mathbb{X}_k|\mathbf{Z}_{1:k-1})\delta\mathbb{X}_k} \tag{4.11}$$

where

$$p(\mathbb{X}_k|\mathbf{Z}_{1:k-1}) = \int f(\mathbb{X}_k|\mathbb{X}_{k-1})p(\mathbb{X}_{k-1}|\mathbf{Z}_{1:k-1})\delta\mathbb{X}_{k-1} \tag{4.12}$$

Note that the above recursions are evaluated via set integration which are taken over all sets of all possible cardinalities of $\mathbb{X}$. Since the closed form solutions of (4.11) and (4.12) are computational intractable, only the first moment of the posterior density is propagated. Therefore, the so called probability hypothesis density (PHD) filter can formulated for the STAMP problem as:

$$D(\mathbf{x}_k, \mathbf{S}_k|\mathbf{Z}_{1:k}) \propto p(\mathbf{x}_k|\mathbf{Z}_{1:k-1})L(\mathbf{Z}_k|\mathbf{x}_k, \mathbf{Z}_{k-1})D(\mathbf{S}_k|\mathbf{x}_k, \mathbf{Z}_{1:k}) \tag{4.13}$$

where $D(\mathbf{S}_k|\mathbf{x}_k, \mathbf{Z}_{1:k})$ is the measurement updated PHD intensity of the daughter process conditioned on $\mathbf{x}_k$. According to [47, 53, 55], the multi-sensor representation of the $D(\mathbf{S}_k|\mathbf{x}_k, \mathbf{Z}_{1:k})$ can be written as

$$D(\mathbf{S}_k|\mathbf{x}_k, \mathbf{Z}_{1:k}) \propto D(\mathbf{S}_k|\mathbf{x}_{k-1}, \mathbf{Z}_{1:k-1}) \times \prod_{i=1,\dots,N} V_i\left(\mathbf{Z}_{i,k}\middle|\mathbf{x}_k, \mathbf{Z}_{1:k-1}\right) \tag{4.14}$$

where

$$L_i\left(\mathbf{Z}_{i,k}\middle|\mathbf{x}_k, \mathbf{Z}_{1:k-1}\right) = (1 - Pd_i(\mathbf{S}_k|\mathbf{x}_k)) + \sum_{z\epsilon\mathbf{Z}_{i,k}} \frac{Pd_i(\mathbf{S}_k|\mathbf{x}_k)\pi_i(z|\mathbf{x}_k, \mathbf{S}_k)}{\eta_{i,z}(\mathbf{x}_k|\mathbf{Z}_{1:k-1})} \tag{4.15}$$

$$D(\mathbf{S}_k|\mathbf{x}_{k-1}, \mathbf{Z}_{1:k-1}) = \int D(\mathbf{S}_{k-1}|\mathbf{Z}_{1:k-1})\, \delta(\mathbf{S}_k - \mathbf{S}_{k-1})d\mathbf{S}_{k-1} + \gamma(\mathbf{S}_k|\mathbf{S}_{k-1}) \tag{4.16}$$

$$\eta_{i,z}(\mathbf{x}_k|\mathbf{Z}_{1:k-1}) = \kappa_i(z) + Pd_i^0(\mathbf{x}_k)\pi_i^0(z|\mathbf{x}_k) + \int Pd_i(\mathbf{S}_k|\mathbf{x}_k)D(\mathbf{S}_k|\mathbf{x}_k, \mathbf{Z}_{1:k-1})\pi_i(z|\mathbf{x}_k, \mathbf{S}_k)d\mathbf{S}_k \tag{4.17}$$

where $Pd_i^0(\mathbf{x}_k)$ and $Pd_i(\mathbf{S}_k|\mathbf{x}_k)$ are the probabilities of detection of LOS and multipath respectively and $\gamma(\mathbf{S}_k|\mathbf{S}_{k-1})$ is the density of newly appearing scatters at time *k*. The first term of $\eta_{i,z}(\mathbf{x}_k|\mathbf{Z}_{1:k-1})$ refer to likelihood of false alarm, the second term refers to the direct path, and the last integration term refers to all multipath modes based on the predicted intensity $D(\mathbf{S}_k|\mathbf{x}_k, \mathbf{Z}_{1:k-1})$. The multi-sensor likelihood of the measurement set $\mathbf{Z}_k$ conditioned on target state $\mathbf{x}_k$ can be inferred as

$$L(\mathbf{Z}_k|\mathbf{x}_k, \mathbf{Z}_{1:k-1}) = \prod_{i=1,\dots,N} L\left(\mathbf{Z}_{i,k}\middle|\mathbf{x}_k, \mathbf{Z}_{1:k-1}\right) = \prod_{i=1,\dots,N} \frac{\prod_{z\epsilon\mathbf{Z}_{i,k}} \eta_{i,z}(\mathbf{x}_k|\mathbf{Z}_{s,1:k-1})}{\exp\{\int Pd_i(\mathbf{S}_k|\mathbf{x}_k)D(\mathbf{S}_k|\mathbf{x}_k, \mathbf{Z}_{1:k-1})d\mathbf{S}_k\}} \quad (4.18)$$

The above PHD recursions of scatters positions, or multipath channel parameters, can be implemented through particle filtering based Sequential Monte Carlo (SMC) and Gaussian Mixture (GM) methods. Due to the Gaussian observation assumption, we utilize the GM-PHD as a more efficient implementation of the proposed STAMP algorithm. The proof of fundamental convergent property of the GM-PHD filter can be found in [26].

4.2. Single-Cluster PHD Filtering For STAMP

The proposed implementations of STAMP algorithm combines a particle representation of the parent process, or the system state vector **x**, and a Gaussian mixture model of the daughter process of scatters multipath state **S**, which is recursively updated based on Finite Set Statistics (FISST) [45] as given in (4.11). The particle

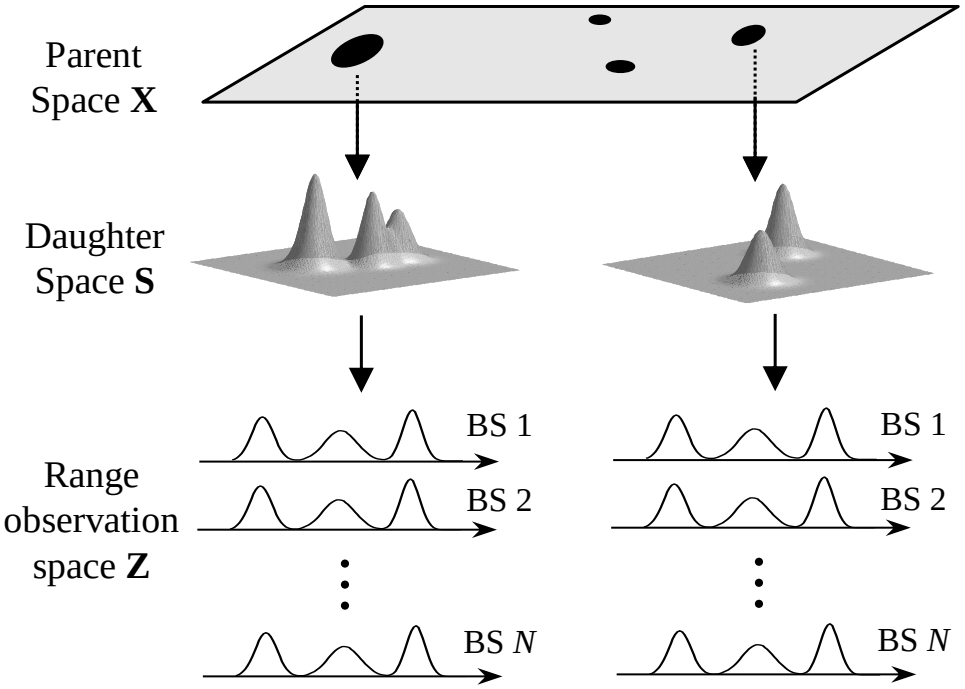

Figure 4.2: Visual illustration of the single-cluster process, where each particle in a parent process of target state is associated with a Gaussian Mixture daughter process of multipath parameters.

approximation of the probability distribution function of the parent process $\mathbf{x}_k$ at time k is given by

$$p(\mathbf{x}_k|\mathbf{Z}_{1:k}) = \sum_{m=1}^{M} \ell_k^{(m)} \delta(\mathbf{x}_k - \mathbf{x}_k^{(m)}) \tag{4.19}$$

The Gaussian mixture intensity functions of the daughter process $\mathbf{S}_k$ conditioned on the mth particle of $p(\mathbf{x}_k)$ is given by

$$D^{(m)}\left(\mathbf{S}_k\middle|\mathbf{x}_k^{(m)}, \mathbf{Z}_{1:k}\right) = \sum_{n=1}^{J_k^{(m)}} w_k^{(m,n)} \mathcal{N}(\mathbf{S}_k; \boldsymbol{\mu}_k^{(m,n)}, \mathbf{C}_k^{(m,n)}), m = 1, \ldots, M \tag{4.20}$$

In (4.20), each Gaussian component of $D^{(m)}(\mathbf{S}_k|\mathbf{x}_k, \mathbf{Z}_{1:k})$ is represented by a hypothesized scatter, and the weight $w_k^{(m,n)} \in (0,1)$ refers to the associated confidence factor. The estimate of the number of scatter multipath channels in $\mathbf{S}_k$ is given by

$$\hat{n}_k^{(m)} = \sum_{n=1}^{J_k^{(i)}} w_k^{(m,n)} \tag{4.21}$$

The main recursion process of the Single-Cluster PHD filtering can be summarized as three steps: prediction of density functions of both parent and daughter process, update of the posterior probability distribution of parent process and iterated update of the posterior PHD surface of daughter process across all BSs. The above three steps will be discussed in detail in the following subsections.

4.2.1 Prediction Step

Based on the Markov transition models of the MS target state and the range bias given in (4.1) and (4.3), the predicted particles of the parent process are drawn as

$$\mathbf{x}_k^{(m)} \sim f\left(\mathbf{x}_k \middle| \mathbf{x}_{k-1}^{(m)}\right),\ m = 1, \ldots, M \tag{4.22}$$

Assume the PHD intensity of the birth of scatter multipath channels are also Gaussian mixture in the form of:

$$\gamma(\mathbf{S}_k) = \sum_{n=1}^{J_\gamma} w_\gamma^{(n)} \mathcal{N}\left(\mathbf{S}_k \middle| \boldsymbol{\mu}_\gamma^{(n)}, \mathbf{C}_\gamma^{(n)}\right) \tag{4.23}$$

According to (4.16), the predicted scatter PHD surface is the sum of the new birth PHD intensity in (4.23) and the intensity of persisting scatters, given by

$$D^{(m)}\left(\mathbf{S}_k \middle| \mathbf{x}_k^{(m)}, \mathbf{Z}_{1:k-1}\right) = \int D^{(m)}(\mathbf{S}_{k-1}|\mathbf{Z}_{1:k-1})\ \delta(\mathbf{S}_k - \mathbf{S}_{k-1}) d\mathbf{S}_{k-1} + \gamma(\mathbf{S}_k)$$

$$= \sum_{n'=1}^{J_{k-1}^{(m)}} w_{k-1}^{(m,n)} \mathcal{N}(\mathbf{S}_k; \boldsymbol{\mu}_{k-1}^{(m,n')}, \mathbf{C}_{k-1}^{(m,n')}) + \sum_{n''=1}^{J_\gamma} w_\gamma^{(n'')} \mathcal{N}\left(\mathbf{S}_k \middle| \boldsymbol{\mu}_\gamma^{(n'')}, \mathbf{C}_\gamma^{(n'')}\right)$$

$$= \sum_{n=1}^{J_{0,k}^{(m)}} w_{0,k}^{(m,n)} \mathcal{N}(\mathbf{S}_k; \boldsymbol{\mu}_{0,k}^{(m,n)}, \mathbf{C}_{0,k}^{(m,n)}), \text{ with } J_{0,k}^{(m)} = J_{k-1}^{(m)} + J_\gamma \tag{4.24}$$

Note that since all scatters are stationary, the dynamic of persisting scatters are simply identity, which is represented as a delta function $\delta(\mathbf{S}_k - \mathbf{S}_{k-1})$ in (4.24).

4.2.2 Update of Parent Process

Before preceding to the update of PHD intensity of scatter state, the probability distribution of the parent process can be primarily computed. According to (4.18), the weights associated to each particle of the parents process is updated as

$$\ell_k^{(m)} = \frac{L\left(\mathbf{Z}_k \middle| \mathbf{x}_k^{(m)}, \mathbf{Z}_{1:k-1}\right) \ell_{k-1}^{(m)}}{\sum_{m'=1}^{M} L\left(\mathbf{Z}_k \middle| \mathbf{x}_k^{(m')}, \mathbf{Z}_{1:k-1}\right) \ell_{k-1}^{(m')}}, m = 1, \dots, M \tag{4.25}$$

where

$$L\left(\mathbf{Z}_k \middle| \mathbf{x}_k^{(m)}, \mathbf{Z}_{1:k-1}\right) = \prod_{i=1,\dots,N} \frac{\prod_{z \in \mathbf{Z}_{i,k}} \eta_{i,z}(\mathbf{x}_k^{(m)} | \mathbf{Z}_{S,1:k-1})}{\exp\left\{\sum_{n=1}^{J_{0,k}^{(m)}} Pd_i\left(\mathbf{S}_k \middle| \mathbf{x}_k^{(m)}\right) w_{0,k}^{(m,n)}\right\}} \tag{4.26}$$

$$\eta_{i,z}\left(\mathbf{x}_k^{(m)} \middle| \mathbf{Z}_{1:k-1}\right) = \kappa_i(z) + Pd_i^0\left(\mathbf{x}_k^{(m)}\right) \pi_i^0\left(z \middle| \mathbf{x}_k^{(m)}\right) + \sum_{n=1}^{J_{0,k}^{(m)}} Pd_i\left(\mathbf{S}_k \middle| \mathbf{x}_k^{(m)}\right) \pi_i\left(z \middle| \mathbf{x}_k^{(m)}, \mathbf{S}_k\right) w_{0,k}^{(m,n)} \tag{4.27}$$

Note that the posterior weight $\ell_k^{(m)}$ is computed based on the predicted PHD intensity $D^{(m)}\left(\mathbf{S}_k \middle| \mathbf{x}_k^{(m)}, \mathbf{Z}_{1:k-1}\right)$ given in (4.24). This provides availability to perform particle management schemes, such as particle resampling [57] and progressive correction [58],

to improve the accuracy of the important sample prorogations. In order to increase the fidelity of the range bias estimate, for each particle, P samples of range bias realizations are drawn, and the sample with highest likelihood $L\left(\mathbf{Z}_k \middle| \mathbf{x}_k^{(m)}, \mathbf{Z}_{1:k-1}\right)$ is kept, i.e.,

$$b_k^{(m)} = \underset{b \in \left\{b^{(1)}, \ldots, b^{(P)}\right\}}{\operatorname{argmax}} L\left(\mathbf{Z}_k \middle| \mathbf{p}_k^{(m)}, b, \mathbf{Z}_{1:k-1}\right) \text{ with } \left\{b^{(1)}, \ldots, b^{(P)}\right\} \sim f\left(b \middle| b_{k-1}^{(m)}\right) \tag{4.28}$$

As shown in (4.26), the likelihood $L\left(\mathbf{Z}_k \middle| \mathbf{p}_k^{(m)}, b, \mathbf{Z}_{1:k-1}\right)$ is represented by a Gaussian mixture structure and non-concave as a function of b. However, in the presence of small clock fluctuation, we can approximate the likelihood is locally concave, so that maximum likelihood formation in (4.28) is valid. The weighted mean MS target location estimate is then given by

$$\widehat{\mathbf{p}}_k = \sum_{m=1}^{M} \ell_k^{(m)} \mathbf{p}_k^{(m)} \tag{4.29}$$

Alternatively, the particle associated with largest weight can be utilized as the output MS position estimate.

4.2.3 Update of Daughter Process

Since multiple BS nodes (or equivalently multi-sensor) are considered for the proposed STAMP problem, the single-sensor PHD update process is inappropriate. In this work, an iterated multi-sensor implementation, referring to the iterated-corrector PHD update, is utilized as in [47, 53]. Starting with the predicted PHD intensity $D^{(m)}\left(\mathbf{S}_k \middle| \mathbf{x}_{k-1}^{(m)}, \mathbf{Z}_{1:k-1}\right)$ in (4.24), the posterior PHD is updated by using the observation

from the first sensor, the second sensor through the last sensor sequentially. In this case, the updated PHD intensity after the ith sensor is given by:

$$D^{(m)}\left(\mathbf{S}_k\middle|\mathbf{x}_k^{(m)},\mathbf{Z}_{1:i,k},\mathbf{Z}_{1:k-1}\right) = \left(1-Pd_i\left(\mathbf{S}_k\middle|\mathbf{x}_k^{(m)}\right)\right)D^{(m)}\left(\mathbf{S}_k\middle|\mathbf{x}_k^{(m)},\mathbf{Z}_{1:i-1,k},\mathbf{Z}_{1:k-1}\right) + \sum_{z\epsilon\mathbf{Z}_{i,k}}\sum_{n=1}^{J_{i-1,k}^{(m)}} w_{i,k}^{(m,n)}\mathcal{N}(\mathbf{S}_k;\boldsymbol{\mu}_{i,k}^{(m,n)},\mathbf{C}_{i,k}^{(m,n)}) \tag{4.30}$$

where

$$w_{i,k}^{(m,n)} = \frac{Pd_i\left(\mathbf{S}_k\middle|\mathbf{x}_k^{(m)}\right)\pi_i\left(z\middle|\mathbf{x}_k^{(m)},\mathbf{S}_k\right)w_{i-1,k}^{(m,n)}}{\eta_{i,z}\left(\mathbf{x}_k^{(m)}\middle|\mathbf{Z}_{1:i-1,k},\mathbf{Z}_{1:k-1}\right)} \tag{4.31}$$

$$\boldsymbol{\mu}_{i,k}^{(m,n)} = \boldsymbol{\mu}_{i-1,k}^{(m,n)} + \frac{\mathbf{C}_{i-1,k}^{(m,n)}(\mathbf{g}_{s,k}^{(m,n)})^T\left(z-g_i\left(\mathbf{x}_k,\boldsymbol{\mu}_{s-1,k}^{(m,n)}\right)\right)}{\epsilon_{i,k}^{(m,n)}} \tag{4.32}$$

$$\mathbf{C}_{i,k}^{(m,n)} = \left(\mathbf{I}_2 - \frac{\mathbf{C}_{i-1,k}^{(m,n)}\mathbf{g}_{s,k}^{(m,n)}(\mathbf{g}_{s,k}^{(m,n)})^T}{\epsilon_{i,k}^{(m,n)}}\right)\mathbf{C}_{i-1,k}^{(m,n)} \tag{4.33}$$

$$\epsilon_{i,k}^{(m,n)} = (\mathbf{g}_{s,k}^{(m,n)})^T\mathbf{C}_{i-1,k}^{(m,n)}\mathbf{g}_{s,k}^{(m,n)} + \sigma_i^2 \tag{4.34}$$

$$\mathbf{g}_{s,k}^{(m,n)} = \nabla_{\mathbf{s}}g_i\left(\mathbf{x}_k^{(m)},\mathbf{s}\right)\Big|_{\boldsymbol{s}=\boldsymbol{\mu}_{s-1,k}^{(m,n)}} = \left[\frac{\mathbf{s}-\mathbf{p}}{\|\mathbf{p}-\mathbf{s}\|} + \frac{\mathbf{s}-\mathrm{r}_i}{\|\mathbf{s}-\mathrm{r}_i\|}\right]_{\boldsymbol{s}=\boldsymbol{\mu}_{s-1,k}^{(m,n)},\mathbf{p}=\mathbf{p}_k^{(m)}} \tag{4.35}$$

Therefore, the multi-sensor PHD update is iteratively performed over N stages, referring to total N BS nodes. The number of Gaussian components at each stage increases geometrically is given by $J_{i,k}^{(m)} = \left(\left|\mathbf{Z}_{i,k}\right|+1\right)J_{i-1,k}^{(m)}$. In order to limit the exponential growth of $J_{i,k}^{(m)}$ over stages and time, Gaussian component pruning and clustering steps described in [59] are employed (in our work, the pruning and merging thresholds are as

0 and 4 respectively, and the maximum number of Gaussian components is limited to 100).

Despite of its implementation simplicity, the major limitation of the iterated multi-sensor PHD filter is the impact of the sensor ordering. It is shown that the PHD estimation performance differs significantly with different permutations of sensor ordering, and the sensor with the lower detectability should be updated in earlier stages [53]. As an alternative implementation, the product multi-sensor PHD filter provides more robust estimation performance against sensor ordering [55]. On the other hand, the probability of detection $Pd_i^0(\mathbf{x})$ and $Pd_i(\mathbf{s}|\mathbf{x})$ is a function of both scatter and target locations and the received signal SNR. Unfortunately, these probabilities are difficult to parameterize and mismatched detection probability would result in false association and over/under-estimated Gaussian component weights, which may cause a scatter multipath channel component being falsely pruned. More sophisticated modeling of target detection profile can be found [60].

The target state has to be initialized at the first scan. In this work, we assume the initial state of MS location is known a priori. Otherwise, different particles of initial guesses of the parent process $\mathbf{x}_0$ can be uniformly drawn from the space of the parent process. As successive observations obtained, incorrect initializations will be eliminated through particle resampling process.

4.3 Localization Identifiability in a NLOS Environment

In this section, the fundamental identifiability of the proposed STAMP problem is studied using the boundedness of the Cramer-Rao Lower Bound (CRLB) on joint target and multipath estimation. Instead of a dynamic tracking problem, we consider a single snapshot of observation interval at particular time k (so that the time index k is omitted for notational simplicity). We also concentrate on the absolute NLOS scenario: all LOS observations of all BSs are miss detected. This worst localization case usually happened during track initiation or lost-track recovery process, which limits the applications of the proposed STAMP scheme. Let the notations consist with the earlier parts of this work, we refresh the assumptions utilized in this section:

1. A MS target receives *known* wideband RF signals at an unknown position $\mathbf{p} \in \mathbb{R}^2$ from a BS beacon network.
2. The BS beacon network has N nodes at known locations$\mathbf{r}_i \in \mathbb{R}^2, i = 1, \dots, N$, and all nodes share the same local oscillator clock but are asynchronized with the MS.
3. Performance under the worst case is considered: the light of sight (LOS) signal is *not* presented while only reflected signals from S unknown random scatters located at $\mathbf{s}_j \in \mathbb{R}^2, j = 1, \dots, S$, are observed at the MS.
4. The statistical property of additive observation noise from each BS node and each path is assumed to be known a priori.

The objective of the proposed STAMP problem is to jointly estimate the $(3+2S)\times 1$ system parameter vector

$$\boldsymbol{\theta} \triangleq^{\text{def}} [\mathbf{p}^T, b, \boldsymbol{s}_1^T, \ldots, \boldsymbol{s}_N^T] \tag{4.36}$$

As introduced in Chapter 2, the CRLB provides lower limits for the covariance matrix of any unbiased estimate of unknown parameter vector $\boldsymbol{\theta}$. Defining $Z = \{z_{1,1}, z_{1,2}, \ldots, z_{N,S}\}$ as the entire observation set of all nodes and all scatters at a single time instance, and denoting $\widehat{\boldsymbol{\theta}}$ as an unbiased estimate of $\boldsymbol{\theta}$, the CRLB provides the lower performance bound of $\widehat{\boldsymbol{\theta}}$ as:

$$\mathbb{E}\left\{\left(\boldsymbol{\theta}-\widehat{\boldsymbol{\theta}}\right)\left(\boldsymbol{\theta}-\widehat{\boldsymbol{\theta}}\right)^T\right\} \geq [\mathbf{J}(\boldsymbol{\theta})]^{-1} = \left[\mathbb{E}\left\{-\nabla_{\boldsymbol{\theta}}\nabla_{\boldsymbol{\theta}}^T \ln p(Z|\boldsymbol{\theta})\right\}\right]^{-1} \tag{4.37}$$

where $\mathbf{J}(\boldsymbol{\theta})$ is the nonsingular Fisher Information matrix (FIM) based on the STAMP likelihood $p(Z|\boldsymbol{\theta})$, and $\mathbf{A} \geq \mathbf{B}$ denotes that matrix **A - B** is positive semidefinite. The expectation is taken over the $\mathbb{R}^{SN}$ observation space conditioned on $\boldsymbol{\theta}$. For notational simplification, we define vector $\mathbf{u}_{i,j}$ and $\mathbf{v}_{i,j}$ for $i = 1, \ldots, N$ and $j = 1, \ldots, S$

$$\mathbf{u}_{i,j} = \sigma_{i,j}^{-1}\nabla_{\mathbf{p}} g_i(\mathbf{p}, \mathbf{s}_j, b) = \frac{\mathbf{p}-\mathbf{s}_j}{\sigma_{i,j}\|\mathbf{p}-\mathbf{s}_j\|} \tag{4.38}$$

$$\mathbf{v}_{i,j} = \sigma_{i,j}^{-1}\nabla_{\mathbf{p}} g_i(\mathbf{p}, \mathbf{s}_j, b) = \frac{\mathbf{s}_j-\mathbf{p}}{\sigma_{i,j}\|\mathbf{p}-\mathbf{s}_j\|} + \frac{\mathbf{s}_j-\mathbf{r}_i}{\sigma_{i,j}\|\mathbf{s}_j-\mathbf{r}_i\|} \tag{4.39}$$

4.3.1 CRLB with Known Data Association

Under the assumption of perfect detection with known data association, the STAMP likelihood $p(Z|\boldsymbol{\theta})$is a single Gaussian written as:

$$p(Z|\boldsymbol{\theta}) \propto \prod_{i=1}^{N}\prod_{j=1}^{S}\exp\left\{-\frac{1}{2\sigma_{i,j}^2}\left(z_{i,j}-g_i(\mathbf{p},\mathbf{s}_j,b)\right)^2\right\} \tag{4.40}$$

where the multipath observation model $g_i(\mathbf{p},\mathbf{s}_j,b)$ shares the same expression given in (4.8). Therefore, the $(3+2S)\times(3+2S)$ FIM for STAMP problem can be written as:

$$\mathbf{J}(\boldsymbol{\theta}) = \sum_{i=1}^{N}\sum_{j=1}^{S}\sigma_{i,j}^{-2}\nabla_{\boldsymbol{\theta}}\nabla_{\boldsymbol{\theta}}^{T}g_i(\mathbf{p},\mathbf{s}_j,b) = \begin{bmatrix} \sum_{j=1}^{S}\mathbf{U}_j\mathbf{U}_j^T & \sum_{j=1}^{S}\mathbf{U}_j\mathbf{e}_j & \mathbf{U}_1\mathbf{V}_1^T & \cdots & \mathbf{U}_S\mathbf{V}_S^T \\ \sum_{j=1}^{S}\mathbf{e}_j^T\mathbf{U}_j^T & \sum_{j=1}^{S}\mathbf{e}_j^T\mathbf{e}_j & \mathbf{e}_1^T\mathbf{V}_1^T & \cdots & \mathbf{e}_S^T\mathbf{V}_S^T \\ \mathbf{V}_1\mathbf{U}_1^T & \mathbf{V}_1\mathbf{e}_1 & \mathbf{V}_1\mathbf{V}_1^T & \mathbf{0} & \vdots \\ \vdots & \vdots & \mathbf{0} & \ddots & \mathbf{0} \\ \mathbf{V}_S\mathbf{U}_S^T & \mathbf{V}_S\mathbf{e}_S & \cdots & \mathbf{0} & \mathbf{V}_S\mathbf{V}_S^T \end{bmatrix} \tag{4.41}$$

where

$$\boldsymbol{U}_j \overset{\text{def}}{=} [\boldsymbol{u}_{1,j},\ldots,\boldsymbol{u}_{N,j}] \tag{4.42}$$

$$\boldsymbol{V}_j \overset{\text{def}}{=} [\boldsymbol{v}_{1,j},\ldots,\boldsymbol{v}_{N,j}] \tag{4.43}$$

$$\boldsymbol{e}_j \overset{\text{def}}{=} \left[\boldsymbol{\sigma}_{1,j}^{-1},\ldots,\boldsymbol{\sigma}_{N,j}^{-1}\right]^T \tag{4.44}$$

Based on the matrix inversion lemma, the 2 × 2 CRLB on the target position estimate $\hat{\mathbf{p}}$ yields the form of

$$CRLB(\mathbf{p}) = [\,\mathbf{J}(\mathbf{p})]^{-1} = \left[\sum_{j=1}^{S}\mathbf{U}_j(\mathbf{I}_N-\mathbf{P}_j^{\perp})\mathbf{U}_j^T-\mathbf{B}\right]^{-1} \tag{4.45}$$

where

$$\boldsymbol{P}_j^{\perp} \overset{\text{def}}{=} \boldsymbol{V}_j\left(\boldsymbol{V}_j^T\boldsymbol{V}_j\right)^{-1}\boldsymbol{V}_j^T \tag{4.46}$$

$$\boldsymbol{B} \overset{\text{def}}{=} \frac{\left(\sum_{j=1}^{S}\boldsymbol{U}_j(\boldsymbol{I}_N-\boldsymbol{P}_j^{\perp})\boldsymbol{e}_j\right)\left(\sum_{j=1}^{S}\boldsymbol{U}_j(\boldsymbol{I}_N-\boldsymbol{P}_j^{\perp})\boldsymbol{e}_j\right)^T}{\sum_{j=1}^{S}\boldsymbol{e}_j^T(\boldsymbol{I}_N-\boldsymbol{P}_j^{\perp})\boldsymbol{e}_j} \tag{4.47}$$

$\mathbf{U}_j(\mathbf{I}_N-\mathbf{P}_j^{\perp})\mathbf{U}_j^T$ represents the Fisher information component carried from the jth scatter for MS position estimate, $\mathbf{B}$ represents the Fisher information due to the unknown range offset b. Note that $\mathrm{P}_j^{\perp}$ stands for the $N \times N$ orthogonal projection matrix onto the range

space of $\mathbf{V}_j$, and $\mathbf{I}_N - \mathbf{P}_j^{\perp}$ represents its orthogonal complement. Clearly, $\mathbf{P}_j^{\perp}$ is a rank-2 matrix, and the rank of matrix $\mathbf{I} - \mathbf{P}_j^{\perp}$ is $N - 2$. Therefore, the non-zero $\mathbf{I}_N - \mathbf{P}_j^{\perp}$ can be achieved only if $N \geq 3$ (we define scatters satisfies this requirement as *valid* scatters). On the other hand, it can be seen that each row of the $2 \times N$ matrix $\mathbf{U}_j$ is linearly dependent and proportional to $\mathbf{e}_j^T$, hence $\mathbf{U}_j(\mathbf{I}_N - \mathbf{P}_j^{\perp})\mathbf{U}_j^T$ is a rank-1 matrix for any N satisfies $N \geq 3$.

In order to investigate the singularity of the FIM given in (4.48), we express its determinant as

$$\det\left(\sum_{j=1}^{S} \mathbf{U}_j(\mathbf{I}_N - \mathbf{P}_j^{\perp})\mathbf{U}_j^T - \mathbf{F}\right) \propto \mathbf{1}^{\boldsymbol{T}}\boldsymbol{\Lambda}^{\frac{\mathbf{1}}{\mathbf{2}}}(\mathbf{I} - \mathbf{P}_{stack}^{\perp})\boldsymbol{\Lambda}^{\frac{\mathbf{1}}{\mathbf{2}}}\mathbf{1} \tag{4.48}$$

where

$$\mathbf{P}_{stack}^{\perp} = \boldsymbol{\Lambda}^{\frac{1}{2}}\mathbf{T}^T(\mathbf{T}\boldsymbol{\Lambda}\mathbf{T}^T)^{-1}\mathbf{T}\boldsymbol{\Lambda}^{\frac{1}{2}} \tag{4.49}$$

$$\boldsymbol{\Lambda} \stackrel{\text{def}}{=} \text{diag}\{\mathbf{e}_1^T(\mathbf{I} - \mathbf{P}_1^{\perp})\mathbf{e}_1, \ldots, \mathbf{e}_S^T(\mathbf{I} - \mathbf{P}_S^{\perp})\mathbf{e}_S\} \tag{4.50}$$

$$\mathbf{T} \stackrel{\text{def}}{=} \left[\frac{\mathbf{p}-\mathbf{s}_1}{\|\mathbf{p}-\mathbf{s}_1\|}, \frac{\mathbf{p}-\mathbf{s}_2}{\|\mathbf{p}-\mathbf{s}_2\|}, \ldots, \frac{\mathbf{p}-\mathbf{s}_S}{\|\mathbf{p}-\mathbf{s}_S\|}\right] \tag{4.51}$$

and $\mathbf{1} \stackrel{\text{def}}{=} [1, \ldots, 1]^T$ is a $S \times 1$ all 1's vector. For invertible 2×2 matrix $\mathbf{T}\boldsymbol{\Lambda}\mathbf{T}^T$, at least two scatters are required, and $\mathbf{p} - \mathbf{s}_{j_1}$ and $\mathbf{p} - \mathbf{s}_{j_2}$ must be linearly independent for any $j_1 \neq j_2$ (i.e., all scatters and target do not lie in a straight line). Since the rank of the orthogonal complement matrix $\mathbf{I} - \mathbf{P}_{\boldsymbol{stack}}^{\perp}$ is $S - 2$, the determinant given in (4.48) is non-zero only if $S \geq 3$.

As a summary of the above analysis, the 2×2 rank-1 matrix $\mathbf{U}_j(\mathbf{I}_N - \mathbf{P}_{\mathbf{j}}^{\perp})\mathbf{U}_j^{\mathrm{T}}$ exists only if signals of three or more nodes contains the reflections from scatter j (i.e.,

$N \geq 3$). In this case, at least three scatters are required for invertible FIM on $\boldsymbol{\theta}$ (i.e., $S \geq 3$). This result accords with the fundamental intuition: three or more nodes are needed to identify the position of a single scatter (i.e., three equations to solve three unknown parameters: 2×1 vector $\mathbf{s}_j$ and $\|\mathbf{p} - \mathbf{s}_j\| + b$); and at least three scatters are essential to find the target position (i.e., three equations to solve three unknown parameters: 2×1 vector $\mathbf{p}$ and b). For the 3D case, since the z coordinate is now included in $\mathbf{p}$ and $\mathbf{s}_j$, one more node is required for each scatter ($N \geq 4$) and one more scatter has to be presented to identify the target position ($S \geq 4$).

If we relax Assumption 3, both LOS path and multipath from the S scatters are observed, and extra Fisher information component contributed by the LOS path will be added to the FIM given in (4.41). Let $j = 0$ denotes the LOS path, and the FIM for $\mathbf{p}$ can be rewritten as

$$\mathbf{J}'(\mathbf{p}) = \sum_{j=0}^{S} \mathbf{U}_j (\mathbf{I}_N - \mathbf{P}_j^{\perp}) \mathbf{U}_j^T - \mathbf{B}' \tag{4.52}$$

where

$$\mathrm{B}' \stackrel{\text{def}}{=} \frac{\left(\sum_{j=0}^{S} \mathrm{U}_j (\mathrm{I}_N - \mathrm{P}_j^{\perp}) \mathrm{E}_j\right) \left(\sum_{j=0}^{S} \mathrm{U}_j (\mathrm{I}_N - \mathrm{P}_j^{\perp}) \mathrm{E}_j\right)^T}{\sum_{j=0}^{S} \mathrm{E}_j^T (\mathrm{I}_N - \mathrm{P}_j^{\perp}) \mathrm{E}_j} \tag{4.53}$$

$$\mathbf{u}_{i,0} = \frac{\mathbf{p} - \mathbf{r}_i}{\sigma_{i,0} \|\mathbf{p} - \mathbf{r}_i\|}, \ \mathrm{P}_0^{\perp} = \mathbf{0} \tag{4.54}$$

In this case, $\mathrm{P}_0^{\perp} = \mathbf{0}$ means there is no Fisher information loss due to the uncertainty of propagation channel. When signal from one node includes the LOS path, the total number of scatter required to invert (4.52) is then reduced by one, and when three or

more nodes include LOS path, (4.52) is always invertible regardless the number of scatter presented.

4.3.2 CRLB with Data Association Uncertainty

In this section, we derive the CRLB in the presence of data association uncertainty. The uncertainty we address in this work contains is from two causes: 1) the occurrence of missed detections and false alarms, and 2) the ambiguity in associating scatters (modes) with observations. In order to capture these uncertainties, the CRLB has to integrate all possible association hypotheses, and the STAMP likelihood function $p(Z|\boldsymbol{\theta})$ in this case is the marginal distribution over all observations and association events, which has Gaussian mixture characteristics.

Let $Z_i \overset{\text{def}}{=} \{z_{i,l}\}_{l=1}^{m_i}$ denotes the TOA measurement set obtained at ith node, with a random number of observations m_i. The likelihood $p(Z_i|\boldsymbol{\theta})$ is then given by:

$$p(Z_i|\boldsymbol{\theta}) = \sum_{m_i=1}^{\infty} p(Z_i, m_i|\boldsymbol{\theta}) = \sum_{m_i=1}^{\infty} \sum_{k=1}^{|\mathcal{E}_{m_i}|} p(Z_i, \mathcal{E}_{m_i}^k, m_i|\boldsymbol{\theta}) \tag{4.55}$$

where $\mathcal{E}_{m_i}^k$, $k = 1,..,|\mathcal{E}_{m_i}|$, is defined as an association event conditioned on the number of observation m_i. Intuitively, each of the association event $\mathcal{E}_{m_i}^k$ can be viewed as a $S \times 1$ vector: $\mathcal{E}_{m_i}^k = [l_{m_i}^{k,1}, \dots, l_{m_i}^{k,S}]$, where non-zero $l_{m_i}^{k,j} = \{1, \dots, m_i\}$ denotes the measurement index associated with scatter j, and $l_{m_i}^{k,j} = 0$ refers to the event that scatter j is not detected. Thus, the joint likelihood $p(Z_i, \mathcal{E}_{m_i}^k, m_i|\boldsymbol{\theta})$ is in the form of

$$p\left(Z_i, \mathcal{E}_{m_i}^k, m_i \middle| \boldsymbol{\theta}\right) = \frac{P\left(\mathcal{E}_{m_i}^k, m_i \middle| \boldsymbol{\theta}\right)}{V^{f_k}} \times \prod_{j:l_{m_i}^{k,j}>0}^{S} \boldsymbol{N}\left(z_{i,l_{m_i}^{k,j}} - g_i(\mathbf{p}, \mathbf{s}_j, b), \sigma_{i,j}^2\right) \tag{4.56}$$

where

$$P\left(\mathcal{E}_{m_i}^k, m_i \middle| \boldsymbol{\theta}\right) = \frac{f_k! \mu(f_k) P_d^{m_i - f_k}}{m_i!(1-P_d)^{m_i - f_k - S}} \tag{4.57}$$

V is the volume of detection space (i.e., maximum detectable range minus minimum detectable range), P_d is the probability of detection, f_k is the number of false alarm assumed by $\mathcal{E}_{m_i}^k$ and $\mu(\cdot)$ is its probabilistic mass function which is modeled as a Poisson distribution.

Assuming all BS nodes are independent with each other, the overall STAMP FIM is then given by

$$\begin{aligned}\mathbf{J}(\boldsymbol{\theta}) &= \sum_{i=1}^{N} \mathbf{J}_i(\boldsymbol{\theta}) = \sum_{i=1}^{N} \mathbb{E}\left\{-\nabla_{\boldsymbol{\theta}} \nabla_{\boldsymbol{\theta}}^T \log p(Z_i|\boldsymbol{\theta})\right\} = \sum_{i=1}^{N} \sum_{m_i=1}^{\infty} \mathbb{E}\left\{-\nabla_{\boldsymbol{\theta}} \nabla_{\boldsymbol{\theta}}^T \log p(Z_i, m_i|\boldsymbol{\theta})\right\} \\ &= \sum_{i=1}^{N} \mathbf{H}_i \, \boldsymbol{\Gamma}_i \mathbf{H}_i^T\end{aligned} \tag{4.58}$$

where

$$\mathbf{H}_i \stackrel{\text{def}}{=} \left[\sigma_{i,1}^{-1} \nabla_{\boldsymbol{\theta}} g_i(\mathbf{p}, \mathbf{s}_1), \ldots, \sigma_{i,S}^{-1} \nabla_{\boldsymbol{\theta}} g_i(\mathbf{p}, \mathbf{s}_S)\right] \tag{4.59}$$

$$[\boldsymbol{\Gamma}_i]_{j_1,j_2} \stackrel{\text{def}}{=} \sum_{m_i=1}^{\infty} \mathbb{E}\left\{\alpha_{i,j_1}(m_i) \alpha_{i,j_2}(m_i)\right\} \tag{4.60}$$

$$\alpha_{i,j}(m_i) \stackrel{\text{def}}{=} \sigma_{i,j} \frac{d \log p(Z_i, m_i|\boldsymbol{\theta})}{d g_i(\mathbf{p}, \mathbf{s}_j)} = \sum_{l=1}^{m_i} \alpha_{i,j}^l(m_i) \tag{4.61}$$

$$\alpha_{i,j}^l(m_i) = \frac{g_i(\mathbf{p}, \mathbf{s}_j) - z_{i,l}}{\sigma_{i,j}} \cdot \frac{\sum_{\mathcal{E}_{m_i}^k : l_{m_i}^{k,j} = l} p\left(Z_i, \mathcal{E}_{m_i}^k, m_i \middle| \boldsymbol{\theta}\right)}{p(Z_i, m_i|\boldsymbol{\theta})} \tag{4.62}$$

Note that the summation in (4.62) sums over all association events $\mathcal{E}_{m_i}^k$ with $l_{m_i}^{k,j} = l$. The expectation in (4.60) refers to a m_i dimensional integration over the whole observation space $z_{i,1}, z_{i,2} \dots z_{i,m_i}$. The $S \times S$ positive semidefinite symmetric matrix $\mathbf{\Gamma}_i$ is defined as the *Information Reduction Matrix* (IRM) due to the data association uncertainty at *i*th node. In the case of perfect detection with known data association, $\mathbf{\Gamma}_i$ is an identity matrix, and (4.58) is reduced to (4.41).

Since the likelihood function $p(Z_i, m_i|\boldsymbol{\theta})$ is in a form of Gaussian mixture, the expectation of cross terms in IRM $\mathbb{E}\{\alpha_{i,j_1}(m_i)\alpha_{i,j_2}(m_i)\}$ for $j_1 \neq j_2$ is not necessary to be zero. Therefore it is complicated to analytically quantify the information loss. However, we may exploit the asymptotic behavior of the IRM. For sufficiently large SNR, the observation noise variance $\sigma_{i,j}^2$ would then become sufficiently small, so that Gaussian density functions approach delta functions. As a result, it can be shown that

$$\mathbb{E}\left\{\alpha_{i,j_1}^{l_1}(m_i) \cdot \alpha_{i,j_2}^{l_2}(m_i)\right\} \to 0 \tag{4.63}$$

and all cross terms in $\mathbf{\Gamma}_i$ trend to zeros. In addition, for any $P_d < 1$ at high SNR, the false alarm rate $P_f \cong 0$ and $\mu(0) \cong 1$, therefore all of the observations are target oriented. As a result, the diagonal elements of IRM is then

$$\begin{aligned}[\mathbf{\Gamma}_i]_{j,j} \cong & \sum_{m_i=1}^{S} \int \sum_{l=1}^{m_i} \left(\frac{g_i(\mathbf{p}, \mathbf{s}_j) - z_{i,l}}{\sigma_{i,j}}\right)^2 \times \sum_{\mathcal{E}_k : l^j = l} p(Z_i, \mathcal{E}_k, m_i|\boldsymbol{\theta})\, dz_{i,1} \dots dz_{i,m_i} \\ & = \sum_{m_i=1}^{S} \binom{S-1}{m_i-1} \frac{P_d^{m_i}}{(1-P_d)^{m_i-S}} = P_d \end{aligned} \tag{4.64}$$

This yields the same CRLB with perfect data associations in (4.45) expect the scaling

factor P_d.

It can be inferred that $\mathbf{\Gamma}_i \leq P_d\mathbf{I}$, with equality asymptotically if SNR is sufficiently large as shown above. Although in [62], the author provides the proof of $\gamma_i \leq P_d$ when the FIM $\mathbf{\Gamma}_i$ is a scalar factor γ_i, a more general proof of this property for matrices such that $\mathbf{\Gamma}_i \leq P_d\mathbf{I}$ is beyond this work. On the other hand, due to the Gaussian mixture characteristics of $p(Z_i|\boldsymbol{\theta})$, Fisher information reduction always exists even in a false alarm free situation. This is due to the unknown correspondence between propagation modes, especially when scatter positions are closely spaced.

Practically, the number of scatters S is an unknown random variable. To incorporate this randomness, the joint likelihood in (4.55) can be modeled as a function of S and its distribution $\mu_S(s)$. However, due to the huge computational complexity, we only consider the case that S is known and deterministic in the simulation section.

4.4 Simulation Result

4.4.1 Numeric Result of CRLB-based Identifiability Analysis

Consider a distributed receiver array with total three BS nodes located at (-200, -200), (200, -200) and (0, 200). The unknown target is located at (30, 50), and three unknown scatters are placed at (-100, 10), (-50, 50) and (90, -100) respectively as shown in Figure 4.3(a). We assume the noise variances are the same for all path and all nodes as:

$$\sigma^2 = \frac{c^2}{B^2 SNR} \tag{4.65}$$

where c denotes the speed of light, and B refers to RF signal bandwidth assumed to be 20MHz. To illustrate the identifiability of STAMP given in Section IV, we compute the CRLB for $\mathbf{p}$ in (4.45) as a function of number scatters S and number of nodes N. For illustrative convenience, we diagonal load the FIM $\mathbf{J}(\mathbf{p})$ with $10^{-6}\mathbf{I}_2$, therefore, when $\mathbf{J}(\mathbf{p})$ given in (4.45) is singular, the resulting CRLB will be a constant independent with SNR. The simulated result is shown in Figure 4.3 (b), and as discussed in section IV, only the case $N = 3$ and $S = 3$ provides a CRLB as a linear function of SNR in logarithm scale, so that the target and scatter positions can be jointly estimated.

The second phase of simulation incorporate the data association uncertainty discussed in Section III. We assume the signal detection profile follows the model as

$$P_d = P_{fa}^{1/(1+SNR)} \tag{4.66}$$

where P_{fa} is the probability of false alarm of given SNR and P_d. Regarding to the m_i dimensional integration for computing CRLB in (4.58), Monte Carlo integration method is utilized, and the number of observation for each node is summed from $m_i = 1$ to $m_i = 30$. The CRLB of $\mathbf{p}$ is illustrated in Figure 4.3 (c) for probability of detection $P_d = 0.9, 0.8, 0.7$ and 0.6. The known data association case for $P_d = 0.9$ is also plotted as a reference for performance bound. Unlike the linear relationship with SNR for known data association, the bounds with data association uncertainty exhibit the nonlinear properties as SNR decreases. This property may be result from the exponential growth of the number of false alarms at low SNR and the increasing ambiguity between each

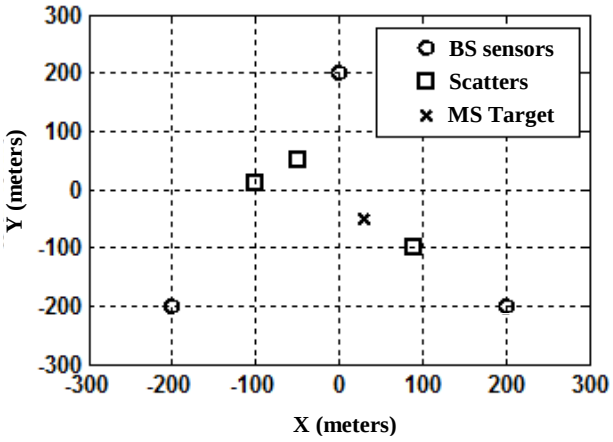

(a)

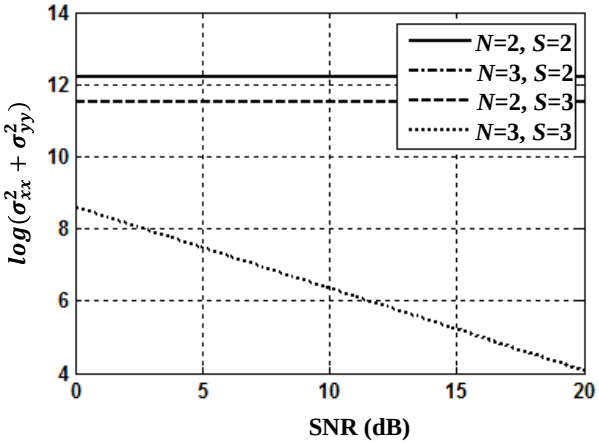

(b)

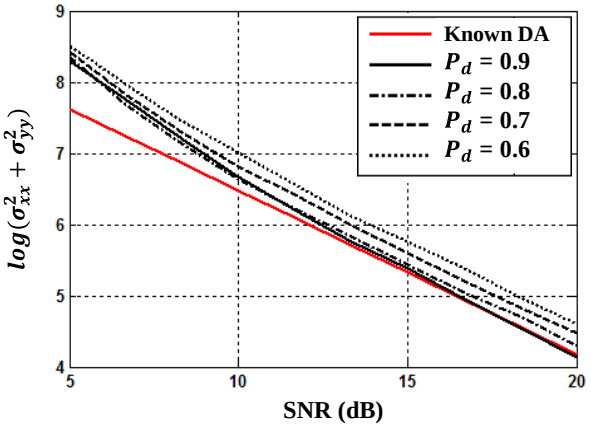

(c)

Figure 4.3: (a) Illustration of simulated scenario (b) CRLB under known data association and (c) CRLB with data association uncertainty

scatter. For high SNR, the bounds trend to linear functions of SNR in logarithm scale and achieve performance comparable to perfect data association case, which is consistent with the discussion in [62].

4.4.2 Numeric Result of the Single-Cluster PHD filter based STAMP Algorithm

This section illustrates the proposed STAMP algorithm derived in Section III for the application of tracking a MS target in a multipath-rich outdoor environment. We consider a 40 × 40 m² area of interest, where three BS nodes locate at (0, 45), (-30, -15) and (30, -15). The BS sensor network shares an overlapping area of surveillance, and produce a set of range Gaussian noisy observations in the presence of imperfect detection. For all BSs, the observation noise variance is assume to be 0.1 m^2. The target starts from the origin of the coordinate system, moves according to the dynamic model in a 2D scenario given in (4.1) and (4.2) over the total 60 time steps. The dynamics of the MS-BS range bias is represented by a random walk process given in (4.3) with variance 0.1 m^2. We assume multipath scatters are uniformly distributed over the area of interest. The number of scatters randomly selected from 3 to 10, so that the localization idenfiability of the absolute NLOS situation is guaranteed.

In the first phase of simulation, both the probability of detection of direct path observation and multipath observation from each scatters are assumed to be 0.5. The probability of false alarm is assumed to be 0.05. With 100 meter range detection interval,

the false detections are modeled by a Poisson point process with the mean number of false detection $\mu = 5$ at each time instant.The total number of particles is set to 600, and a resampling scheme described in [57] is utilized. Figure 4.4 (a) illustrates a realization of the estimated target paths over the true target trajectory (black solid lines) using the LOS-only method (blue solid lines) and proposed STAMP algorithm (red solid lines). In this realization, the LOS-only method failed due to the low probability of detection of the LOS observations, while the proposed STAMP algorithm continuously maintained relative small localization error by exploiting the multipath observations (almost overlap with the ground truth). Extracting the Gaussian components with weights greater than 0.25 from the estimated PHD intensity, the estimates of the scatter positions (red plus signs) are marked with the ground truth (black circles). The logarithm of the estimated PHD surface is also plotted in Figure 4.4 (b), with a dynamic range from -15 to 5. Although several "false peaks" are presented, all of the eight scatters can be correctly identified on both figures.

In the second phase of the simulation, Monte Carlo (MC) simulations were performed to evaluate the localization performance in the presence of different LOS detection profiles of the proposed STAMP algorithm. We set the probability of detection of LOS path to 0, 0.3 and 0.5 respectively, while maintaining the probability of detection of multipath to 0.5 for all BSs. By randomly generating MS trajectories and scatter distributions, 100 independent MC simulations are performed with other parameters

utilized in the first phase. The curves of mean squared localization error of both the STAMP and the LOS-only methods are plotted as a function of time index in Figure 4.5 (a). The cumulative density function of the localization error over the total 60 time intervals and 100 MC runs are also shown in Figure 4.5 (b). As the probability of detection of LOS path decreases, the performance of LOS-only method decreases significantly, while the localization error of STAMP method almost maintains within 2 meters for all of the three LOS detectabilities. Note that the scenario with probability of detection of LOS path equal to 0 corresponds to the absolute NLOS case as discussed in Section 3.3. In this case, the proposed STAMP method is still able to jointly estimate the MS state and the scatter positions, since the number of BS nodes and scatters are both greater than three, which guarantees the STAMP identifiability.

In addition, the estimation performance of scatter position, or multipath channel was qualified by using the Optimal SubPattern Assignment (OSPA) metric [61]. In Figure 4.6(a), the OSPA distances are shown with the three different LOS detection profiles, which measures the differences in both localization and cardinality, and in Figure 4.6 (b) and (c), the localization error and cardinality error of OSPA metric are also plotted respectively. For all of the three metrics, the error curves decrease as a function of time since all scatters are assumed to be stationary. Also, as the probability of detection for LOS path increases, the scatter localization performance also enhanced.

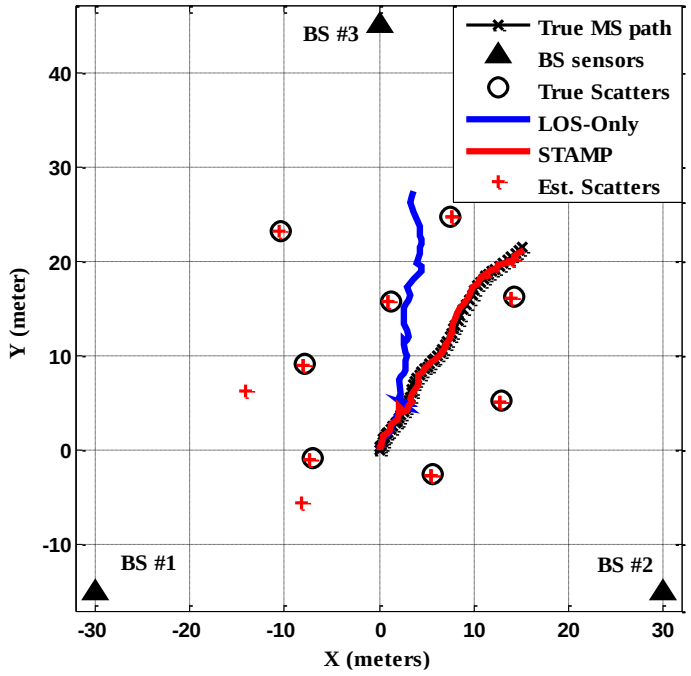

(a)

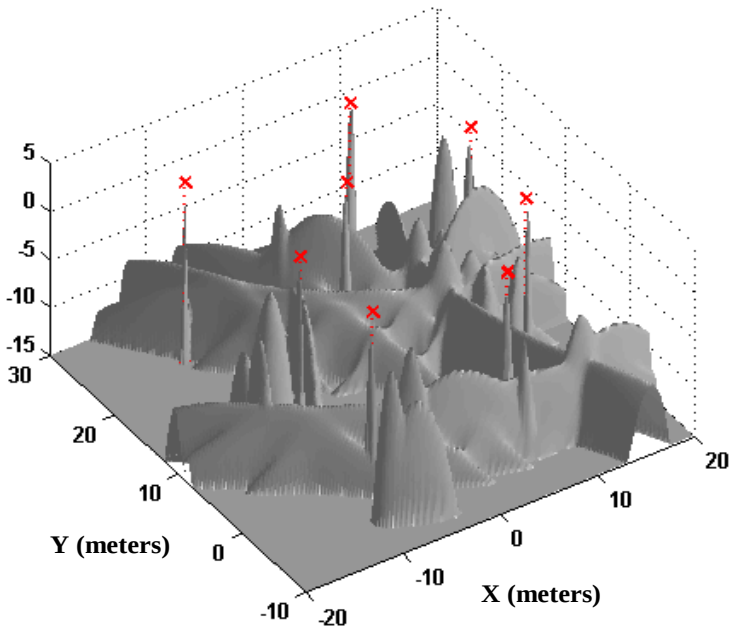

(b)

Figure 4.4: (a) Illustration of the simulated scenario: three BS nodes (triangles) and eight scatters (circles) and the true MS trajectory; the estimation results of STAMP and LOS-only method are both shown. (b) Logarithm of the estimated PHD surface of scatters, with ground truth marked as red crosses.

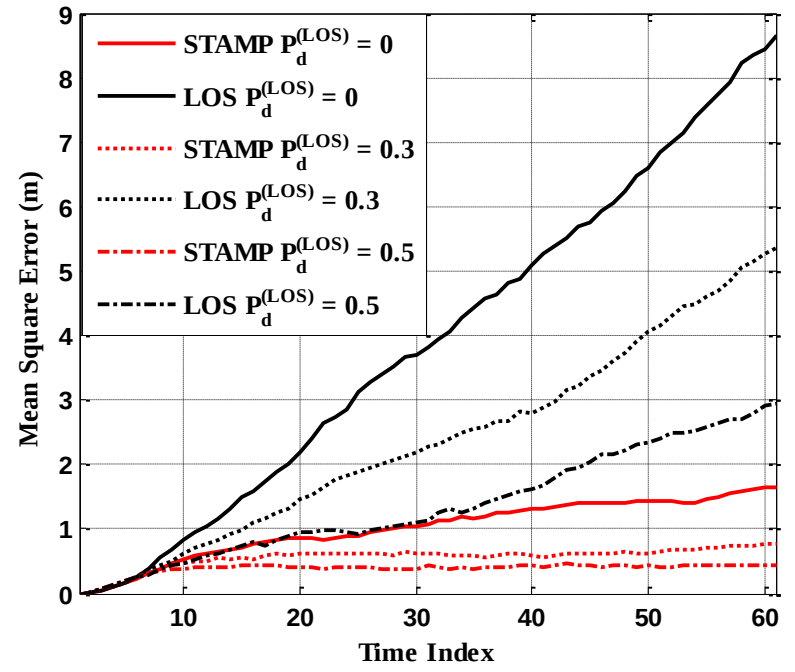

(a)

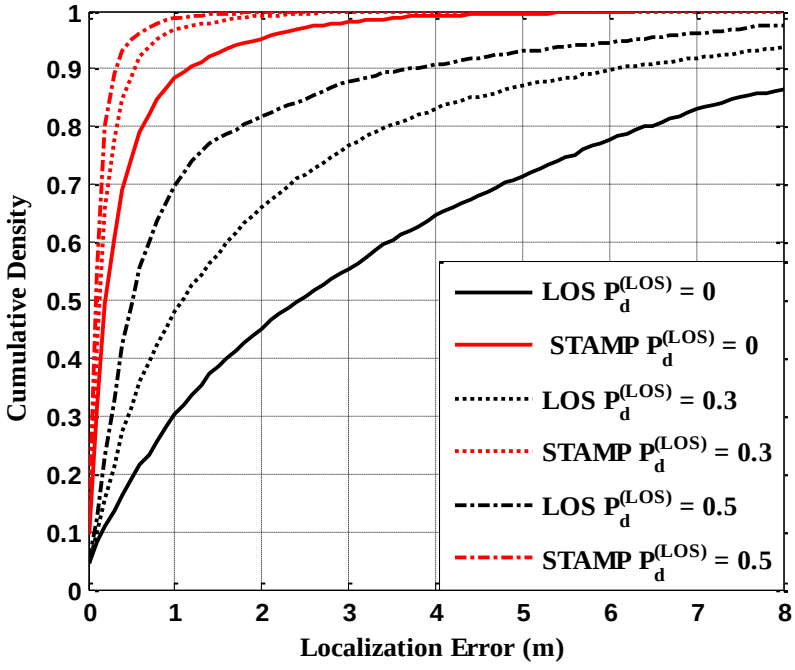

(b)

Figure 4.5: MC simulation for probability of detection of LOS path equal to 0, 0.3 and 0.5. Plots contains (a) mean squared MS localization error over time and (b) cumulative density function of MS localization error over all time interval and MC runs

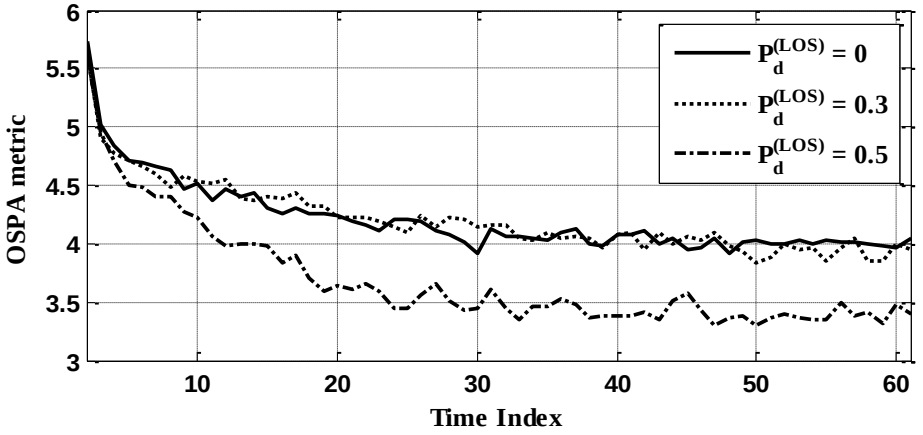

(a)

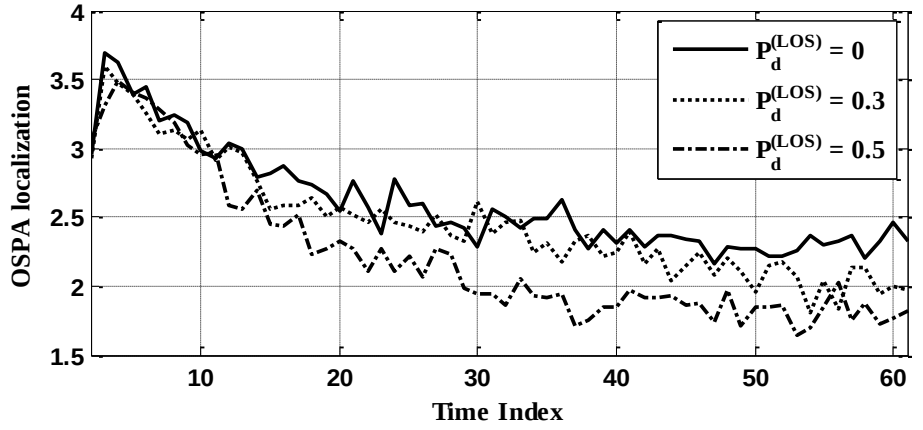

(b)

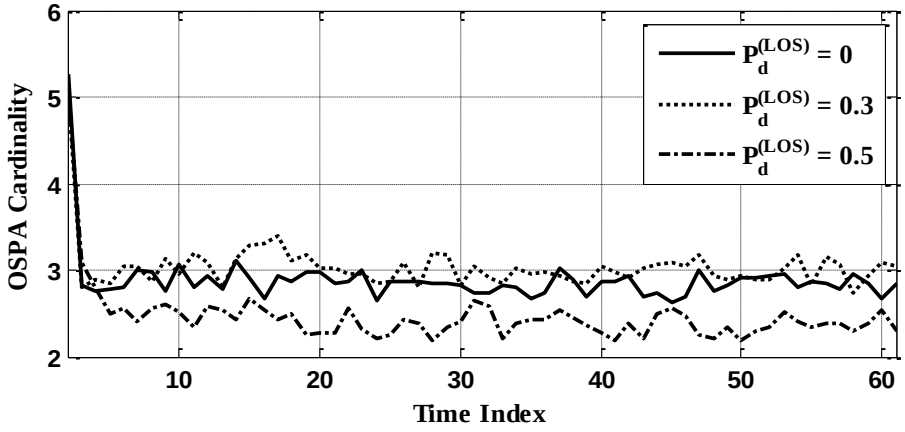

(c)

Figure 4.6: OSPA metric of scatter localization performance over time with (a) OSPA distance, (b) localization error and (c) cardinality error

4.5 Real-data Experiment Result

This section describes the results of applying STAMP to real data from an experiment conducted on the first floor atrium of an engineering building at Duke University. We consider an equivalent RF sources tracking problem by using a multistatic receiver BS nodes. A multi-channel S-band radar testbed system [41, 42] was utilized to track a RF transmitter. Figure 4.7 provides views of the experiment environment with the actual floor plan and the measured trajectory (black solid line) of the transmitter that was used as the target in this experiment. Three omnidirectional receiver antenna locating at (7.4, 1.7), (0, 3.18) and (4.5, -1.8) respectively. The NLOS areas are given in the gray regions due to the blockage of two large reinforced concrete pillars. The information about the building floor plan was assumed to be unavailable. However, since an indoor environment is considered, instead of the point scattering model utilized earlier, we explore the specular reflection model from flat planes reflectors as discussed in earlier chapters: the planes reflectors are essentially straight lines based on Hessian normal form: $x\cos\psi + y\sin\psi + \rho = 0$, with parameter vector $\mathbf{s} = [\psi, \rho]^T$. The reflective surfaces are assumed to be smooth enough and are able to produce images sources with a distance depending on the position of the incident source. Therefore, the multipath range observation model in (4.8) is modified as

$$g_i(\mathbf{x}_k, \mathbf{s}) = \left\| \mathbf{p}_k^{img} - \mathbf{r}_j \right\| + b_k \tag{4.67}$$

where

$$\mathbf{p}_k^{img} = \begin{bmatrix} -x_k \cos 2\psi - y_k \sin 2\psi - 2\rho \cos \psi \\ -x_k \sin 2\psi + y_k \cos 2\psi - 2\rho \sin \psi \end{bmatrix} \tag{4.68}$$

The proof of identifiability of the specular reflection model is similar as the point scattering model analyzed in Section IV, which is not included in this work.

We implemented the Single-Cluster PHD filter based STAMP algorithm with the number of particles equal to M = 100. The estimated target path (red solid line) are shown in Figure 4.7, which visually overlaps with the measured path ground truth (black solid line). The localization error of STAMP algorithm and LOS-only method are shown in Figure 4.8. Note that when the target is in a NLOS region (i.e., gray areas of Figure 4.8), the positioning errors are larger compared to the LOS regions. However, by exploiting the multipath observations with estimated multipath parameters, STAMP is able to maintain the target localization errors to within ±1 m for both x and y dimensions. On the other hand, estimation error of the LOS-only method in the LOS region approximates that of STAMP, however, since no observation is present in the NLOS regions, the location estimates diverge rapidly with time compared the STAMP results.

The logarithm of estimated GM-PHD surfaces of multipath parameter at four time instances (i.e., scan t = 11, 31, 61 and 85) are shown in Figure 4.9. The ground truth positions of the five walls (as denoted in Figure 4.7) are marked as red dots in Figure 4.9. For the given indoor scene, four planar reflectors of the area of interest, corresponding to four dominant Gaussian components, can be identified on estimated PHD surfaces, which are closed to the true values as marked by red dots.

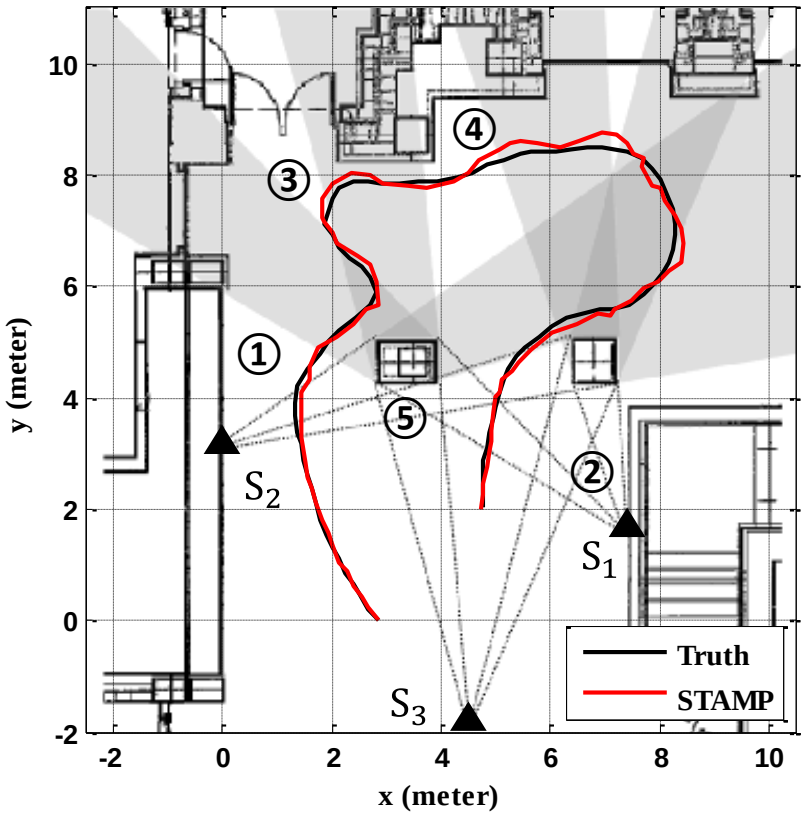

Figure 4.7: Illustration of the experiment scenario: three BSs are denoted by squares, the target trajectory are marked with solid lines and five plane reflectors are noted in circled numbers; the gray areas represent NLOS regions. Estimated target trajectory with the STAMP algorithm is marked in red line.

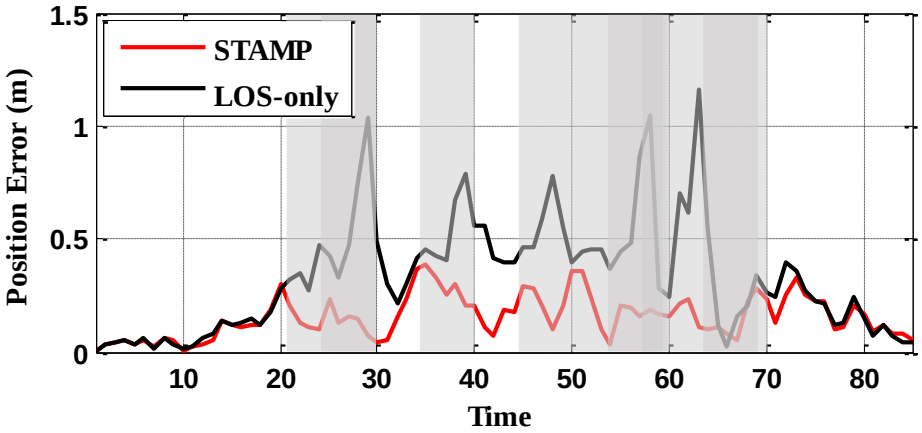

Figure 4.8: Localization error (Euclidean distance) of the STAMP method and LOS-only method.

The residual Guassian components in the estimated PHD surfaces may be caused by false alarms or other unmolded multipath propagations, e.g., 3D or multiple bounces reflections.

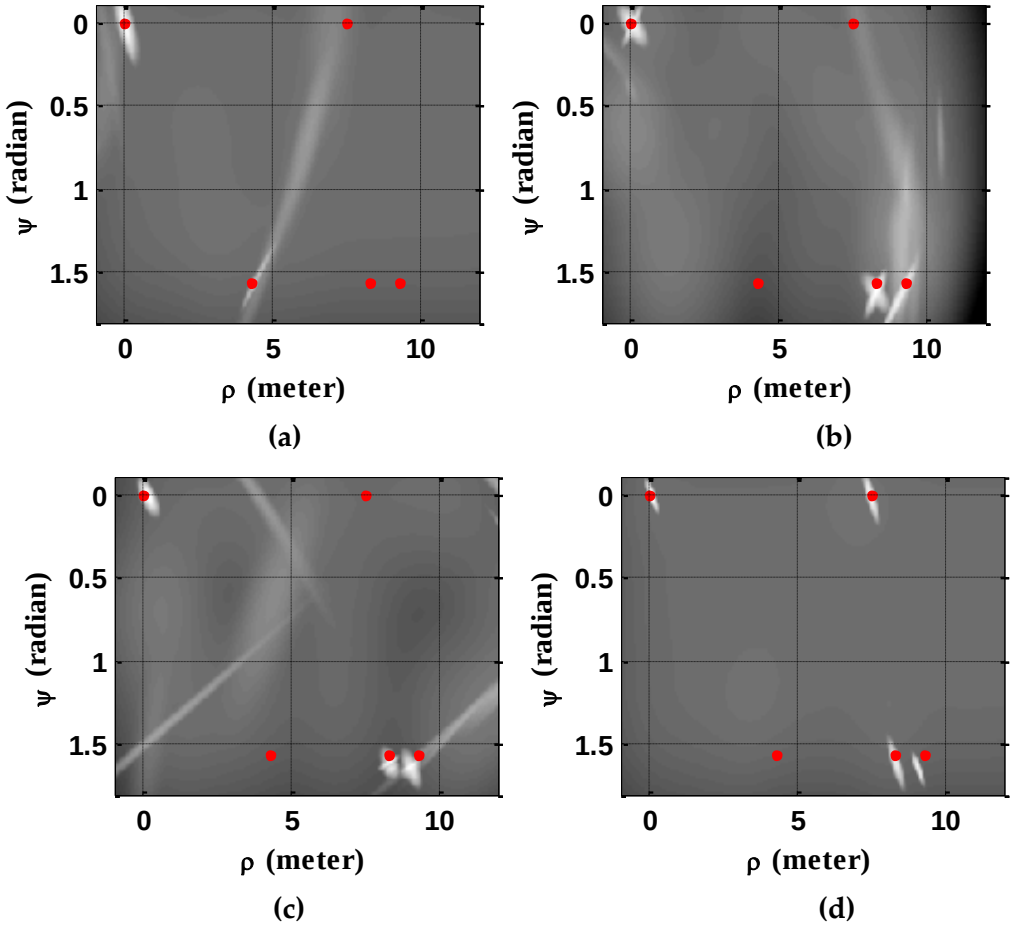

Figure 4.9: Estimated PHD intensity of multipath channels parameters at (a) t = 11, (b) t = 31, (c) t = 61 and (d) t = 85. The true values of plane reflectors are marked with red dots.

4.6 Summary

This chapter proposed a single-cluster PHD filter implementation of the simultaneous target and multipath positioning (STAMP) problem. The multipath

propagation was modeled with single bounce reflections from unknown random scatters. The proposed recursive Bayesian algorithm coupled a particle filter to obtain posterior probability distribution of mobile station (MS) position and MS-BS oscillator clock bias, which defined the parent process. By modeling the scatter state as a random finite set, a multi-sensor iterated Gaussian mixture PHD filter, defined as a daughter process, was utilized to estimate the PHD intensity of the scatter locations conditioned on the each particle of parent process. The CRLB based identifiability analysis has shown that, at least three BS nodes for each scatter and at least three scatters, were required to provide a finite CRLB on target position estimates. We also extended the CRLB in the case of data association uncertainty. Ambiguities due to the probability of erroneous propagation modes association hypotheses was discussed in terms of the information reduction matrix. A set of simulations and an illustrative real-data experiment for indoor target tracking problem were implemented using the proposed method; and improved target localization accuracy has been achieved even when the LOS propagation was not present over the course of the track.

5

Multi-static AOA STAMP

This chapter extends the application of STAMP to the problem of tracking a RF source (target) in complex multipath environments using Angle-of-Arrival (AOA) observations produced by a multi-static sensor array network. In the presence of time-varying number of multipath modes, the single cluster process, as introduced in Chapter 4, is formulated using a recursive Bayesian estimation framework: the target state is defined as the parent process and the multipath parameter state is defined as the daughter process. Instead of using particle presentations for the distribution of parent process, a multi-hypothesis data association method is used with Probability Hypothesis Density (PHD) filtering to improve the accuracy of the target state estimate. The Gaussian target state is updated based on classic multiple-scan maximum likelihood data association, and the update of multipath channel parameters is solved by a Gaussian Mixture PHD filtering conditioned on the target state estimate. Simulation and experimental results

using real data for an indoor target positioning problem demonstrates substantial improvements in localization accuracy with this method.

5.1 Problem Formulation

Consider the problem of tracking a moving RF source (target) in a two-dimensional space. Let target state vector $\mathbf{x}_k = [x_k, y_k, \dot{x}_k, \dot{y}_k]^T$, be the target x-y ground coordinates and vector velocity at scan k. The linear target dynamics with Gaussian process noise is given in (4.1) and (4.2).

The localization system is constituted with S multi-static sensor arrays with overlapping coverage. All sensors, with different locations and array orientations, produce a set of angle-of-arrival (AOA) observations. Let $z_{k,s}$ denote a single AOA observation from sth sensor array at time k, the Gaussian observation noise model is given by:

$$f(z|\boldsymbol{\Theta}_s, \mathbf{x}_k) = \begin{cases} \mathcal{N}\left(z_{s,k}; h_s^d(\mathbf{x}_k), \sigma^2\right), & \text{direct-path} \\ \mathcal{N}\left(z_{s,k}; h_s(\mathbf{x}_k, \boldsymbol{\theta}_s), \sigma^2\right), & \text{multipath} \end{cases}, \tag{5.1}$$

where the model $h_s^d(\mathbf{x}_k)$ and $h_s(\mathbf{x}_k, \boldsymbol{\theta}_s)$ denote nonlinear observation models for the LOS path and the multipath propagation respectively. Instead of using common multipath parameter for all sensors (e.g., the point scatter model as utilized in Chapter 4), this chapter assumes that each ULA observes independent multipath channel parameters, so that the $L \times 1$ vector $\boldsymbol{\theta}_s$ denotes the time invariant multipath parameters associated to the sth sensor array.

At each time k, there is only one source or target presented. However, the number of multipath propagation modes at each sensor array $N_{k,s}$ is a time-varying random variable. Previous solution of multi-hypothesis data association based STAMP algorithm estimates the stacked state vector $[\mathbf{x}_k^T, \boldsymbol{\theta}_{1,1}^T, \dots, \boldsymbol{\theta}_{1,N_{k,1}}^T, \boldsymbol{\theta}_{2,1}^T, \dots, \boldsymbol{\theta}_{S,N_{k,S}}^T]^T$, where the number of multipath channels $N_{k,s}, s = 1, \dots, S$ are estimated via a channel initiation and validation process. In this chapter, we represent the multipath channel parameter state as a random finite set (RFS) on $\mathcal{P} \in \mathbb{R}^L$.

$$\boldsymbol{\Theta}_s = \{\boldsymbol{\theta}_{s,1}, \dots, \boldsymbol{\theta}_{s,N_k}\} \in \mathcal{F}(\mathcal{P}) \tag{5.2}$$

Similarly, in the presence of imperfect detection, the observation set at time k is also modeled as a random finite set on space $\mathcal{Z} \in \mathbb{R}^2$

$$\mathbf{Z}_{s,k} = \{z_{s,k,1}, \dots, z_{s,k,|Z_k|}\} = Z_d(\mathbf{x}_k) \cup Z(\mathbf{x}_k, \boldsymbol{\Theta}_s) \cup C_{s,k} \in \mathcal{F}(\mathcal{Z}) \tag{5.3}$$

where $Z_d(\mathbf{x}_k)$ denotes the direct path observation, $Z(\mathbf{x}_k, \boldsymbol{\Theta}_s)$ represents the observation set of multipath, and $C_{s,k}$ denotes the set of false alarms detected at time k. In order to estimate the joint STAMP state $\mathbb{X}_k = \{\mathbf{x}_{1:k}, \boldsymbol{\Theta}_1, \dots, \boldsymbol{\Theta}_S\}$, single-cluster point process is modeled, where the target state $\mathbf{x}$ represents the parent state vector and the multipath mode parameter $\boldsymbol{\Theta}_s, s = 1, \dots, S$ represent its daughter process. Therefore, the single cluster PHD recursion is written as:

$$D(\mathbf{x}_k, \boldsymbol{\Theta}_1, \dots, \boldsymbol{\Theta}_S | \mathbf{Z}_{1:k}) = \frac{\alpha f(\mathbf{x}_k | \mathbf{Z}_{1:k-1}) L(\mathbf{Z}_k | \mathbf{x}_k, \mathbf{Z}_{k-1})}{f(\mathbf{x}_k | \mathbf{Z}_{1:k})} \prod_{S=1}^{S} D\left(\boldsymbol{\Theta}_S \middle| \mathbf{x}_k, \mathbf{Z}_{s,1:k}\right) \tag{5.4}$$

where α is a normalized coefficient. $D\left(\boldsymbol{\Theta}_s|\mathbf{x}_k, \mathbf{Z}_{s,1:k}\right), s = 1, \ldots, S$ is the measurement updated PHD intensity the of daughter process conditioned on $\mathbf{x}_k$

$$D\left(\boldsymbol{\Theta}_s|\mathbf{x}_k, \mathbf{Z}_{s,1:k}\right) = \left[1 - P_d(\boldsymbol{\Theta}_s|\mathbf{x}_k) + \sum_{z\epsilon\mathbf{Z}_{s,k}} \frac{P_d(\boldsymbol{\Theta}_s|\mathbf{x}_k) f(z|\boldsymbol{\Theta}_s, \mathbf{x}_k)}{\eta_z(\mathbf{x}_k|\mathbf{Z}_{s,1:k-1})}\right] \times \left[D\left(\boldsymbol{\Theta}_s|\mathbf{x}_k, \mathbf{Z}_{s,1:k-1}\right)\right] \tag{5.5}$$

$$\eta_z\left(\mathbf{x}_k|\mathbf{Z}_{s,1:k-1}\right) = \kappa(z) + P_d^{(d)}(\mathbf{x}_k) g(z|\mathbf{x}_k) + \int P_d(\boldsymbol{\Theta}_s|\mathbf{x}_k) D\left(\boldsymbol{\Theta}_s|\mathbf{x}_k, \mathbf{Z}_{s,1:k-1}\right) f(z|\mathbf{x}_k, \boldsymbol{\Theta}_s) d\boldsymbol{\Theta}_s \tag{5.6}$$

where $P_d(\boldsymbol{\Theta}|\mathbf{x}_k)$ is the probability of detection. The first term of $\eta_z(\mathbf{x}_k|\mathbf{Z}_{1:k-1})$ refer to likelihood of false alarm, the second term refers to the direct path, and the last term refers to all multipath modes based on intensity $D\left(\boldsymbol{\Theta}_s|\mathbf{x}_k, \mathbf{Z}_{s,1:k-1}\right)$. Similar to (4.18), the multi-component likelihood of the measurement set $\mathbf{Z}_k$ conditioned on target state $\mathbf{x}_k$ is given by

$$L\left(\mathbf{Z}_{s,k}|\mathbf{x}_k, \mathbf{Z}_{s,1:k-1}\right) = \frac{\prod_{z\epsilon\mathbf{Z}_k} \eta_z(\mathbf{x}_k|\mathbf{Z}_{s,1:k-1})}{\exp\{\int P_d(\boldsymbol{\Theta}_s|\mathbf{x}_k) D(\boldsymbol{\Theta}_s|\mathbf{x}_k, \mathbf{Z}_{s,1:k-1}) d\boldsymbol{\Theta}_s\}} \tag{5.7}$$

5.2 Multi-Hypothesis Single-Cluster PHD filtering for STAMP

The STAMP problem is divided into two stages to update the target state and multipath parameters successively. A single-cluster PHD filter is used to update the multipath parameters based on Finite Set Statistics (FISST), while an explicit multi-hypothesis EKF is introduced to update the target state. Therefore, instead of using

particle representations, the parent process $\mathbf{x}_k$ (i.e., target state) at time k is modeled a single Gaussian distribution,

$$f(\mathbf{x}_k|\hbar_{1:k}, \mathbf{Z}_{1:k}) = \mathcal{N}(\mathbf{x}_k; \hat{\mathbf{x}}_k, \mathbf{P}_k) \tag{5.8}$$

and the intensity functions of the daughter process, $\mathbf{\Theta}_s$, $s = 1, \ldots, S$, are modeled as a Gaussian mixture distribution conditioned on $\mathbf{x}_k$ as

$$D\left(\mathbf{\Theta}_s \middle| \mathbf{x}_k, \mathbf{Z}_{s,1:k}\right) = \sum_{j=1}^{J_{s,k}} w_{s,k}^{(j)} \mathcal{N}(\mathbf{\Theta}_s; \boldsymbol{\mu}_{s,k}^{(j)}, \mathbf{C}_{s,k}^{(j)}), \quad s = 1, \ldots, S \tag{5.9}$$

In (4.8), $\hbar_{1:k} = \{\hbar_1, \hbar_2, \ldots, \hbar_k\}$ is defined as a *data association hypothesis sequence* up to time *k*. At each time *k*, the classic maximum likelihood data association (i.e., 2D assignment) is performed to find the optimal correspondence $\hbar_k$ between observations $z \epsilon \mathbf{Z}_{s,k}$ and the direct path, false alarm and multipath modes. In this case, the mean vector $\boldsymbol{\mu}_{s,k}^{(j)}$ of each Gaussian component of $D\left(\mathbf{\Theta}_s \middle| \mathbf{x}_{k-1}, \mathbf{Z}_{s,1:k-1}\right)$ is represented by a hypothesized multipath channel, and the weight $w_{s,k}^{(j)} \in (0, 1)$ refers to the associated confidence factor. The estimated number of multipath channels in $\mathbf{\Theta}_s$ is given by

$$n_{k,s} = \sum_{j=1}^{J_{s,k}} w_{s,k}^{(j)} \tag{5.10}$$

The principle idea of Multi-Hypothesis Single-Cluster PHD filtering is to obtain an enhanced estimate of the parent distribution $f(\mathbf{x}_k|\hbar_{1:k}, \mathbf{Z}_{1:k})$ by applying the multi-dwell data association via the joint association likelihood optimization up to time *k*. The estimated $f(\mathbf{x}_k|\hbar_{1:k}, \mathbf{Z}_{1:k})$ is then utilized to update the daughter process $D(\mathbf{\Theta}_s|\mathbf{x}_k, \mathbf{Z}_{1:k})$

via conventional GM-PHD update steps. Note that the multi-dwell data association $\hbar_{1:k}$ is only utilized to update $f(\mathbf{x}_k|\hbar_{1:k}, \mathbf{Z}_{1:k})$, while the update of $D(\mathbf{\Theta}_s|\mathbf{x}_k, \mathbf{Z}_{1:k})$ is solely conditioned on $\mathbf{x}_k$ independent of any data association but via FISST. The general flow chart of the proposed STAMP algorithm is shown in Figure 5.2.

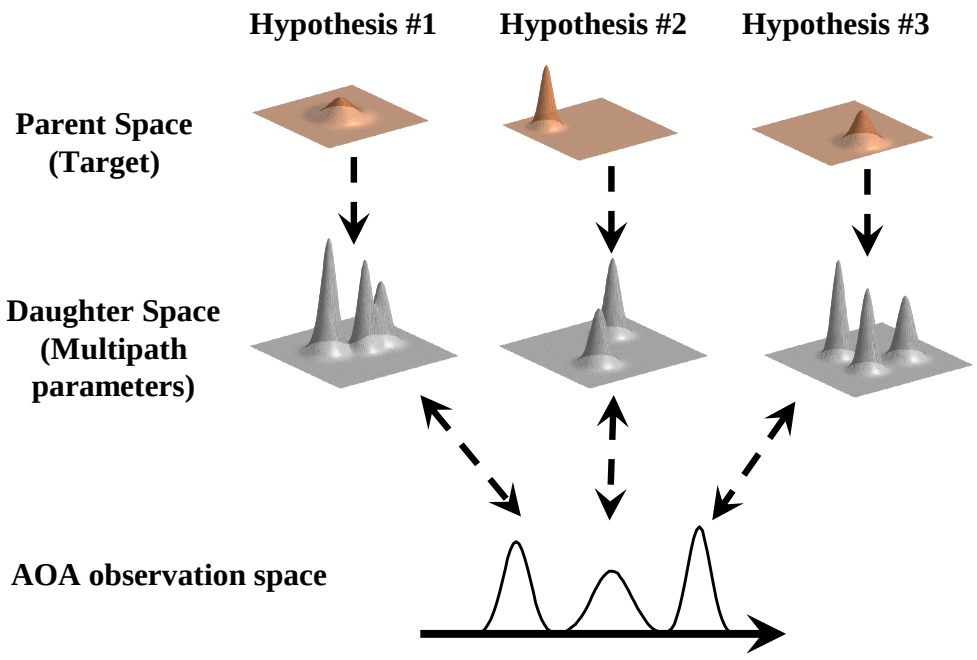

Figure 5.1: Visual illustration of the multi-hypothesis based cluster process. Each data association produces a parent process of target state, and the associated daughter process of multipath parameters is conditioned on the given parent process.

By incorporating the multi-hypothesis framework, the recursion in (5.4) can be modified as:

$$D(\mathbf{x}_k, \mathbf{\Theta}_1, \ldots, \mathbf{\Theta}_S|\hbar_{1:k}, \mathbf{Z}_{1:k}) = \alpha \frac{f(\mathbf{x}_k|\hbar_{1:k-1}, \mathbf{Z}_{1:k-1}) L(\mathbf{Z}_{1:k}|\mathbf{x}_{1:k}, \hbar_{1:k},)}{f(\mathrm{x}_k|\mathbf{Z}_{1:k}, \hbar_{1:k})} \prod_{s=1}^{S} D\left(\mathbf{\Theta}_s \middle| \mathbf{x}_k, \mathbf{Z}_{s,1:k}\right) \tag{5.11}$$

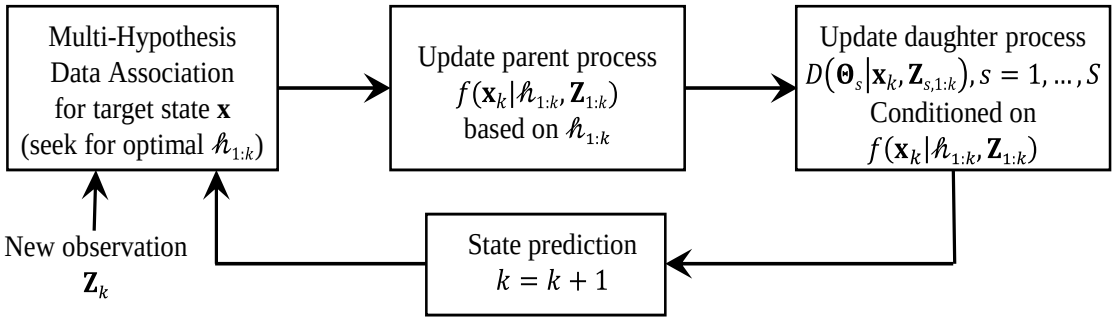

Figure 5.2: General flow-chart of the proposed multi-hypothesis single cluster PHD filter for STAMP.

where $L(\mathbf{Z}_{1:k}|\mathbf{x}_k, \hbar_{1:k},)$ is the joint association likelihood to be evaluated. Multi-hypothesis data association, as introduced in Chapter 2 and 3, seeks to find the optimal hypothesis sequence by maximizing the joint association likelihood function of the cumulative observation set $\mathbf{Z}_{1:k}$ given cumulative target state $\mathbf{x}_{1:k}$, so that the optimal association sequence $\hbar^*_{1:k}$ could be obtained by,

$$\hbar^*_{1:k} = \underset{\hbar_{1:k}}{\operatorname{argmax}}\, L(\mathbf{Z}_{1:k}|\mathbf{x}_{1:k}, \hbar_{1:k}) \tag{5.12}$$

Therefore, each association sequence $\hbar_{1:k}$ includes its own pair of parent process $f(\mathbf{x}_k|\mathbf{Z}_{1:k}, \hbar_{1:k})$ and daughter process $D(\boldsymbol{\Theta}_s|\mathbf{x}_k, \mathbf{Z}_{1:k})$. In order to recursively estimate the optimal $\hbar^*_{1:k}$, the joint association likelihood can be decomposed as:

$$L(\mathbf{Z}_{1:k}|\mathbf{x}_k, \hbar_{1:k}) \propto \underbrace{\frac{\prod_{s=1}^{S} L(\mathbf{Z}_{s,k}, \hbar_{s,k}|\mathbf{x}_k, \hbar_{1:k-1}, \mathbf{Z}_{1:k-1})}{L(\mathbf{Z}_k, \hbar_k|\mathbf{x}_k, \hbar_{1:k-1}, \mathbf{Z}_{1:k-1})}} \times L(\mathbf{Z}_{1:k-1}|\hbar_{1:k-1}) \tag{5.13}$$

where $\hbar_{s,k}$ represents the temporal data hypothesis for sth sensor array only, i.e., $\hbar_k = \{\hbar_{1,k}, \ldots, \hbar_{S,k}\}$. According to the target dynamics model given in (4.1) and (4.2), the predicted distribution density of the parent process from time index k-1 to k is given as

$$f(\mathbf{x}_k|\hbar_{1:k-1}, \mathbf{Z}_{1:k-1}) = \mathcal{N}(\mathbf{x}_k; \mathbf{F}_t\bar{\mathbf{x}}_{k-1}, \mathbf{F}_t\mathbf{P}_{k-1}\mathbf{F}_t^T + \mathbf{D}\mathbf{Q}_k\mathbf{D}^T) = \mathcal{N}(\mathbf{x}_k; \bar{\mathbf{x}}_{k|k-1}, \mathbf{P}_{k|k-1}) \tag{5.14}$$

Denote the observation set $\mathbf{Z}_{s,k} = \{z_{s,k,1}, z_{s,k,2}, \ldots, z_{s,k,|\mathbf{Z}_{s,k}|}\}$, where $|\mathbf{Z}_{s,k}|$ is the total number of observations for sth sensor array at time k. Under the assumption of stationary multipath channel parameters, i.e., $\mathbf{\Theta}_s$ is time-invariant, the temporal likelihood $L(\mathbf{Z}_{s,k}, \hbar_{s,k}|\mathbf{x}_k, \hbar_{1:k-1}, \mathbf{Z}_{1:k-1})$ in (17) can be computed by

$$L(\mathbf{Z}_{s,k}, \hbar_{s,k}|\mathbf{x}_k, \hbar_{1:k-1}, \mathbf{Z}_{1:k-1}) = \frac{\prod_{i=1}^{|\mathbf{Z}_{s,k}|}\sum_{j=-1}^{J_{s,k-1}} C_{i,j}(\hbar_{s,k}) l_{s,j}(z_{s,k,i}|\bar{\mathbf{x}}_{k|k-1})}{\exp\{\sum_{j=1}^{J_{s,k-1}} P_d^{(j)} w_{s,k-1}^{(j)}\}} \tag{5.15}$$

with

$$l_{s,j}(z|\bar{\mathbf{x}}_{k|k-1}) = \begin{cases} w_{s,k-1}^{(j)} P_d^{(j)} \mathcal{N}(z; h_{s,k}^{(j)}, \epsilon_{s,k}^{(j)}), & j \geq 0 \\ \kappa(\mathbf{z}) + w_0^{\gamma}, & j = -1 \end{cases} \tag{5.16}$$

$$h_{s,k}^{(j)} = \begin{cases} h_s(\bar{\mathbf{x}}_{k|k-1}, \boldsymbol{\mu}_{s,k-1}^{(j)}), & j \geq 1 \\ h_s^d(\bar{\mathbf{x}}_{k|k-1}), & j = 0 \end{cases} \tag{5.17}$$

$$\epsilon_{s,k}^{(j)} = \begin{cases} (\mathbf{h}_{s,k}^{(j)})^T \mathbf{P}_{k|k-1} \mathbf{h}_{s,k}^{(j)} + (\mathbf{g}_{s,k}^{(j)})^T \mathbf{C}_{s,k-1}^{(j)} \mathbf{g}_{s,k}^{(j)} + \sigma^2, j \geq 1 \\ (\mathbf{h}_k^{(d)})^T \mathbf{P}_{k|k-1} \mathbf{h}_k^{(d)} + \sigma^2, \quad j = 0 \end{cases} \tag{5.18}$$

where 4×1 vector $\mathbf{h}$ and L×1 vector $\mathbf{g}$ are gradient vectors of the observation function with respect to target state $\mathbf{x}$ and multipath parameter $\boldsymbol{\theta}$ evaluated using $\bar{\mathbf{x}}_{k|k-1}$ and $\boldsymbol{\mu}_{s,k-1}^{(j)}$. The binary assignment variable $C_{i,j}(\hbar_{s,k}) = \{0,1\}$ is based on a given association

hypothesis $\hbar_{s,k}$: for sth sensor array, $C_{i,j}(\hbar_{s,k}) = 1$ represents that ith observation corresponds to jth component, and $C_{i,j}(\hbar_{s,k}) = 0$ otherwise. In particular, $C_{i,0}(\hbar_{s,k}) = 1$ implies that ith observation corresponds to LOS observation, while $C_{i,-1}(\hbar_{s,k}) = 1$ denotes ith observation corresponds to false alarm or a new birthed mode. Under the assumption of one-to-one correspondence between components and observations, each multipath propagation channel can produce at most one observation and vice versa, which can be expressed as following constraints:

$$\sum_{i=0}^{|Z_k|} C_{i,j}(\hbar_{s,k}) = 1, \;\; j = 0,1,\dots,J_{k-1} \quad \sum_{j=-1}^{J_{k-1}} C_{i,j}(\hbar_{s,k}) = 1, \;\; i = 1,\dots,|\mathbf{Z}_k| \qquad (5.19)$$

where $i = 0$ corresponds to a pseudo-observation state for unassociated components (i.e., the raymode is not detected). It can be seen that $L\left(\mathbf{Z}_{s,k}, \hbar_{s,k} \middle| \mathbf{x}_k, \hbar_{1:k-1}, \mathbf{Z}_{1:k-1}\right)$ is in a Gaussian distributed form. If we sum over all possible $\hbar_{s,k}$ for a given $\hbar_{1:k-1}$, the multi-component likelihood (13) will be yielded which integrates all possible data associations h_k, and a Gaussian mixture multi-component likelihood distribution $L\left(\mathbf{Z}_{s,k} \middle| \mathbf{x}_k, \hbar_{1:k-1}, \mathbf{Z}_{1:k-1}\right)$ is obtained.

Since the number of $\hbar_k$ grows exponentially as k increases, only the H-best sequences are kept at each time instance in order to ensures the computational feasibility of the multi-hypothesis method. Therefore, for given $\hbar_{k-1}$, we firstly compute the H-best temporal association $\hbar_k$ for each association parent $h_{1:k-1}$ based on (5.13) and (5.15). Then from the total H^2 candidates for all parents $\hbar_{1:k-1}$, only H-best $\hbar_{1:k}$ sequences are kept while the rest $H(H-1)$ are pruned (i.e., the H largest values in (5.13) for all $\hbar_{1:k-1}$).

Hence, the number of hypothesis sequence kept at each time step is maintained as H, which ensures real-time computational feasibility.

After the H-best hypotheses are obtained, the posterior of the parent process can be updated for a given data association sequence $\hbar_{1:k}$ as

$$f(\mathbf{x}_k|\hbar_{1:k}, \mathbf{Z}_{1:k}) = \mathcal{N}(\mathbf{x}_k; \bar{\mathbf{x}}_k, \mathbf{P}_k) \tag{5.20}$$

where

$$\bar{\mathbf{x}}_k = \bar{\mathbf{x}}_{k|k-1} + \mathbf{P}_{k|k-1}\mathbf{H}_{\hbar_k}\mathbf{S}_{\hbar_k}^{-1}\mathbf{y}_{\hbar_k} \tag{5.21}$$

$$\mathbf{P}_k = \left(\mathbf{I}_4 - \mathbf{P}_{k|k-1}\mathbf{H}_{\hbar_k}^T\mathbf{S}_{\hbar_k}^{-1}\mathbf{H}_{\hbar_k}\right)\mathbf{P}_{k|k-1} \tag{5.22}$$

$$\mathbf{y}_{\hbar_k} = \bigoplus_{\substack{C_{i,j}(\hbar_{s,k})=1 \\ s=1,\ldots,S}} \left(z_{s,k,i} - h_{s,k}^{(j)}\right), \quad \mathbf{H}_{\hbar_k} = \bigoplus_{\substack{C_{i,j}(\hbar_{s,k})=1 \\ s=1,\ldots,S}} \left(\mathbf{h}_{s,k}^{(j)}\right)^T, \quad \mathbf{S}_{\hbar_k} = \underset{\substack{C_{i,j}(\hbar_{s,k})=1 \\ s=1,\ldots,S}}{Diag} \epsilon_{s,k}^{(j)} \tag{5.23}$$

and $\bigoplus$ and $Diag$ denote vertical and diagonal concatenation operation when the observation-raymode pair is valid $C_{i,j}(\hbar_{s,k}) = 1$ according to $\hbar_{s,k}$.

Once the posterior distribution of the parent process $f(\mathbf{x}_k|\hbar_{1:k}, \mathbf{Z}_{1:k})$ is obtained, the conditional daughter process for multipath channel parameter $\mathbf{\Theta}_s$ is then updated according to (5.5) and (5.6). As mentioned in the last section, the posterior intensity $D(\mathbf{\Theta}_s|\mathbf{x}_k, \mathbf{Z}_{1:k})$ is the sum of three terms: the detected pre-observed channels, the miss-detected pre-observed channels and newly appearing channels. Assume the PHD intensity of the birth of multipath channels are also Gaussian mixture in the form of:

$$\gamma(\mathbf{\Theta}_s) = \sum_{j=1}^{J_\gamma} w_{\gamma,s}^{(j)} \mathcal{N}\left(\mathbf{\Theta}_s \middle| \boldsymbol{\mu}_{\gamma,s}^{(j)}, \mathbf{C}_{\gamma,s}^{(j)}\right) \tag{5.24}$$

where J_γ, $w_{\gamma,s}^{(j)}$, $\boldsymbol{\mu}_{\gamma,s}^{(j)}$ and $\mathbf{C}_{\gamma,s}^{(j)}, j = 1, \ldots, J_\gamma$ characterize the shape of the birth intensity. Therefore, the GM-PHD solution of (5.5) for the sth sensor array can be written as:

$$D(\boldsymbol{\Theta}_s|\mathbf{x}_k, \mathbf{Z}_{1:k}) = \sum_{j=1}^{J_{s,k-1}} \left(1 - P_d^{(j)}\right) w_{s,k-1}^{(j)} \mathcal{N}\left(\boldsymbol{\Theta}_s \middle| \boldsymbol{\mu}_{s,k-1}^{(j)}, \mathbf{C}_{s,k-1}^{(j)}\right)$$

$$+ \sum_{i=1}^{|Z_{s,k}|} \left[\frac{\sum_{j=1}^{J_{s,k-1}} l_{s,j}(z_{s,k,i}|\bar{\mathbf{x}}_k) \mathcal{N}\left(\boldsymbol{\Theta} \middle| \boldsymbol{\mu}_{s,k}^{(i,j)}, \mathbf{C}_{s,k}^{(i,j)}\right) + \sum_{j'=1}^{J_\gamma} l_{s,j'}(z_{s,k,i}|\bar{\mathbf{x}}_k) \mathcal{N}\left(\boldsymbol{\Theta} \middle| \boldsymbol{\mu}_{s,k}^{(i,j')}, \mathbf{C}_{s,k}^{(i,j')}\right)}{\sum_{j=-1}^{J_{s,k-1}} l_j(z_{s,k,i}|\bar{\mathbf{x}}_k) + \sum_{j'=1}^{J_\gamma} l_{s,j'}(z_{s,k,i}|\bar{\mathbf{x}}_k)} \right] \tag{5.25}$$

Here $l_j\left(z_{s,k,i}\middle|\bar{\mathbf{x}}_k\right)$ is with the same form as (5.15) except it is evaluated with the posterior distribution $f(\mathbf{x}_k|h_{1:k}, \mathbf{Z}_{1:k})$, or $\mathcal{N}(\mathbf{x}_k; \bar{\mathbf{x}}_k, \mathbf{P}_k)$, given in (5.20). The updated Gaussian mean and covariance matrix in (5.9) are given by:

$$\boldsymbol{\mu}_{s,k}^{(i,j)} = \boldsymbol{\mu}_{s,k-1}^{(j)} + \frac{\mathbf{C}_{s,k-1}^{(j)} (\mathbf{g}_{s,k}^{(j)})^T \left(z_{s,k,i} - h_{s,k}^{(j)}\right)}{\epsilon_{s,k}^{(j)}} \tag{5.26}$$

$$\mathbf{C}_{s,k}^{(i,j)} = \left(\mathbf{I}_L - \frac{\mathbf{C}_{s,k-1}^{(j)} \mathbf{g}_{s,k}^{(j)} (\mathbf{g}_{s,k}^{(j)})^T}{\epsilon_{s,k}^{(j)}}\right) \mathbf{C}_{s,k-1}^{(j)} \tag{5.27}$$

In order to limit the exponential growth of $J_{s,k}$ over time, Gaussian component pruning and clustering steps described in [59] are employed (in our work, the pruning and merging thresholds are 0.001 and 4 respectively). Note that, for computational efficiency, we decouple the correlation between target process and the reflector parameters to yield a suboptimal solution. This decoupling provides satisfactory estimation results as shown in the next section. However if necessary, the correlation can be recovered as discussed in [64].

5.3 Simulation Evaluation

This section illustrates the proposed STAMP algorithm for the application of multi-sensor AOA target tracking problem in an indoor environment. Two sensor arrays operate asynchronously and produce a set of AOA observations at each dwell in the presence of imperfect detection. The target dynamic model in a 2D scenario is given in (4.1) and (4.2). Since indoor environment is considered, physical optics based multipath propagating models of specular reflections from flat planes reflectors, which are defined as straight lines based on Hessian normal form: $x\cos\psi + y\sin\psi + \rho = 0$, with parameter vector $\boldsymbol{\theta} = [\psi, \rho]^T$. The planes are assumed to be specular reflectors and are able to produce images source with a bearing depending on the position of the incident source. The AOA observation model for a direct path measurement is given by

$$h_s^d(\mathbf{x}_k) = \frac{\cos\theta_s(x_k - x_s) + \sin\theta_s(y_k - y_s)}{\sqrt{(x_k - x_s)^2 + (y_k - y_s)^2}} \tag{5.28}$$

and for multipath measurements:

$$h_s(\mathbf{x}_k, \boldsymbol{\theta}) = \frac{\cos\theta_s(x'_{k,s} - x_s) + \sin\theta_s(y'_{k,s} - y_s)}{\sqrt{(x'_{k,s} - x_s)^2 + (y'_{k,s} - y_s)^2}} \tag{5.29}$$

$$x'_{k,s} = -x_k\cos 2\psi - y_k\sin 2\psi - 2\rho\cos\psi \tag{5.30}$$

$$y'_{k,s} = -x_k\sin 2\psi + y_k\cos 2\psi - 2\rho\sin\psi \tag{5.31}$$

where (x_s, y_s) and θ_s are x-y coordinate and orientation of sth sensor array.

The simulation scenario is illustrated in Figure 5.3(a). Two static sensor arrays, with an overlapping area of surveillance, locate at (0, 8) and (8, 0) with orientation 0 and $\pi/2$ respectively. Each array produces zero-mean Gaussian observation noise with AOA error standard deviation $\sigma = 0.005$. The probability of detection of direct path

observation is assumed to be 0.95, and probability of detection of multipath observation is assumed to be 0.8. The probability of false alarm is assumed to be 0.1. With 20 array elements for both arrays, the false detections are modeled by a Poisson point process with the mean number of false detection $\mu = 2$ at each time instant. The two arrays locate at two sides of a square room, where the direct path observations are occasionally undetectable due to blockage, as shown in Figure 5.3(a). Six planar reflector (i.e., walls of the room) are indicated from ① to ⑥ with parameter vectors (0, 1.2), (π/2, 1.2), (0, 15.2), (π/2, 5.2), (0, 5) and (π/2, 15.2). The target starts from lower-left corner (3.7, 4.9), moves along the black solid line based on a constant velocity dynamic model and ends in (3, 8). The total number of observation dwells is K = 95. The NLOS area for each array is represented by the gray region: for array s_1, the target NLOS stays in NLOS from k = 53 to 94, and for array s_2, the target moves in NLOS from k = 21 to 81.

Letting the number of hypothesis $\hbar_{1:k}$ at each dwell $H = 100$, Figure 5.3(b) illustrates the estimated target path over the true target trajectory using the proposed STAMP algorithm. It can be observed that the localization error is small for both LOS and NLOS situation by exploiting the multipath observations. The estimation of the GM-PHD surfaces of multipath parameter for both arrays are shown in Figure 5.4. All of the planar reflectors can be correctly identified on estimated PHD surfaces: reflector 1, 3 and 4 are observed by array s_1 and reflector 1, 3 and 4 are observed by array s_2. Several additional reflectors (Gaussian components) with can be also observed on the PHD surfaces, which are due to the false AOA measurements.

To evaluate the effectiveness of multi-hypothesis data association, Monte Carlo

simulations were performed to compare the tracking performance for different values of H, i.e., the number of hypothesis sequence kept at each dwell. The performance metric utilized is the offtrack rate at each dwell, i.e., the percentage of the number of realizations with an instantaneous target position estimation error greater 1 meter. Figure 5.5 illustrates the off-track error rate as a function of time for 100 independent runs for the values of H as 1, 10, 30 and 100 (when H = 1, the multi-hypothesis data association yields the single dwell nearest-neighbor method). Moving from LOS condition to NLOS, the off-track error rate generally increases with time. As the value of H increases, lower off-track rates, or improved tracking performances, can be obtained. For the scene of simulation, the case when H = 100, the maximum off-track rate at the end of the track is approximately 50%, representing half of the realizations could maintain a maximum localization error within 1 m for both LOS and NLOS situation.

5.4 Real data Experiment

This section describes the results of applying STAMP to real data from an experiment conducted on the first floor atrium of an engineering building at Duke University. A multi-static indoor S-band radar testbed system [36, 37] was used to track a RF transmitter, where the two receiver array locate at (5, 0) and (0, 5) with orientation 0 and $\pi/2$ respectively. Each receiver array contains 16 array elements and both transmit and receive antennas were omnidirectional. Figure 5.6(a) provides views of the experiment environment with black solid line as the measured trajectory of the transmitter which was used as the target in this experiment. The NLOS areas are given in the gray regions due to the blockage of two large reinforced concrete pillars. The

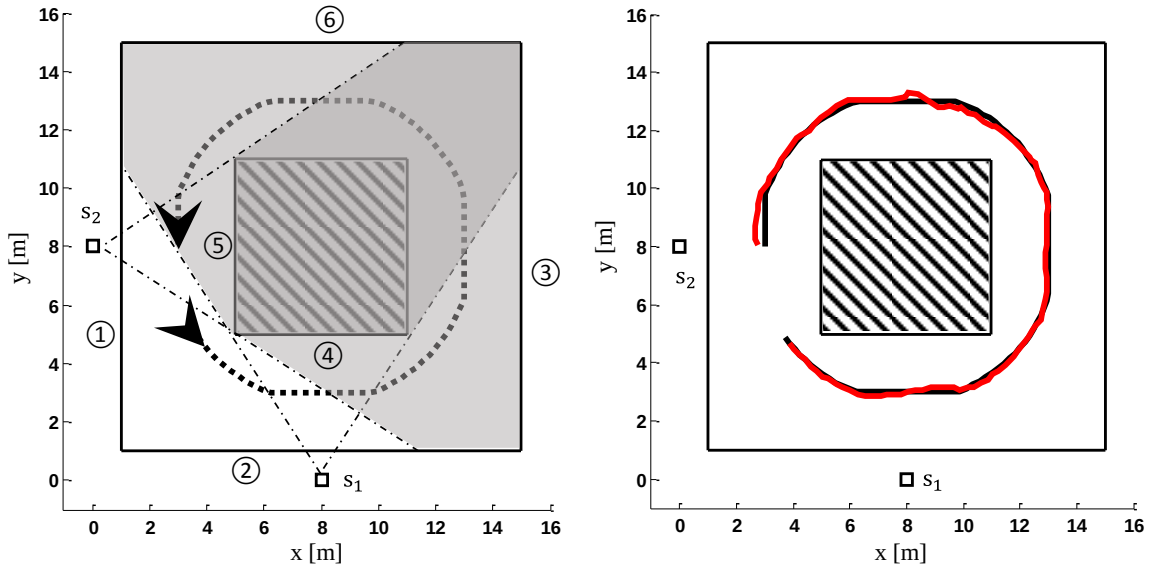

Figure 5.3: (a) illustration of the simulated scenario: two sensor arrays are denoted by squares, the target trajectory are marked with dashed lines and six plane reflectors are noted in circled numbers; the gray areas represent NLOS regions (b) Estimated target trajectory is marked in red line with the ground truth in the black solid line.

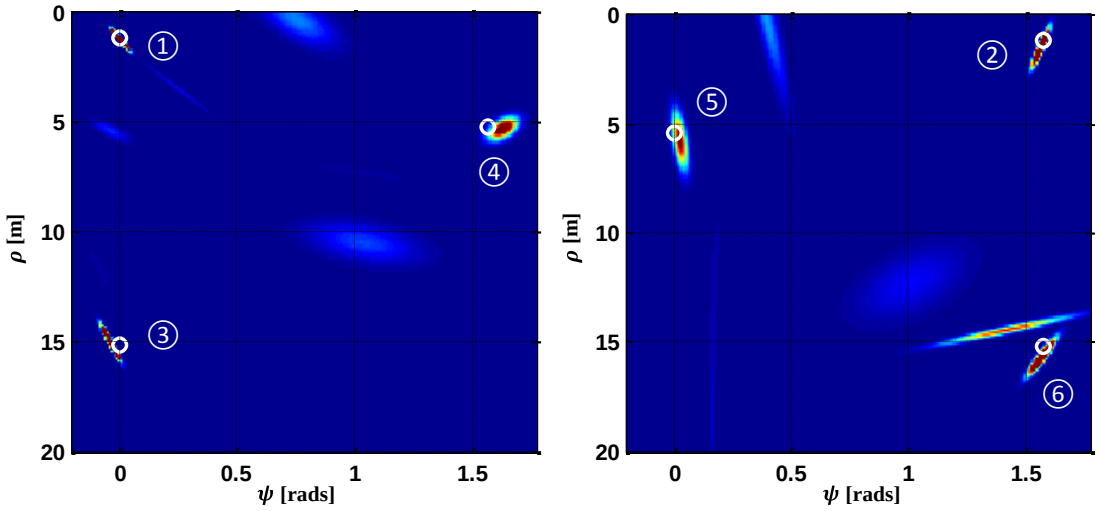

Figure 5.4: Estimated PHD intensities of multipath channels parameters (i.e., positions of planar reflectors in the room) with (a) array 1 and (b) array 2. The true values of plane reflectors are marked with white circles, and marked by circled numbers.

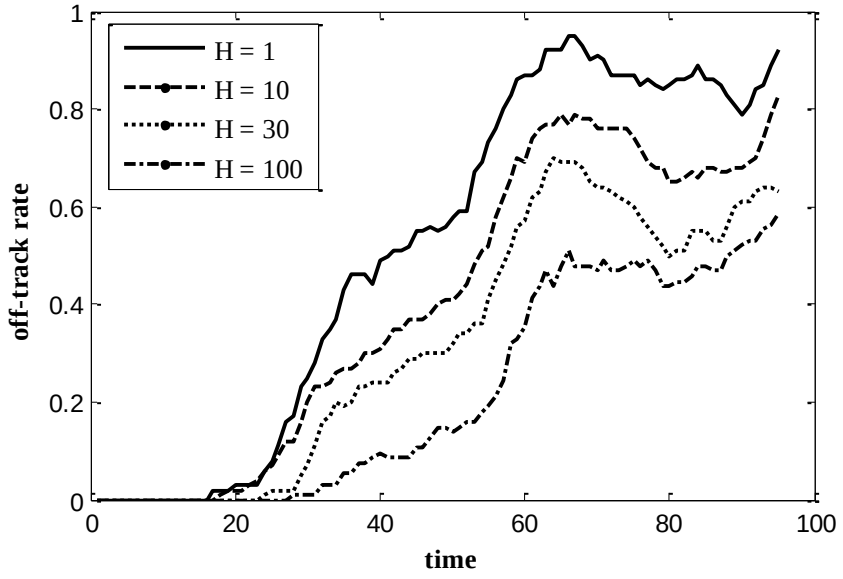

Figure 5.5: Off-track rate (i.e., probability of that instantaneous target position estimation error greater 1 meter) as a function of time index for different values of H (number of hypothesis kept at each time dwell). The result is generated by averaging 100 independent Monte Carlo runs.

specular reflection based multipath model is utilized, and no information about the building floor plan was used by the geolocation algorithm.

We implemented the multi-hypothesis tracking algorithm with the number of hypothesis per dwell as $H = 100$. The estimated target path are shown in Figure 5.6(b), with the measured path ground truth (black solid line) and the actual floor plan. The result using the proposed STAMP algorithm is marked as red line, while the estimated path using LOS observations only is represented by the red line. The difference between the target position estimates and the ground truth versus time is plotted in Figure 5.7. Assuming the measured ground truth has RMS error of 0.1 m in both x and y directions, the 95% (2σ) confidence intervals of the estimate error (computed from the EKF

posterior error covariance matrix), incorporating the ground truth uncertainties, are also illustrated in this figure as dashed lines. Note that when the target is in a NLOS region (i.e., time dwells 62-71 and 90-100 for sensor s_1, and time dwells 72-93 for sensor s_2), the positioning errors are larger compared to the LOS regions. However, using the multipath observations with estimated multipath parameters, STAMP is able to maintain the target localization errors to within ±1.5 m for both x and y dimensions as shown in Figure 5.7(a). For comparison, target localization errors using LOS observations only are shown in Figure 5.7(b) with 95% error bounds. In this case, the estimation error in the LOS region approximates that of STAMP, however, since no observation is present in the NLOS regions, the location error and bounds diverge rapidly with time compared the STAMP results in Figure 5.7(a).

The estimated GM-PHD surface of multipath parameter is shown in Figure 5.8, which is the sum of the PHDs from both sensor s_1 and s_2. For the given scene, two planar reflectors of the building (i.e., strong Gaussian components) can be identified on estimated PHD surfaces with parameter vectors (0.04, 0.3) and (-0.01, 7.32), which are closed to the true values (0, 0.1) and (0, 7.4) as marked by 1 and 2 in Figure 5.6(a) respectively. Notice that the roughness of the building wall surface would result in slowly varying estimates of multipath from dwell to dwell. Fortunately, this effect is empirically negligible, so that the support of the estimated posterior PHD, $D\left(\boldsymbol{\Theta}_s \middle| \mathbf{x}_k, \mathbf{Z}_{s,1:k}\right)$, always contains the true values of the multipath parameters.

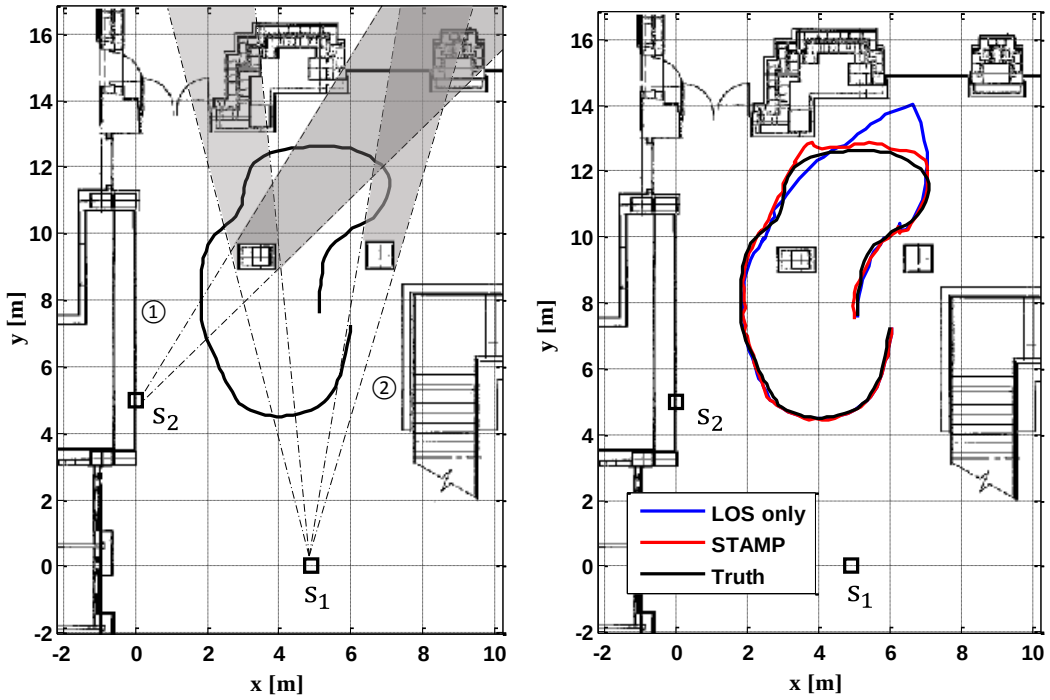

(a) (b)

Figure 5.6: (a) Illustration of the experiment scenario: two sensor arrays are denoted by squares, the target trajectory are marked with solid lines and two plane reflectors are noted in circled numbers; the gray areas represent NLOS regions (b) Estimated target trajectory with proposed STAMP algorithm is marked in red line, estimated target trajectory with LOS-only is marked in blue line.

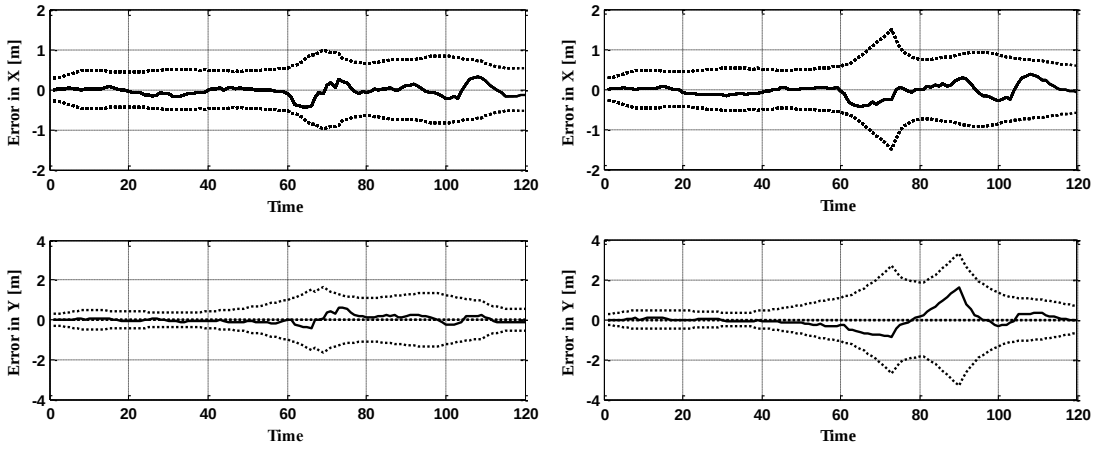

(a) (b)

Figure 5.7: Target location estimate error in x and y (solid line), with 95% confidence bounds (dotted lines) via (a) via STAMP and (b) direct path observations only

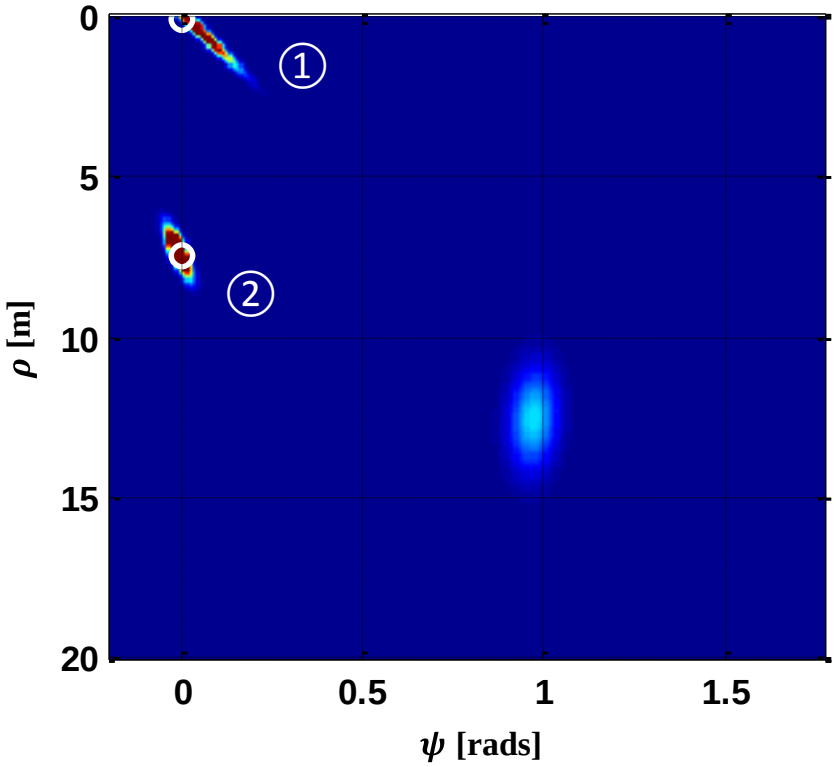

Figure 5.8: Estimated PHD intensity of multipath channels parameters (i.e., positions of planar reflectors in the room) by summing PHDs of the two arrays. The true values of plane reflectors are marked with white circles, and marked by circled numbers with respect to Figure 5.6(a).

5.5 Summary

In this chapter, we propose a multi-hypothesis single-cluster PHD filtering method for the simultaneous target and multipath positioning (STAMP) problem. Assuming the target state follows a single Gaussian process, the proposed recursive Bayesian algorithm employs a multi-hypothesis tracker to obtain an enhanced target state estimate, which defines the parent process. By modeling the multipath channel state as a random finite set, a Gaussian mixture PHD filter is utilized to estimate the

PHD intensity of the multipath channels parameters conditioned on the target state estimate. A set of illustrative simulation and real-data experiment for indoor target tracking problem are implemented using the proposed method, and enhanced target localization accuracy has been achieved even when LOS propagation is not present over the course of the track.

6

Conclusions and Future Work

For conventional geolocation system such as radar and Global Positioning System (GPS), both of the availability of the Line-Of-Sight (LOS) observations and the intensity of multipath observations impact the localization performance. For the GPS network, target position information is extracted based on LOS distances from a set of RF signal beacons to the mobile terminal. In urban or indoor environments, the received signal strength via LOS paths is often much weaker than multipath signals or even undetectable. In such cases, conventional LOS based positioning methods are inappropriate to apply. A number of works have been proposed to explore multipath observations as information sources when the LOS path is denied. Theses NLOS localization schemes typically require accurate priori information of the multipath propagation channel. For example, in order to predict detailed physical models of multipath observations, knowledge of the reflective geometry from meticulous building

floor plans and local maps are utilized, which is unfortunately difficult to obtain due to expensive labor and time costs.

In order to avoid the need for high fidelity multipath channel pre-probing, this work proposed the concept of Simultaneous Target and Multipath Positioning (STAMP), where the estimation of multipath parameters was included in the geolocation process with the dynamics of the target position. The STAMP state vector coupled both the target position and multipath channel parameters, which were jointly estimated based on the recursive Bayesian framework. In Chapter 2 and 3, the STAMP technique was applied to the target positioning problem by using a single-station hybrid TOA/AOA system and a monostatic MIMO radar system respectively. Assuming the multipath channels were stationary and time-invariant, the multi-hypothesis STAMP algorithm tracked the moving object and learned the physical multipath environmental parameters along an entire historical set of observation intervals. This method employed a multi-hypothesis data association to resolve fundamental ambiguities caused by the unknown correspondence between multipath channels and observed data in the presence of high observation noise levels and false alarms. Moreover, fundamental identifiability analysis of STAMP was provided based the Cramer-Rao Lower Bound (CRLB) for joint target and multipath parameter estimation. The estimation theoretic CRLB, or Fisher Information Matrix (FIM), could be regarded as a measure to qualify how each propagation modes contributes to the Fisher information and when the target and

multipath propagation parameters are identifiable as a function of available observations. The multi-hypothesis STAMP algorithm was evaluated based on a set of illustrative simulations and real data experiments by using an indoor multi-channel radar testbed, and substantial improvement in localization accuracy was observed.

In practice, the number of multipath propagation modes (e.g., the number of scatters in the scene of interest) is an unknown time-varying random variable. The multiple-hypothesis based STAMP algorithm modeled the target state and multipath parameter state as a single system state vector, and mode validation process was utilized over successive dwells in order to obtain an estimate of the number of modes. Alternatively, the multipath channel state could be modeled as a random finite set, characterizing both the cardinality and associated parameters of the entire multipath channel space, which was estimated using the first moment approximation of the Bayesian multi-target filter, or the probability hypothesis density (PHD) filter. The single-cluster PHD filter, exploring a hierarchical point process model, was extended to the STAMP problem: the target state was defined as a parent process; the random finite set of the multipath channel state was defined as the daughter process conditioning on the parent process. In Chapter 4 and 5, the single-cluster PHD filter STAMP algorithm was applied to multistatic range-based and AOA-based localization systems respectively. In Chapter 4, the propagation of the distribution of parent process was updated by using a particle filter, while in Chapter 5, the parent process was modeled

by a single Gaussian distribution and updated by a multi-hypothesis EKF. For both cases, the PHD intensity of the daughter process was represented by a Gaussian mixture model conditioned on the distribution of the parent process, and a GM-PHD filter was employed. The Single-Cluster PHD filter based STAMP algorithm was evaluated via a set of simulations and an illustrative real-data indoor RF source tracking experiment.

Future works of the STAMP problem include methodology to enhance the feasibility of real world multipath exploration. In complex indoor/urban multipath environments, the multipath propagations model of single bounce reflections from planar/point reflectors may be inappropriate. Sophisticated multipath modeling, such as the multiple reflections model, should be explored. Beside the discrete and resolved multipath returns, unresolvable multipath components and diffusely scattered energy will also be present. Alternative approaches for geolocation using a statistical model of the RF propagation has been proposed in [21, 44]. On the other hand, more robust and computational efficient particle filtering and data association algorithms will also be studied in the presence of large scale data, imperfect detections and highly frequented mode birth/death process. More realistic real data experiment will be also conducted in various multipath environments. Other possible extensions, for example, include the combination between the STAMP algorithm and the track-before-detection method in presence of low received signal SNR. Based on the CRLB analysis, optimal sensor management/selection problem for large distributed sensor network can be also studied.

In addition, partially STAMP that incorporates prior multipath channel information such as local maps and floor plans of building) is also a potential extension for real world implementation of STAMP concept.

In summary, this work has shown that the STAMP technique can be used to obtain enhanced target tracking/geolocation accuracies in dense and uncertain multipath environment such as indoor and urban areas. The mathematical identifiability analysis and the derivation of STAMP algorithm create a framework for many potential applications for joint multipath exploiting and target positioning. The STAMP concept has been proofed based on a set of numerical simulations and real data experiment. In some of these new applications, multipath will play a significant role, and the proposed STAMP can be utilized to solve the problems that arise.

Appendix A

This appendix provides the full derivation of equations (2.17) and (2.18), i.e., the CRLB for target position estimate $\hat{\mathbf{p}}$ and the multipath parameter vector $\hat{\boldsymbol{\theta}}_k$ for mode k, from the information matrix $\mathbf{J}(\mathbf{x})$ given in (2.12). Recall that the matrix inverse identity is given by:

$$\begin{bmatrix} A & B \\ C & D \end{bmatrix}^{-1} = \begin{bmatrix} E & F \\ G & H \end{bmatrix} \tag{A.1}$$

where

$$E = (A - B \cdot D^{-1} \cdot C)^{-1} \tag{A.2}$$

$$H = (D - C \cdot A^{-1} \cdot B)^{-1} \tag{A.3}$$

The CRLB for $\hat{\mathbf{p}}$ is the upper 2 by 2 sub-matrix of the inverse of $\mathbf{J}(\mathbf{x})$ given by

$$[\mathbf{J}(\mathbf{x})^{-1}]_{\mathbf{p}} = \left(\mathbf{L}_d + \sum_i \mathbf{L}_i + \boldsymbol{\Gamma}_{\mathbf{p}}^{-1} - \begin{bmatrix} \mathbf{C}_{1,\mathbf{p}}^T \\ \mathbf{C}_{2,\mathbf{p}}^T \\ \vdots \\ \mathbf{C}_{N,\mathbf{p}}^T \end{bmatrix}^T \begin{bmatrix} \boldsymbol{\Lambda}_1 + \boldsymbol{\Gamma}_1^{-1} & 0 & \dots & 0 \\ 0 & \boldsymbol{\Lambda}_2 + \boldsymbol{\Gamma}_2^{-1} & & \vdots \\ \vdots & & \ddots & 0 \\ 0 & \dots & 0 & \boldsymbol{\Lambda}_N + \boldsymbol{\Gamma}_N^{-1} \end{bmatrix}^{-1} \begin{bmatrix} \mathbf{C}_{1,\mathbf{p}}^T \\ \mathbf{C}_{2,\mathbf{p}}^T \\ \vdots \\ \mathbf{C}_{N,\mathbf{p}}^T \end{bmatrix} \right)^{-1}$$

$$= \left(\mathbf{L}_d + \sum_i \mathbf{L}_i + \boldsymbol{\Gamma}_{\mathbf{p}}^{-1} - \sum_i \mathbf{C}_{1,\mathbf{p}} (\boldsymbol{\Lambda}_1 + \boldsymbol{\Gamma}_1^{-1})\, \mathbf{C}_{1,\mathbf{p}}^T \right)^{-1}$$

$$= \left(\mathbf{L}_d + \boldsymbol{\Gamma}_{\mathbf{p}}^{-1} + \textstyle\sum_i \mathbf{L}_i - \mathbf{C}_{i,\mathbf{p}} (\boldsymbol{\Lambda}_i + \boldsymbol{\Gamma}_i^{-1})^{-1} \mathbf{C}_{i,\mathbf{p}}^T \right)^{-1} \tag{A.4}$$

This is the derivation of (2.17). For the CRLB on multipath parameter estimates $\widehat{\boldsymbol{\theta}}_k$, we first let the lower right sub-matrix D as $\boldsymbol{\Lambda}_k + \boldsymbol{\Gamma}_k^{-1}$, and thus H as $[\mathbf{J}(\mathbf{x})^{-1}]_{\boldsymbol{\theta}_k}$

$$[\mathbf{J}(\mathbf{x})^{-1}]_{\boldsymbol{\theta}_k} = \left(\boldsymbol{\Gamma}_k^{-1} + \boldsymbol{\Lambda}_k - \begin{bmatrix} \mathbf{C}_{k,\mathbf{p}}^T \\ 0 \\ \vdots \\ 0 \end{bmatrix} \begin{bmatrix} \mathbf{L}_d + \sum_i \mathbf{L}_i + \boldsymbol{\Gamma}_{\mathbf{p}}^{-1} & \mathbf{C}_{1,\mathbf{p}} & \cdots & \mathbf{C}_{N,\mathbf{p}} \\ \mathbf{C}_{1,\mathbf{p}}^T & \boldsymbol{\Lambda}_1 + \boldsymbol{\Gamma}_1^{-1} & \cdots & 0 \\ \vdots & \vdots & \ddots & 0 \\ \mathbf{C}_{N,\mathbf{p}}^T & 0 & 0 & \boldsymbol{\Lambda}_N + \boldsymbol{\Gamma}_N^{-1} \end{bmatrix}^{-1} \begin{bmatrix} \mathbf{C}_{k,\mathbf{p}}^T \\ 0 \\ \vdots \\ 0 \end{bmatrix}^T \right)^{-1}$$

$$= \left(\boldsymbol{\Gamma}_k^{-1} + \boldsymbol{\Lambda}_k - \mathbf{C}_{1,\mathbf{p}}^T (\boldsymbol{\Gamma}_k^{-1} + \underbrace{\mathbf{L}_d + \boldsymbol{\Gamma}_{\mathbf{p}}^{-1} + \sum_{i \neq k} \mathbf{L}_i - \mathbf{C}_{i,\mathbf{p}} (\boldsymbol{\Lambda}_i + \boldsymbol{\Gamma}_i^{-1})^{-1} \mathbf{C}_{i,\mathbf{p}}^T}_{\triangleq \left([\mathbf{J}(\mathbf{x})^{-1}]_{\mathbf{p}}^{(k)} \right)^{-1}})^{-1} \mathbf{C}_{1,\mathbf{p}} \right)^{-1}$$

$$= \left(\boldsymbol{\Gamma}_k^{-1} + \boldsymbol{\Lambda}_k - \mathbf{C}_{1,\mathbf{p}}^T (\boldsymbol{\Gamma}_k^{-1} - \boldsymbol{\Gamma}_k^{-1} (\boldsymbol{\Gamma}_k^{-1} + [\mathbf{J}(\mathbf{x})^{-1}]_{\mathbf{p}}^{(k)})^{-1} \boldsymbol{\Gamma}_k^{-1}) \mathbf{C}_{1,\mathbf{p}} \right)^{-1}$$

$$= \left(\boldsymbol{\Gamma}_k^{-1} + \boldsymbol{\Lambda}_k - \mathbf{C}_{1,\mathbf{p}}^T \mathbf{L}_k^{-1} \mathbf{C}_{1,\mathbf{p}} + \mathbf{C}_{k,\mathbf{p}}^T \mathbf{L}_k^{-1} (\mathbf{L}_k^{-1} + [\mathbf{J}(\mathbf{x})^{-1}]_{\mathbf{p}}^{(k)})^{-1} \mathbf{L}_k^{-1} \mathbf{C}_{k,\mathbf{p}} \right)^{-1} \quad \text{(A.5)}$$

The term $[\mathbf{J}(\mathbf{x})^{-1}]_{\mathbf{p}}^{(k)}$ denotes the CRLB on $\widehat{\mathbf{p}}$ excluded the contribution from mode k. Thus the derivation of (2.17) and (2.18) is done.

Bibliography

[1] Cheung, K.W.; So, H.C.; Ma, W.-K.; Chan, Y.T.; , "Least squares algorithms for time-of-arrival-based mobile location," Signal Processing, IEEE Transactions on , vol.52, no.4, pp. 1121- 1130, April 2004.

[2] Mensing, C.; Plass, S.; , "Positioning Algorithms for Cellular Networks Using TDOA," Acoustics, Speech and Signal Processing, 2006. ICASSP 2006 Proceedings. 2006 IEEE International Conference on , vol.4, no., pp.IV, 14-19 May 2006

[3] Gavish, M.; Weiss, A.J.; , "Performance analysis of bearing-only target location algorithms," Aerospace and Electronic Systems, IEEE Transactions on , vol.28, no.3, pp.817-828, Jul 1992.

[4] Seshadri, V.; Zaruba, G.V.; Huber, M.; , "A Bayesian sampling approach to in-door localization of wireless devices using received signal strength indication," Pervasive Computing and Communications, 2005. PerCom 2005. Third IEEE International Conference on , vol., no., pp. 75- 84, 8-12 March 2005.

[5] Bahl, P.; Padmanabhan, V.N.; , "RADAR: an in-building RF-based user location and tracking system ," INFOCOM 2000. Nineteenth Annual Joint Conference of the IEEE Computer and Communications Societies. Proceedings. IEEE , vol.2, no., pp.775-784 vol.2, 2000.

[6] T.P. Deasy and W.G. Scanlon, “Stepwise Algorithms for Improving the Accuracy of Both Deterministic and Probabilistic Methods in WLAN-Based Indoor User Localization,” Int’l J. Wireless Information Networks, vol. 11, Oct. 2004.

[7] Patwari, N.; Ash, J.N.; Kyperountas, S.; Hero, A.O., III; Moses, R.L.; Correal, N.S.; , "Locating the nodes: cooperative localization in wireless sensor networks," Signal Processing Magazine, IEEE , vol.22, no.4, pp. 54- 69, July 2005.

[8] Torrieri, D.J.; , "Statistical Theory of Passive Location Systems," Aerospace and Electronic Systems, IEEE Transactions on , vol.AES-20, no.2, pp.183-198, March 1984.

[9] Gustafsson, F.; Gunnarsson, F.; , "Mobile positioning using wireless networks: possibilities and fundamental limitations based on available wireless network measurements," Signal Processing Magazine, IEEE , vol.22, no.4, pp. 41- 53, July 2005.

[10] Mao, Guoqiang, Baris Fidan, and Brian Anderson. "Wireless sensor network localization techniques." Computer network 51.10 (2007): 2529-2553.

[11] Krolik, J.L.; Farrell, J.; Steinhardt, A.; , "Exploiting multipath propagation for GMTI in urban environments," Radar, 2006 IEEE Conference on , vol., no., pp. 4 pp., 24-27 April 2006.

[12] Yihong Qi; Suda, H.; Kobayashi, H.; , "On time-of-arrival positioning in a multipath environment," Vehicular Technology Conference, 2004. VTC2004-Fall. 2004 IEEE 60th , vol.5, no., pp. 3540- 3544 Vol. 5, 26-29 Sept. 2004.

[13] Caffery, J.J.; Stuber, G.L.; , "Radio location in urban CDMA microcells," Personal, Indoor and Mobile Radio Communications, 1995. PIMRC'95. 'Wireless: Merging onto the Information Superhighway'., Sixth IEEE International Symposium on , vol.2, no., pp.858-862 vol.2, 27-29 Sep 1995.

[14] Van Trees, Harry L. Detection, estimation, and modulation theory. Wiley-Interscience, 2004.

[15] Narasimhan, Sunil, and Jeffrey L. Krolik. "Fundamental limits on acoustic source range estimation performance in uncertain ocean channels." *The Journal of the Acoustical Society of America* 97 (1995): 215.

[16] B.W Reinisch, D.M Haines, R.F Benson, J.L Green, G.S Sales, W.W.L Taylor, Radio sounding in space: magnetosphere and topside ionosphere, Journal of Atmospheric and Solar-Terrestrial Physics, Volume 63, Issues 2–3, January 2001, Pages 87-98.

[17] Setlur, P.; Amin, M.; Ahmad, F., "Multipath Model and Exploitation in Through-the-Wall and Urban Radar Sensing," Geoscience and Remote Sensing, IEEE Transactions on , vol.49, no.10, pp.4021,4034, Oct. 2011.

[18] Porretta, M.; Nepa, P.; Manara, G.; Giannetti, F.; Dohler, M.; Allen, B.; Aghvami, A.H.; , "A novel single base station location technique for microcellular wireless networks: description and validation by a deterministic propagation model," Vehicular Technology, IEEE Transactions on , vol.53, no.5, pp. 1502- 1514, Sept. 2004.

[19] P. Meissner and K. Witrisal, "Multipath-assisted single-anchor indoor localization in an office environment," in 19th International Conference on Systems, Signals and Image Processing, IWSSIP 2012, 2012.

[20] G. V. Zaruba, M. Huber, F. A. Kamangar, and I. Chlamtac. 2007. Indoor location tracking using RSSI readings from a single Wi-Fi access point. Wirel. Netw. 13, 2 (April 2007), 221-235.

[21] Tsalolikhin, E.; Bilik, I.; Blaunstein, N.; , "A Single-Base-Station Localization Approach Using a Statistical Model of the NLOS Propagation Conditions in Urban Terrain," Vehicular Technology, IEEE Transactions on , vol.60, no.3, pp.1124-1137, March 2011.

[22] Azizyan, Martin, Ionut Constandache, and Romit Roy Choudhury. "SurroundSense: mobile phone localization via ambience fingerprinting." *Proceedings of the 15th annual international conference on Mobile computing and networking*. ACM, 2009.

[23] Yu, Jason; Krolik, Jeffrey, "MIMO multipath clutter mitigation for GMTI automotive radar in urban environments," Radar Systems (Radar 2012), IET International Conference on , vol., no., pp.1,5, 22-25 Oct. 2012doi: 10.1049/cp.2012.1565

[24] Gustafson, D.E.; Elwell, J.M.; Soltz, J.A.; , "Innovative Indoor Geolocation Using RF Multipath Diversity," Position, Location, And Navigation Symposium, 2006 IEEE/ION , vol., no., pp. 904- 912, April 25-27, 2006.

[25] Honglei Miao; Kegen Yu; Juntti, M.J.; , "Positioning for NLOS Propagation: Algorithm Derivations and Cramer–Rao Bounds," Vehicular Technology, IEEE Transactions on , vol.56, no.5, pp.2568-2580, Sept. 2007.

[26] Li Li; Krolik, J.L.; , "Target tracking in uncertain multipath environments using Viterbi data association," Information Fusion (FUSION), 2011 Proceedings of the 14th International Conference on , vol., no., pp.1-7, 5-8 July 2011.

[27] Dissanayake, M.W.M.G.; Newman, P.; Clark, S.; Durrant-Whyte, H.F.; Csorba, M.; , "A solution to the simultaneous localization and map building (SLAM) problem," Robotics and Automation, IEEE Transactions on , vol.17, no.3, pp.229-241, Jun 2001.

[28] Quach, T.; Farooq, M.; , "Maximum likelihood track formation with the Viterbi algorithm," Decision and Control, 1994., Proceedings of the 33rd IEEE Conference on , vol.1, no., pp.271-276 vol.1, 14-16 Dec 1994.

[29] Pulford, G.W.; La Scala, B.F.; , "Multihypothesis Viterbi Data Association: Algorithm Development and Assessment," Aerospace and Electronic Systems, IEEE Transactions on , vol.46, no.2, pp.583-609, April 2010.

[30] Bar-Shalom, Y.; Daum, F.; Huang, J.; , "The probabilistic data association filter," Control Systems Magazine, IEEE , vol.29, no.6, pp.82-100, Dec. 2009.

[31] K.G. Murty. “An algorithm for ranking all the assignments in order of increasing cost,” Operations Research, 16(3):682–687, 1968.

[32] Pattipati, K.R.; Deb, S.; , "Comparison of assignment algorithms with applications to the passive sensor data association problem," Control and Applications, 1989. Proceedings. ICCON '89. IEEE International Conference on , vol., no., pp.317-322, 1989.

[33] Poore, A., and Rijavec, N. (1991) Multitarget tracking, multidimensional assignment problems, and Lagrangian relaxation. Proceedings of SDI Panels on Tracking (Aug. 1991), 51—74.

[34] Maksarov, D.; Durrant-Whyte, H.; , "Mobile vehicle navigation in unknown environments: a multiple hypothesis approach," Control Theory and Applications, IEE Proceedings - , vol.142, no.4, pp.385-400, Jul 1995.

[35] Miller, M.L.; Stone, H.S.; Cox, I.J.; , "Optimizing Murty's ranked assignment method," Aerospace and Electronic Systems, IEEE Transactions on , vol.33, no.3, pp.851-862, July 1997.

[36] Yu, J.; Reynolds, M.; Krolik, J.; , "An indoor S-band radar receive array testbed," Radar Conference, 2010 IEEE , vol., no., pp.712-717, 10-14 May 2010.

[37] Li Li; Yu, J.; Krolik, J.; , "Software-defined calibration for FMCW phased-array radar," Radar Conference, 2010 IEEE , vol., no., pp.877-881, 10-14 May 2010.

[38] Botteron, C.; Host-Madsen, A.; Fattouche, M.; , "Cramer-Rao bounds for the estimation of multipath parameters and mobiles' positions in asynchronous DS-CDMA systems," Signal Processing, IEEE Transactions on , vol.52, no.4, pp. 862- 875, April 2004.

[39] Yihong Qi; Kobayashi, H.; Suda, H.; , "Analysis of wireless geolocation in a non-line-of-sight environment," Wireless Communications, IEEE Transactions on , vol.5, no.3, pp. 672- 681, March 2006.

[40] Y. Bar-Shalom and T. E. Fortman, Tracking and Data Association, NewYork: Academic, 1988.

[41] Yu, J.; Reynolds, M.; Krolik, J.; , "An indoor S-band radar receive array testbed," *Radar Conference, 2010 IEEE* , vol., no., pp.712-717, 10-14 May 2010.

[42] Li Li; Yu, J.; Krolik, J.; , "Software-defined calibration for FMCW phased-array radar," Radar Conference, 2010 IEEE , vol., no., pp.877-881, 10-14 May 2010.

[43] Wijesoma, W. Sardha, L. D. L. Perera, and Martin D. Adams. "Toward multidimensional assignment data association in robot localization and mapping." Robotics, IEEE Transactions on 22.2 (2006): 350-365.

[44] Bilik, I.; Adhikari, K.; Buck, J.R., "Shannon Capacity Bound on Mobile Station Localization Accuracy in Urban Environments," *Signal Processing, IEEE Transactions on* , vol.59, no.12, pp.6206,6216, Dec. 2011.

[45] R. Mahler, Statistical Multisource Multitarget Information Fusion. Norwood, MA, USA: Artech House, 2007.

[46] Mahler, Ronald PS. "Multitarget Bayes filtering via first-order multitarget moments." Aerospace and Electronic Systems, IEEE Transactions on 39.4 (2003): 1152-1178.

[47] Lian, F., et al. "Joint spatial registration and multi-target tracking using an extended probability hypothesis density filter." *Radar, Sonar & Navigation, IET*5.4 (2011): 441-448.

[48] Mullane, John, et al. "A random-finite-set approach to bayesian slam." Robotics, IEEE Transactions on 27.2 (2011): 268-282.

[49] Lee, C., D. Clark, and Joaquim Salvi. "SLAM with dynamic targets via single-cluster PHD filtering." (2013): 1-1.

[50] Lundquist, Christian, K. Granstrom, and Umut Orguner. "Estimating the Shape of Targets with a PHD Filter." Information Fusion (FUSION), 2011 Proceedings of the 14th International Conference on. IEEE, 2011.

[51] Granstrom K, Lundquist C, Orguner U. "A Gaussian mixture PHD filter for extended target tracking." Information Fusion (FUSION), 2010 13th Conference on. IEEE, 2010: 1-8.

[52] Ristic, B.; Clark, D.E.; Gordon, N., "Calibration of Multi-Target Tracking Algorithms Using Non-Cooperative Targets," Selected Topics in Signal Processing, IEEE Journal of , vol.7, no.3, pp.390,398, June 2013.

[53] Nagappa, Sharad, and Daniel E. Clark. "On the ordering of the sensors in the iterated-corrector probability hypothesis density (PHD) filter." *SPIE Defense, Security, and Sensing*. International Society for Optics and Photonics, 2011.

[54] M. I. Skolnik, *Introduction to Radar System* 3E, McGraw-Hill, New York, NY, USA, 2001.

[55] Mahler, Ronald. "Approximate multisensor CPHD and PHD filters." *Information Fusion (FUSION), 2010 13th Conference on*. IEEE, 2010.

[56] Clark, Daniel, and Ba-Ngu Vo. "Convergence analysis of the Gaussian mixture PHD filter." *Signal Processing, IEEE Transactions on* 55.4 (2007): 1204-1212.

[57] Sanjeev Arulampalam, M., et al. "A tutorial on particle filters for online nonlinear/non-Gaussian Bayesian tracking." *Signal Processing, IEEE Transactions on* 50.2 (2002): 174-188.

[58] Musso, Christian, Nadia Oudjane, and Francois Le Gland. "Improving regularised particle filters." *Sequential Monte Carlo methods in practice*. Springer New York, 2001. 247-271.

[59] Vo, Ba-Ngu, and Wing-Kin Ma. "The Gaussian mixture probability hypothesis density filter." *Signal Processing, IEEE Transactions on* 54.11 (2006): 4091-4104.

[60] Mahler, Ronald PS, Ba-Tuong Vo, and Ba-Ngu Vo. "CPHD filtering with unknown clutter rate and detection profile." Signal Processing, IEEE Transactions on 59.8 (2011): 3497-3513.

[61] Schuhmacher, Dominic, Ba-Tuong Vo, and Ba-Ngu Vo. "A consistent metric for performance evaluation of multi-object filters." *Signal Processing, IEEE Transactions on* 56.8 (2008): 3447-3457.

[62] X. Song, P. Willett, and S. Zhou, "On Fisher information reduction for range-only localization with imperfect detection," IEEE Transactions on Aerospace and Electronic Systems, vo. 48, no. 4, pp. 3694-3702, October 2012.

[63] Hue, C.; Le Cadre, J.-P.; Perez, P.; , "Posterior Cramer-Rao bounds for multi-target tracking," Aerospace and Electronic Systems, IEEE Transactions on , vol.42, no.1, pp. 37- 49, Jan. 2006.

[64] Swain, Anthony, and Daniel Clark. "The single-group PHD filter: an analytic solution." Information Fusion (FUSION), 2011 Proceedings of the 14th International Conference on. IEEE, 2011.

Biography

Li Li joined the Ph.D. program of Electrical Engineering at Duke University in 2009. As a senior research assistant in the Sensor Array and Multipath Signal Processing Lab, his research interests include statistical sensor array signal modeling and processing with an emphasis on low SNR radar target imaging, detection and tracking in dense multipath environments. He received a BS degree in Communications Engineering from the University of Electronic Science and Technology of China (UESTC) in 2009, followed by a MS degree in Electrical Engineering from Duke University in 2011.